Estimation of Glucose using Fixed Wavelength Light Sources

Thesis submitted to Goa University

for the award of the Degree of

DOCTOR OF PHILOSOPHY

In

Electronics

By

Marlon Darius Sequeira

Under the guidance of

Prof. Gourish M. Naik

School of Physical and Applied Sciences

Goa University, Taleigao-Goa

August 2020

CERTIFICATE

This is to certify that the thesis titled **"Estimation of Glucose using Fixed Wavelength Light Sources"** submitted by Mr. Marlon Darius Sequeira for the award of the degree of Doctor of Philosophy in Electronics, is based on his original and independent work carried out by him during the period of study under my supervision. The thesis or any part thereof has not been previously submitted for any other degree or diploma in any University or Institute.

`

(Prof. Gourish M. Naik)
Research Guide

Place: Goa University
Date: 26/01/2021

DECLARATION

I state that the present thesis entitled **"Estimation of Glucose using Fixed Wavelength Light Sources",** is my original contribution and the same has not been submitted on any occasion for any other degree or diploma of this or any other University or Institute. To the best of my knowledge the present study is the first comprehensive work of its kind in the area mentioned. The literature related to the problem investigated has been cited. Due acknowledgements have been made whenever facilities and suggestions have been availed of.

(Marlon Darius Sequeira)
Candidate

Place: Goa University
Date : 25/01/2021

Dedicated to my Parents

Caetano F. Sequeira

and

Magdalena E. Sequeira

ACKNOWLEDGEMENTS

Foremost, I would like to thank the Almighty GOD for showering upon me countless blessings and graces required by me during these years.

I would like to express my deepest gratitude to my supervisor, Prof. G. M. Naik, for his constant support and motivation throughout my research work. I will treasure the invaluable guidance that he gave me during these years. He has always been patient with me and inspired me to take up challenges during my research work. I consider myself privileged to have worked under his guidance.

I would like to convey my gratitude to Dr. M. Kunhanandan, Assistant professor, Department of Mathematics, Goa University, for his feedback and suggestions during the Department Research Committee (DRC) meetings which enabled me to improve in various facets of my research work.

I extend a big thank you to my teacher, Prof. R. S. Gad, Head of Department, Department of Electronics, Goa University, for his insightful comments and encouragement throughout. He has always supported me by providing the various research facilities available at the department. I am sincerely grateful to my teacher, Dr. J. S. Parab, Associate professor, Department of Electronics, Goa University, who has been a constant source of encouragement and inspiration to me. He guided me through the process of understanding the multivariate analysis and exposed me to the various FPGA embedded platforms available at the department.

My many thanks and appreciation goes to Dr. N. Tavares, Dr. N. T. Vetrekar, Dr. I. Nazareth, Dr S. R. Vernekar, Dr. V. R. Gad, Dr. U. V. Rane, Dr. S. R. Ghanti, Dr. N. Marchon, Dr. S. A. Patil, Mr. C. Pinto, Mr. S. M. Patil, Mrs. V. Fernandes, Mr. G. Abhyankar, Mr. D. Gonsalves, Mrs. Y. Prabhu, Mr. A. Gaonkar, Mr. C. Panem, Mr. A. Pednekar, Mr. A. Prabhu and Mr. D. Chodankar for the valuable scientific discussions we have had during my research work.

I would like to thank the Ministry of Electronics and Information Technology, New Delhi, for the scholarship provided under the Visvesvaraya Ph.D. Scheme for Electronics and Information Technology (MEITY-PHD-488).

I am grateful to the supporting staff of the Department of Electronics, Goa University, Mr. W. D'Souza, Mr. V. Malik, Mrs. A. Velip, Mrs. P. Andrade, who have always extended their helping hand whenever needed. I also thank Mr. M. Lanjewar, Technical Officer, and Mr. A. Lopes, USIC, Goa University, for their wise and encouraging words shared from time to time.

Words are not enough to express my gratitude to my parents, Caetano F. Sequeira and Magdalena E. Sequeira for their selfless sacrifices, patience, love and encouragement. This accomplishment wouldn't be possible without the support of my beloved wife, Elita Fernandes, who has always been a source of strength, encouragement, and love to me. I would like to thank my dear siblings Carlton Sequeira and Lwellon Sequeira who have been pillars of support in good and bad times.

Marlon Darius Sequeira

August 2020

TABLE OF CONTENTS

LIST OF FIGURES

LIST OF TABLES

LIST OF ABBREVIATIONS

ADC: Analog to Digital Converter

ANN: Artificial Neural Network

ASCII: American Standard Code for Information Interchange

ASIC: Application Specific Integrated Circuit

ATR: Attenuated total reflection

BSP: Board Support Packages

BUN: Blood Urea Nitrogen

CAD: Computer Aided Design

CBC: Complete Blood Cell Count

CGM: Continuous Glucose Monitoring

CLB: Configurable Logic Block

CLS: Classical Least Squares

DIP: Diabetes in pregnancy

EGA: Error Grid Analysis

FPGA: Field Programmable Gate Array

GDM: Gestational Diabetes Mellitus

GOx: Glucose Oxidase

GPIO: General Purpose Input Output

GUI: Graphical User Interface

HAL: Hardware Abstraction Layer

HDL: Hardware Description Language

I2C: Inter Integrated Circuit

ICR: Independent Component Regression

IDE: Integrated Development Environments

IDF: International diabetes Federation

ILS: Inverse Least-Squares

IP: Intellectual Property

IR: Infrared

LED: Light Emitting Diode

LOOCV: Leave One Out Cross Validation

LUT: Look Up Table

MIPS: Million Instructions Per Second

MLR: Multiple Linear Regression

MSC: Multiplicative Scatter Correction

MUX: Multiplexer

NADH: Nicotinamide Adenine Dinucleotide Reduced

NIPALS: Non-linear Iterative Partial Least Squares

NIR: Near-Infrared

OCT: Optical Coherence Tomography

OGTT: Oral Glucose Tolerance Test

PCA: Principal Component Analysis

PCR: Principal Component Regression

PLSR: Partial Least Squares Regression

QCL: Quantum Cascade Laser

QTH: Quartz Tungsten Halogen

RBC: Red Blood Cell

RBF: Radial Basis Function

RBFNN: Radial Basis Function Neural Network

RISC: Reduced Instruction Set Computer

RMSE: Root Mean Square Error

RMSEP: Root Mean Square Error of Prediction

SBT: Software Build Tools

SDRAM: Synchronous Dynamic Random Access Memory

SEA: South-East Asia

SEP: Standard Error of Prediction

SIMPLS: Statistical Inspired Modification of PLS

SMBG: Self-Monitoring Of Blood Glucose

SNR : Signal to Noise Ratio

SNV: Standard Normal Variate

SPI: Serial Peripheral Interface

SVD: Singular Value Decomposition

UART: Universal Asynchronous Receiver Transmitter

UV: Ultraviolet

VHDL: Very High Speed Integrated Circuit Hardware Description Language

WHO: World Health Organization

PREFACE

This thesis is on “Estimation of Glucose using Fixed Wavelength Light Sources”. A system has been developed to estimate the glucose concentration non-invasively on an Altera NIOS-II soft-core platform using a DE-0 Nano board having a Cyclone-IV FPGA. Fixed wavelengths were used to probe the sample and a PLSR calibration model is built to estimate glucose concentration of unknown samples. The whole exercise is done to reduce the resources required for development of a portable, low cost glucose monitoring device.

Chapter 1 contains an introduction to the thesis along with overview of diabetes, the different types of diabetes, the global prevalence of diabetes, confounding effects of other blood constituents, history of blood glucose monitoring devices, economic impact of diabetes and finally ends with objective of research work.

Chapter 2 contains a detailed literature review of various methods used for determination of glucose. It classifies these methods into invasive, minimally-invasive and non-invasive. Under invasive methods the laboratory methods and home monitoring methods are described. Minimally invasive methods such as reverse iontophoresis, sonophoresis, and microporation are discussed. In non-invasive section, methods such as mid-infrared spectroscopy, Raman spectroscopy, optical polarimetry, photoacoustic spectroscopy, bioimpedance spectroscopy, Optical Coherence Tomography, Near Infrared spectroscopy are reviewed. The chapter ends with highlight on the need of a non-invasive glucometer.

Chapter 3 discusses how to use near-infrared radiation to estimate glucose. It contains the theory behind the near-infrared absorption. The chapter also discusses the major interferents and the optical properties of human tissue.

Chapter 4 elucidates the methodology adopted for determination of glucose concentration. It contains the spectroscopic measurements for glucose estimation, spectrophotometer for measurement for glucose absorption, sample preparation, path length considerations and system design.

Chapter 5 describes how glucose estimation can be done using a FPGA soft-core processor. It contains structure of an FPGA, soft-core processor for embedded systems, a survey of soft-core processors, DE-0 Nano board used to configure the NIOS-II soft

core, Qsys system integration tool, SDRAM interface to NIOS-II, ADC controller interface and programming the NIOS-II soft core.

Chapter 6 describes multivariate calibration model for glucose estimation. It discusses various multivariate methods available, PLSR along with NIPALS and SIMPLS algorithm, the ParLes software for preliminary analysis.

Chapter 7 gives results obtained and conclusion drawn from the various experiments. A PLSR calibration model was built to estimate glucose for three different cases. The model for glucose estimation is assessed using root mean square error and Clarke error grid analysis. In the end, the future scope of research in the area is given.

LIST OF PUBLICATIONS

Journal Publications

1. "**Estimation of glucose using fixed wavelength NIR light sources**", Journal of Advanced Research in Dynamical and Control Systems, Vol. 10, 03-Special Issue, 2018, pp.119-126 **(Scopus).**

2. "**Altera computational platform for blood glucose monitoring**", Int. J. of Recent Technology and Engineering. Accepted **(Scopus).**

3. "**Effect of Reduced Point NIR Spectroscopy on Glucose Prediction Error in Human Blood Tissue**", Biomedical Engineering and Computational Intelligence **(Springer Lecture Notes in Computational Vision and Biomechanics, Volume 32**), pp. 93-103.

4. "**Glucose signal estimation using high performance ADC and light probes",** Int. J. of researches in biosciences, agriculture and technology, Vol. V, Special Issue (3), Nov-2017, pp.162-165 (UGC approved Journal No. 43906)

Conferences

1. "**Fixed wavelength light source estimation of glucose**" Nat. Conf. Science Education & Research, Basaweswara College, Bangalore, 29-30th Jan 2016, pp. 21-23.

2. "**Non-Invasive Estimation of Glucose using Fixed Wavelength Visible Light Sources** " 10th Annual Symposium on VLSI and Embedded Systems, Electrical & Electronics Engineering Department, Goa College of Engineering. Goa, 27-28thApril 2017.

3. "**Electrometer amplifier using FPGA interface**" 11th annual National symposium on VLSI and Embedded Systems, Goa University, 23rd March 2018, pp. 44-46.

4. "**Development of instrumentation for reflectance parameter measurement for non-invasive glucose estimation**" in 11th annual National symposium on VLSI and Embedded Systems, Goa University, 23rd March 2018, pp. 47-49.

In the present days cures have been found for so many ailments, which were historically thought to be incurable. The advances in medical sciences have enabled people to manage their health in a more efficient manner, which has resulted in leading a long and healthy life. One of the diseases which plays havoc if not managed well is diabetes. There are severe long term conditions that result from diabetes like kidney failure, neuropathy and eye damage, leading to blindness, slow healing of wounds, amputation of limbs, accompanied by acute cardiovascular conditions. Hence, it is of utmost importance that blood sugar levels should be tightly controlled to avoid the above complications. Another confounding factor is that these above condition do not surface themselves up until many years. These can lead to a serious financial burden in the later stage. A good healthy lifestyle involving regular physical activity, normal body weight, healthy diet, can go a long way to prevent diabetes.

The above listed reasons make it imperative for a person having diabetes to regulate his blood sugar which requires them to measure the blood sugar at regular intervals during the day. Traditionally used laboratory techniques are very accurate but come with an inherent delay due to time taken to process the samples. The self-monitoring devices in the market today rely on finger pricking and collecting the blood on disposable strips. The pain associated with the finger pricking causes apprehension in the patients mind and lead to less frequent measurement. Thus a tight control of one's blood glucose levels is not achieved. Additionally these devices come with a serious danger of infection. Hence, there is a shift of attention to non-invasive methods to monitor glucose. Traditional use of spectroscopy for glucose estimation used a white light source, which makes the entire equipment very bulky. If a portable device has to be fabricated, fixed wavelength light sources like LEDs must be used in place of a white light source. These sources can offer a manifold increase in signal to noise ratio. Use of fixed wavelength light sources not only reduces the equipment size but also relaxes the power, memory and computing requirements.

Thus the problem was formulated to develop a method to acquire glucose signal using fixed wavelength light sources and to implement multivariate algorithm to estimate the glucose concentration.

1.1 Overview of Diabetes

Diabetes is a serious, long-term condition that occurs due to raised levels of glucose in the blood, which is a result of body's inability or insufficient production of the hormone insulin, or the ineffectiveness of the hormone it produces. The pancreas is the organ which produces the hormone insulin required by the body. Insulin allows the uptake of glucose from the bloodstream into the cells. The cells utilize glucose by converting it to energy. Hyperglycemia or high blood glucose levels are a result of either inability of cells to respond to insulin or insufficient insulin. Hyperglycemia is used as the clinical indicator for diabetes [1].

1.1.1 Types of Diabetes

Type 1 diabetes results from an autoimmune reaction of the body. The immune system attacks the insulin producing beta cells situated in the pancreas although small percentage are a result of idiopathic failure of the beta cells[2]. This leads to very little or no production of insulin by the body. Of the total diabetes population, type 1 diabetes accounts for 5 - 10 % of the cases [3]. Type 1 diabetes was previously known as insulin dependent, childhood-onset or juvenile diabetes.

Type 2 diabetes is a condition where the body cells cannot respond to insulin fully, known as insulin resistance. As a result of ineffectiveness of insulin the body prompts an increased production of insulin, which overtime leads to the failure of beta cells to keep up with the demand [1]. This type of diabetes accounts for 90 - 95 % of the cases of diabetes [3]. This type of diabetes was formally known as adult-onset diabetes or non-insulin dependent diabetes. Increasing age**,** obesity, fat distribution, sedentary lifestyle, stress may be considered as potential risk factors in type 2 diabetes.

Hyperglycemia during pregnancy can be classified as either Diabetes In Pregnancy (DIP) or Gestational Diabetes Mellitus (GDM) [4,5]. Hyperglycemia which is diagnosed for the first time during pregnancy is termed as GDM. This may occur anytime during pregnancy period but most likely after 24 weeks [6]. Pregnant women with a history of diabetes or high blood sugar level during pregnancy and fall within the WHO criteria when not pregnant are said to have DIP. DIP can occur anytime during pregnancy, even during the first trimester [5]. Around 75–90% cases of hyperglycemia during pregnancy are GDM [7].

Diabetes needs to be managed well, if not it leads to many life threatening complications. Diabetic ketoacidosis in case of type 1 and 2 and hyperosmolar coma in type 2 can occur if blood glucose levels are allowed to become abnormally high. Exercising more than usual, skipping a meal, or if there is a over dosage of anti diabetic medication, the blood glucose levels can drop to abnormally low levels which may lead to loss of consciousness or seizures.

Over a long period, diabetes can cause damages to eyes, heart, blood vessels, nerves and kidneys, which increase the incidence of heart disease and stroke. Reduced blood flow to the extremities due to the above condition coupled with neuropathy (nerve damage) can increase the chances of foot ulcers and infection which eventually may lead to amputation of limbs. Another serious issue to health is diabetic retinopathy, which occurs due to long-term compounded damage to retinal blood vessels. Diabetes can have serious damage to kidney and may result in kidney failure. Gestational diabetes can lead to serious complication to both mother and child which may result in fetal death, congenital defects, stillbirths, maternal morbidity and mortality. The above reasons make it very clear why it is imperative to manage the blood glucose levels in the prescribed clinical range.

1.2 Global prevalence of Diabetes

According to the latest finding of International diabetes Federation (IDF) as of 2019, 463 million people suffer from diabetes and this figure is estimated to grow to 578 million by 2030[1]. It is estimated that 79.4% diabetic patients live in low and middle income countries. According to “Diabetes atlas” published by IDF, China has the highest number of diabetes in the age group of 20 to 79 years followed by India and United States of America [1].India and United States of America are expected to occupy the position until 2030, then Pakistan is anticipated to reach the third position by 2045.

India falls in the IDF South-East Asia (SEA) region. In 2019, 8.8% of the adult population aged 20–79 years in the SEA region had diabetes which is equal to 87.6 million people. India has 77 million adults having diabetes and is ranked second in the world. India along with Sri Lanka and Bangladesh amount to 98.9% of the entire adult population having diabetes in the SEA region.

Table 1.1: Country ranks for number of adults (20 to 79 years) having diabetes in 2019, and estimate for 2030 and 2045.

2019			2030			2045		
Rank	Country	Number of people with diabetes (millions)	Rank	Country	Number of people with diabetes (millions)	Rank	Country	Number of people with diabetes (millions)
1	China	116.4	1	China	140.5	1	China	142.2
2	India	77	2	India	101	2	India	134.2
3	USA	31	3	USA	34.4	3	Pakistan	37.1
4	Pakistan	19.4	4	Pakistan	26.2	4	USA	36
5	Brazil	16.8	5	Brazil	21.5	5	Brazil	26
6	Mexico	12.8	6	Mexico	17.2	6	Mexico	22.3
7	Indonesia	10.7	7	Indonesia	13.7	7	Egypt	16.9
8	Germany	9.5	8	Egypt	11.9	8	Indonesia	16.6
9	Egypt	8.9	9	Bangladesh	11.4	9	Bangladesh	15
10	Bangladesh	8.4	10	Germany	10.1	10	Turkey	10.4

1.3 Physiological Ranges of Glucose

Glucose acts as the most essential energy source for a human being. Ideally pre-prandial glucose must be below 100 mg/dL(5.5 mmol/L) in plasma and below 89 mg/dL(4.9 mmol/L) in whole blood and capillary. Recommended ideal goals for postprandial are 140 mg/dL(7.8 mmol/L) in plasma and less than 125 mg/dL(6.9 mmol/L) in whole blood and capillary [8]. Most diabetic patients are using blood glucose self-monitoring devices for surveillance of their glucose levels and adjustment of their insulin dosage to achieve normoglycemia with glucose concentrations between 3.9 and 7.8 mmol/l (70–140 mg/dl) [9]

1.4 The Glucose Metabolism

Glucose is an essential fuel for the body. The amount of glucose in the bloodstream is regulated by different hormones, the most important being insulin. Glucose is used for many purposes in the body. It can be converted into energy via pyruvate and the tricarboxylic acid cycle (citric acid cycle), as well as being converted to fat (long-term storage) and glycogen (short-term storage)[10].

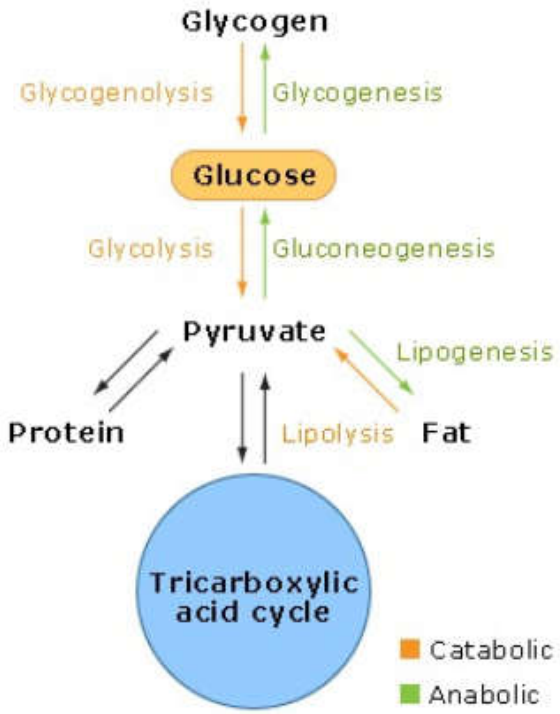

Figure 1.1: Anabolism and catabolism of glucose

Insulin is one of the myriad of hormones produced by the body for its proper functioning. The insulin making cells of the body are called beta cells, and they are found in the pancreas gland. These cells clump together to form the "islets of Langerhans". Insulin controls the metabolism of proteins, fats, and carbohydrates by facilitating the uptake of glucose into skeletal muscle cells, fat and liver from the blood [11]. Not all tissues require insulin for glucose uptake. Tissues such as liver cells, red blood cells, the gut mucosa, the kidneys, and cells of the nervous system use a glucose transporter that is not insulin dependent.

Glucagon is secreted by the alpha cells of the pancreatic islets in much the same manner as insulin. Glucagon is the main hormone opposing the action of insulin and is

released when food is scarce. Whereas insulin triggers the formation of glycogen (an energy-requiring process, or an anabolic effect), glucagon triggers glycogen breakdown, which releases energy (a catabolic effect). Glucagon also helps the body to switch to using resources other than glucose, such as fat and protein. Blood glucose levels are not constant; they rise and fall depending on the body's needs, regulated by hormones. This results in glucose levels normally ranging from 70 to 110 mg/dl.

After a meal, a rise in blood glucose is detected by the pancreatic beta cells, which respond by releasing insulin. Insulin increases the uptake and use of glucose by tissues such as skeletal muscle and fat cells. This rise in glucose also inhibits the release of glucagon, inhibiting the production of glucose from other sources, e.g., glycogen break down. Glucose once inside the cell, is used immediately via glycolysis. This is a central pathway of carbohydrate metabolism as it occurs in all cells in the body, and because all sugars can be converted into glucose and enter this pathway. During the well fed state, the high levels of insulin and low levels of glucagon stimulate glycolysis, which releases energy and produces carbohydrate intermediates that can be used in other metabolic pathways.

Any glucose that is not used immediately is taken up by the liver and muscle where it can be converted into glycogen (glycogenesis). Insulin also encourages glycogen formation in muscle, but by a different method. Here it increases the number of glucose transporters on the cell surface. This leads to a rapid uptake of glucose that is converted into muscle glycogen. When glycogen stores are fully replenished, excess glucose is converted into fat in a process called lipogenesis. Glucose is converted into fatty acids that are stored as triglycerides (three fatty acid molecules attached to one glycerol molecule) for storage. Insulin also has an anabolic effect on protein metabolism. It stimulates the entry of amino acids into cells and stimulates protein production from amino acids.

Fasting is defined as more than eight hours without food. The resulting fall in blood sugar levels inhibits insulin secretion and stimulates glucagon release. Glucagon opposes many actions of insulin. Most importantly, glucagon raises blood sugar levels by stimulating the mobilization of glycogen stores in the liver, providing a rapid burst of glucose. In 10–18 hours, the glycogen stores are depleted, and if fasting continues,

glucagon continues to stimulate glucose production by favoring the hepatic uptake of amino acids, the carbon skeletons of which are used to make glucose. In addition to low blood glucose levels, many other stimuli stimulate glucagon release including eating a protein-rich meal (the presence of amino acids in the stomach stimulates the release of both insulin and glucagon, glucagon prevents hypoglycemia that could result from unopposed insulin) and stress (the body anticipates an increased glucose demand in times of stress).

1.5 Confounding Effect of other Blood constituents.

Blood is a specialized body fluid that delivers necessary substances to the body's cells. Blood has different function in the human body which include oxygen and nutrients supply to the various parts of the body, removal of waste products such as carbon dioxide, lactic acid and urea, immunological function such as transport of white blood cells and detection of foreign bodies by antibodies, self repair by coagulation, messenger functions by transport of hormones and tissue damage signals, pH regulation of the body in the range of (7.35 - 7.45) and temperature regulation of body.

The blood volume in an average adult is around 5 litres. The blood contains plasma and several kinds of cells. The three different types of formed elements in the blood are leukocytes (white blood cells), erythrocytes (red blood cells), and thrombocytes (platelets) [12]. Plasma constitutes about 55% of the whole blood by volume and the red blood cells constitute about 45% of the blood. The white blood cells constitute a miniscule volume. The normal appearance of plasma is straw yellow color.

The total volume of plasma is around 2.7 - 3.0 litres in an average human being. It is basically an aqueous solution which containing 92% water, 8% blood plasma proteins and other trace materials. Nutrients such as glucose, fatty acids and amino acids are dissolved in the plasma and therefore plasma is responsible to circulate these nutrients to the various parts of the body. Water is a major component of blood and tissue, hence absorption due to water plays dominant contributors to any absorbance studies. We must choose optical windows which present low water absorption. In addition to water, blood matrix consists of around 118 constituents. All of them present an overlapping absorbance signature, which makes it very difficult to isolate the glucose signature. Below table gives the reference physiological range of different blood constituents.

Table 1.2: Clinical range of blood constituents

Sr. No.	Blood Constituent	Clinical Range
1	Acetoacetate	< 3 mg/dL
2	Acidity (pH)	7.35 - 7.45
3	Alanine aminotransferase	7–41 units/L
4	Alcohol	0 mg/dL(blood alcohol content of 30 mg/dL is the limit of intoxication)
5	Ammonia	15 - 50 µg of nitrogen/dL
6	Amylase	53 - 123 units/L
7	Ascorbic Acid	0.4 - 1.5 mg/dL
8	Aspartate aminotransferase	12-38 units/L
9	Bicarbonate	18 - 23 mEq/L (carbon dioxide content)
10	Bilirubin	0.3–1.3 mg/dL (total) 0.0–1 mg/dL (indirect) 0.0–0.4 mg/dL (direct)
11	Blood	8.5 - 9.1% of the body weight
12	Calcium	8.5 - 10.5 mg/dL (normally slightly higher in children)
13	Carbon Dioxide Pressure	35 - 45 mm Hg
14	Carbon Monoxide	Less than 5% of total hemoglobin
15	CD4 Cell Count	500 - 1500 cells/µL
16	Ceruloplasmin	15 - 60 mg/dL
17	Chloride	98 - 106 mEq/L
18	Complete Blood Cell Count (CBC)	White blood cell 3.5–9.1x 10^9/L Red blood cell 4–5.2 x 10^{12}/L
19	Copper	70 - 150 µg/dL
20	Creatine Kinase	38 - 174 units/L (Male) 96 - 140 units/L (Female)

21	Creatine Kinase Isoenzymes	5% MB or less
22	Creatinine	0.6 - 1.2 mg/dL
23	Erythrocyte Sedimentation Rate	< 50 mm/hr
24	Glucose	70 - 110 mg/dL (Fasting)
25	Hematocrit	45 – 62 % (Male) 37 – 48 % (Female)
26	Hemoglobin	13 - 18 gm/dL (Male) 12 - 16 gm/dL (Female)
27	Iron	60 - 160 µg/dL (normally higher in males)
28	Iron-binding Capacity	250 - 460 µg/dL
29	Lactate (lactic acid)	4.5-19.8mg/dL (Venous) 4.5 - 14.4 mg/dL (Arterial)
30	Lactic Dehydrogenase	50 - 150 units/L
31	Lipase	10 - 150 units/L
32	Lipids	< 200 mg/dL(Cholesterol) <150 mg/dL(Triglycerides) < 60 mg/dL(HDL Cholesterol) < 60 - 130 mg/dL(LDL Cholesterol) < 4.0 (Cholesterol/HDL ratio)
33	Magnesium	1.5 - 2.0 mEq/L
34	Mean Corpuscular Hemoglobin (MCH)	26 - 31 pg/cell
35	Mean Corpuscular Hemoglobin Concentration (MCHC)	32 - 36% hemoglobin/cell
36	Mean Corpuscular Volume (MCV)	79 – 93.3 fL
37	Osmolality	280 - 296 mOsm/kg water

38	Oxygen Pressure	83 - 100 mm Hg
39	Oxygen Saturation (arterial)	96 - 100%
40	Phosphatase Prostatic	0 - 3 units/dL (Bodansky units) (acid)
41	Phosphatase	50 - 160 units/L (normally higher in infants and adolescents)(alkaline)
42	Phosphorus	3.0 - 4.5 mg/dL (inorganic)
43	Platelet Count	150000 - 350000/mL
44	Potassium	3.5 - 5.0 mEq/L
45	Prostate Specific Antigen	0 - 4 ng/mL (likely higher with age)
46	Proteins	6.7–8.6 gm/dL (Total) 3.5–5.5 gm/dL (Albumin) 2–3.5 gm/dL (Globulin)
47	Pyruvic Acid	0.3 - 0.9 mg/dL
48	Red Blood Cell Count	4.2 - 6.9 million/µL/cu mm
49	Sodium	135 - 145 mEq/L
50	Thyroid-Stimulating Hormone	0.5 - 6.0 µ units/mL
51	Urea Nitrogen (BUN)	7 - 18 mg/dL
52	BUN/Creatinine Ratio	5 – 35
53	Uric Acid	2.1 to 8.5 mg/dL (Male) 2.0 to 7.0 mg/dL (Female)
54	Vitamin A	30 - 65 µg/dL
55	WBC (leukocyte count and white blood cell count)	4.3-10.8 × 10^3/mm^3
56	White Blood Cell Count	4300 - 10800 cells/µL/cu mm
57	Zinc B-Zn	70 - 102 µmol/L

1.6 History of Blood Glucose Monitoring

Diabetes has been known since ancient times, as the level of blood glucose rises above the normal range, kidneys pass the glucose into urine. In ancient times the Chinese used to test for the disease by checking if ants were attracted to sugar in a patient's urine. Prior to modern chemical techniques, tasting of a urine sample was even considered a valid test. Chemical testing of urine for diabetes has been done over a century. In 1908, Stanley Benedict made the pioneering development of improved copper reagent for estimating glucose in urine. This method was used for over 50 years to estimate glucose in urine [13].

In 1941, the Ames Division of Miles Laboratories (the division name reportedly came from that of the president, a physician named Walter Ames Compton), in Elkhart, Indiana, introduced a tablet based on a standard test for certain sugars involving copper sulphate, called Benedict's solution. One of these "Clinitest" tablets could be added to a few drops of urine and noting the colour change from bright blue to orange, was compared to a series of printed colours on the instruction sheet and the approximate level of glucose in the urine was estimated.Urine testing for glucose, however has very serious problems. When a person first develops diabetes, the level of glucose in urine is a reasonable indication of excessive amounts in the blood; however, because both normal and low blood glucose levels results in no glucose in urine, it is never possible to assess low blood levels using urine tests. As the disease progresses over a period of time, it becomes much less reliable as a marker of high blood glucose. Even otherwise, it's never an accurate measurement, and even though improved testing devices ("dipsticks") have been developed over the years, it's never been more than a "semi-quantitative" test.

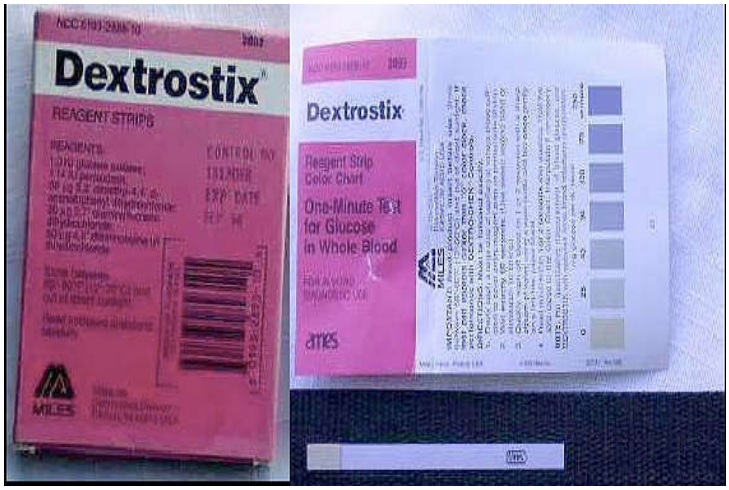

Figure 1.2: Dextrostix

Dextrostix, the first blood glucose strip was developed by Ames in 1965. The color developed on the strip after placing a blood drop for 60 seconds was compared to a color chart printed on the bottle for a semi quantitative assessment of blood glucose levels [14]. Dextrostix used a biochemical reaction, with an enzyme called Glucose Oxidase (GOx), which reacts with glucose to produce hydrogen peroxide. The hydrogen peroxide produced a colour from another chemical called o-tolidine and the amount of colour on the strip after exposing it to a drop of blood was a good measure of the amount of glucose present

Figure 1.3: Ames Reflectance Meter

The Ames reflectance meter was developed in 1970 by Anton H. Clemens. It had a needle that indicated the intensity of blue light reflected from Dextrostix. Unfortunately it had some reliability problems, mostly from its rechargeable lead acid batteries, and its use did not become widespread. The next electronic strip reader appeared in about 1972, called the Eyetone, and was manufactured by a Japanese company, Kyoto Dai-ichi (which later changed the company name to Ark-Ray). It also read Dextrostix, but used a plug-in AC adapter for power instead of batteries. In about 1979, Kyoto Dai-ichi introduced an improved Dextrostix meter with a digital readout, called the Dextrometer.

The meters and the associated strips developed during the 1980s required less blood and were became much more affordable. Subsequently self-monitoring of blood glucose (SMBG) devices became the standard of care. Boehringer Mannheim, which had developed a parallel blood glucose test strip for visual colour comparison called the Chemstrip bG, kept pace by introducing a meter to read the strips, the Accu-Chek bG in about 1982. The Chemstrip bG was preferred by many over Dextrostix because the blood could be wiped off the strip (with a cotton ball) after a minute's contact instead of washing off with water. Later versions of the meters were called Accu-Chek in the U.S. and "Reflolux in the rest of the world. LifeScan entered the market in about 1981, with a meter (first called Glucocheck, then GlucoScan) developed in England by Medistron and test strips developed in Japan by the Eiken corporation—the first product in which the meter was not preceded by a strip intended for visual comparison. Some of the early GlucoScan meters had their own reliability problems, but they sustained the company until it was purchased by Johnson & Johnson in 1986. Exactech a photometric based meter, with a strip developed in England, manufactured by MediSense and marketed originally in the U.S. by Baxter. Exactech came in the form of either a slim pen or a credit card sized, thin plastic package. Early versions of the device had both accuracy and reliability problems, which hampered its early market acceptance.

Cygnus developed the first real time glucose monitoring device called Glucowatch Biographer. It used reverse iontophoresis to stimulate the secretion of subcutaneous fluid, which was in turn was used to estimate glucose. It did not do well on the market as there were issues related to site irritation. Medtronic introduced a real time Continuous Glucose Monitoring (CGM) device named Guardian in 2004. This device had the capacity to notify its users of potentially dangerous eventualities such as

hyperglycemia and hypoglycemia. The same company launched an integrated insulin pump and sensor in 2006.

Figure 1.4: the Glucowatch Biographer (Cygnus, Redwood, CA)

FreeStyle Navigator CGM was available commercially in 2008 from Abbott which measures glucose concentration in interstitial fluid. All of the above CGMs require one to perform calibration with more reliable glucose meters, usually done by self monitoring blood glucose device. Dexcom in 2012 launched the G4 Platinum, and soon followed by G5 Mobile. The G5 Mobile is a CGM which allows the transmission of data to ones cell phone. In 2013 Medtronic became the first company to introduce the first insulin pump with a "threshold suspend" in case of hypoglycemia by the introduction of MiniMed 530G Enlite sensor.

FreeStyle Libre Pro introduced by Abbott in 2016 is a CGM which requires no fingerstick calibration during wear as they are factory calibrated .The CGM works with a special sensor that can be worn for 14 days. The entire system is made up of two units the "sensor" and the "reader", the sensor communicates with the reader using a wireless interface.

1.7 Economic impact of diabetes

Diabetes is one of the biggest health challenges of the 21st century. Diabetes and its complications have a significant economic impact on individuals, families, health systems and countries. Diabetes is one of the costliest health problems in the world. The

direct cost includes the expenditures incurred due to diabetes, irrespective of whether it is borne by the individual or by public/private players or by government. Since 2006, the International Diabetes Federation (IDF) has been publishing the estimates of health expenditure due to diabetes in "Diabetes Atlas". The expenditure was 232 billion dollars in 2007, 727 billion dollars in 2017, and rose to 760 billion dollars in 2019 for adults in the age group of 20-70 years [15–20]. There is a substantial growth of 4.5% form 2017. It is estimated that by 2030 the expenditure will reach 825 billion dollars [1].

According to IDF, United States of America has the highest diabetes related expenditure of 294.6 billion dollars, followed by China with 109.0 billion dollars and Brazil with 52.3 billion dollars. One study estimates that losses in Gross Domestic Product (GDP) worldwide from 2011 to 2030, including both the direct and indirect costs of diabetes, will amount to 1.7 trillion dollars, comprising 900 billion dollars for high-income countries and 800 billion dollars for low and middle income countries [21].

There are also indirect expenditures to be taken into account such as lost productivity due to the inability to work, sickness, absence, disability, premature retirement or premature death. Bommer et al. calculates the indirect expenditures of diabetes to constitute 34.7% of the entire global expenditures of diabetes of 1.31 trillion dollars in 2015 [22]. The indirect expenditure taken into account by Bommer et al. are presenteeism, absenteeism, mortality and labor-force drop out.

Above paragraphs, give a clear picture of the economic impact of diabetes hence a need is felt more than ever before for the development of an inexpensive, and reliable non invasive method for estimating glucose.

1.8 Objective of research work

A tight control of blood glucose is imperative for a person diagnosed by diabetes. The methods used for this not only needs to be accurate but also must have minimum waiting time. Current pathological test involves sending the sample to a laboratory hence has an inherent long waiting time. All methods, which involve withdrawal of blood by either a syringe or a lancing device, have the perilous possibility of infection, not to mention the recurring cost for each measurement. Self-monitoring blood glucose meters and the above mentioned pathological test fall under this category. The frequent pricking of fingers for blood glucose monitoring has generated an apprehension of pain

involved in this method. Near Infrared spectroscopy has proven to be an option which circumvents all the above disadvantages and issues. The current trend is to utilize the advances in embedded and optical technology to harness the capabilities to perform a fast and reliable estimation of blood glucose levels. Our aim here to develop a novel FPGA based design using fixed wavelengths near-infrared light sources to probe. The criteria for choosing the wavelengths was set as the peaks and valleys which glucose present in the combination band of near-infrared region. After probing, the absorbance analysis requires the use of multivariate algorithm as the glucose signals are concealed in overlapping signatures of other constituent in the aqueous ensemble which is made up of five major blood constituents namely glucose, ascorbate, analine, lactate and urea. Thus the objective of research work can be categorized as follows.

1. Design a soft-core FPGA based hardware to estimate the glucose level in human blood.
2. Use fixed wavelength NIR light sources to probe.
3. Implement multivariate algorithm for estimation of glucose.

Previous attempts to use NIR technique involved using a while light source with a broad emission spectrum and utilized a monochromator. By using fixed wavelength, we can bypass the use of white light source, in turn relaxing the power consumption, computing and memory requirements. In the future, these wavelengths can be replaced by Laser diodes and Light emitting diodes which guarantee us an increase of signal to noise ratio.

References

[1] "IDF Diabetes Atlas, Ninth edition 2019", International Diabetes Federation, [Online] Available at: https://www.diabetesatlas.org/upload/resources/material/20200302_133351_IDFATLAS9e-final-web.pdf

[2] D.M. Maahs, N.A. West, J.M. Lawrence, E.J. Mayer-Davis, "Epidemiology of type 1 diabetes", Endocrinol Metab Clin North Am., Vol.39(3), 2010, pp. 481–497.

[3] M.A. Atkinson, G.S. Eisenbarth, A.W. Michels, "Type 1 diabetes", The Lancet, Vol. 383 (9911), 2014, pp. 69–82.

[4] "Diagnostic criteria and classification of hyperglycaemia first detected in pregnancy: a World Health Organization Guideline", Diabetes Res Clin Pract., Vol. 103, 2014, pp. 341–363.

[5] M. Hod, A. Kapur , D.A. Sacks, E. Hadar, et al., "The International Federation of Gynecology and Obstetrics (FIGO) Initiative on gestational diabetes mellitus: A pragmatic guide for diagnosis, management, and care", Int. J. Gynaecol Obstet., Vol. 131, 2015, pp. S173-S211.

[6] J. Immanuel, D. Simmons, “Screening and treatment for earlyonset gestational diabetes mellitus: a systematic review and meta-analysis”, Curr. Diab. Rep., Vol. 17, 2017, p. 115.

[7] L. Guariguata, U. Linnenkamp, J. Beagley, D.R. Whiting, et al., “Global estimates of the prevalence of hyperglycaemia in pregnancy”, Diabetes Res. Clin. Pract., Vol.103, 2014, pp. 176–185.

[8] E. Renard, “Monitoring glycemic control: the importance of self-monitoring of blood glucose”, Am J Med, Vol. 118, 2005, pp. 12S-19S.

[9] S. Delbeck, T. Vahlsing, S. Leonhardt, et al., “ Non-invasive monitoring of blood glucose using optical methods for skin spectroscopy—opportunities and recent advances”, Anal. Bioanal Chem.Vol. 411, 2019, pp. 63–77.

[10] L. Dean, J. McEntyre, “The Genetic Landscape of Diabetes”, National Center for Biotechnology Information (US), 2004.

[11] L. Stryer, “Biochemistry”, W.H. Freeman and Company, 1995.

[12] “An Overview of Blood”, [Online] Available at: www.pentextbc.ca/anatomyand physiology/chapter/an-overview-of-blood/

[13] S.F. Clarke, J.R. Foster, “A history of blood glucose meters and their role in self-monitoring of diabetes mellitus”, Br. J. Biomed. Sci., Vol. 69 (2), 2012, pp. 83–93

[14] “History of Glucose Monitoring”, [Online] Available at: www.professional.diabetes.org/sites/professional. diabetes.org/files/media/db201811.pdf

[15] “IDF Diabetes Atlas, Third edition”, International Diabetes Federation, 2006.

[16] “IDF Diabetes Atlas, Fourth edition”, International Diabetes Federation, 2009.

[17] “IDF Diabetes Atlas, Fifth edition”, International Diabetes Federation, 2011.

[18] “IDF Diabetes Atlas, Sixth edition”, International Diabetes Federation, 2013.

[19] “IDF Diabetes Atlas, Seventh edition”, International Diabetes Federation, 2015.

[20] “IDF Diabetes Atlas, Eight edition”, International Diabetes Federation, 2017.

[21] D.E. Bloom, E.T. Cafero, E. Jané-Llopis, S. Abrahams-Gessel, et al., “The global economic burden of non-communicable diseases (Working Paper Series)”, Geneva: Harvard School of Public Health and World Economic Forum, 2011.

[22] C. Bommer, E. Heesemann, V. Sagalova, J. Manne-Goehler, R. Atun, T. Bärnighausen, et al., “The global economic burden of diabetes in adults aged 20-79 years: a cost-of-illness study”, Lancet Diabetes Endocrinol, Vol. 5(6), 2017, pp. 423–430.

Diabetes is the underlying reason for many health complications such as stroke, cardiovascular diseases, kidney failure, blindness etc. Hence it becomes crucial to monitor the blood glucose levels in the prescribed range. Many different methods are used to monitor glucose, these methods can be broadly classified into invasive, minimally invasive and non-invasive. In this chapter we discuss the different methods used in detail.

2.1 Invasive Methods

Whole blood, plasma, or serum samples are used to estimate the glucose concentration, but the whole blood is seldom used as the readings are 15% lower due to additional water content in blood cells. In these methods there is a need of withdrawing blood, hence theses methods are known as invasive.

The laboratories exploited the reducing and condensation properties of glucose, but the issues of toxicity, non-specificity and cross-reaction saw these methods being phased out from the clinical practices. Currently the pathological laboratories rely on enzymatic and hexokinase methods. Both the above methods are highly glucose specific, accurate, and offer minimum cross-reaction. Many market players have come out with home monitoring devices, which employ finger pricking to withdraw blood in conjunction with a glucose strip to estimate glucose concentration.

2.1.1 Laboratory Methods

All of the standard laboratory methods rely on withdrawing certain amount of blood and hence are invasive in nature. Most laboratories prefer the Enzymatic-amperometric and hexokinase method. The above methods offer wide range of operation including hypoglycemic and hyperglycemic ranges as well as excellent specificity and sensitivity [1]. As such, these methods are often used as standard of reference for other less accurate glucose measuring devices.

In the first method, an enzyme glucose oxidase (GOx) which is specific to glucose is used. Glucose, oxygen, water react in the presence of glucose oxidase to form hydrogen peroxide and gluconic acid. At the anode of an electrochemical probe, the hydrogen peroxide produced then get oxidized, which in turn produces a current (amperometric signal) which is proportional to the glucose concentration [2].

Hexokinase method involves the presence of the enzyme hexokinase. There are a sequence of chemical reactions which are carried out. In the first phase, the glucose reacts with adenosine triphosphate along with biocatalyst hexokinase and magnesium ions to form adenosine diphosphate and glucose-6-phosphate. During the next phase, glucose-6-phosphate dehygrogenase catalyzes the oxidization of nicotinamide adenine dinucletide and glucose-6-phosphate to form nicotinamide-adenine-dinucleotide-reduced and 6-phosphogluconate respectively. Nicotinamide-adenine-dinucleotide-reduced (NADH) has a special property of absorbing light at 340nm and the amount produced is proportional to glucose present. Standard spectrophotometeric techniques are used to record the absorption of NADH and therefore this method is also called as photometric method [3,4].

2.1.2 Home Monitoring Methods

All of the current monitoring devices used at home use finger pricking with a lancet in order to access the capillary blood. These portable devices are sometimes knows as self-monitoring blood glucose (SMBG) devices. Based on the type of diabetes, medication and diet these devices are used to monitor glucose at specific times of the day at the patients home itself. These devices use a glucose test strip which collects the blood drop on it. These strips contain an enzyme and electrodes. The glucose in the blood oxidizes in the presence of an enzyme present on the strip. This produces a current proportional to the glucose concentration which is conditioned by a signal conditioning circuit before being readout on display of the device [5-8].

2.2 Minimally-Invasive Methods

Minimally invasive methods use some fluid such as tears, sweat or interstitial fluid extracted from the body, but do not require withdrawal of blood from the body. The procedure of extraction of body fluid causes minimal irritation to the skin. This body fluid is then used for measurement of glucose concentration by enzymatic reaction. The glucose from capillary blood and the glucose in interstitial fluid are not quite the same as there is a certain delay involved for glucose from capillary blood to reach the interstitial fluid.

2.2.1 Reverse Iontophoresis

In reverse iontophoresis, electrodes are located on the skin and a small electric current is allowed to flow between the electrodes. A minute quantity of interstitial fluid is obtained by means of this small electric current, hence this becomes a minimally invasive method. The current which is primarily produced by sodium ions also causes an electro-osmotic-flow of the interstitial fluid, also carrying along with it small amount glucose towards the cathode [9]. This glucose can be quantified using the standard enzymatic method such as oxidation by enzyme such as glucoses oxidase.

2.2.2 Sonophoresis

A low frequency pressure wave is used to drive glucose molecules out of the skin. The direction of propagation of the any sound wave is the same as the direction of oscillation [10].This process improves the skin permeability and is known as cavitation. This process employs a successive compression and expansions of substantial magnitude to extract gas out of tissue, which also carries with it other permeants such as glucose [11]. This glucose can then be measured using enzymatic method.

2.2.3 Microporation

Methods to perforate the stratum corneum, without penetrating the entire skin, attempt to punch micro-pathways through the outermost part of the barrier. For example a transdermal glucose sensing system developed by SpectRx uses a pulsed laser beam to create micropores of less than 100 μm in diameter by thermal ablation of the stratum corneum [12,13]. Transdermal fluid is then collected, by applying a vacuum, into a disposable collection device. Glucose is subsequently quantified electrochemically.

2.3 Non-Invasive Methods

There are several kinds of interactions between electromagnetic radiation and biological tissues depending on the properties of target tissues and the characteristics of illuminating sources. The interactions can be mainly categorized into absorption, transmission, emission, reflection, scattering and optical rotation. Non-invasive technologies rely solely on some form of radiation and its interaction with glucose without the need of accessing any body fluid.

2.3.1 Mid-Infrared Spectroscopy

Mid-Infrared spectroscopy is a vibrational spectroscopy technique which uses radiation in the range of 2.5 μm ton 10μm however some claim to use radiation up to 25μm [14,15]. The MIR radiation scatters less in tissue due to longer wavelength, which in turn leads to sharp absorption lines in the spectrum in between 8-10 μm [16-17]. Many functional groups have a unique spectrum in this region which serves a vital role in molecular identification. Hence, this region is often called as finger print region. Unfortunately, water also strongly absorbs in the region, which makes it impractical the use of MIR in tissue probing as the penetration depth is only a few micrometers in the tissue [18]. To circumvent this problem we require sources with high optical power such as quantum cascade laser [19] and the use of complementary technologies in conjunction with it such as photoacoustic spectroscopy for successful glucose estimation [20].

2.3.2 Raman Spectroscopy

In Raman spectroscopy we try to determine the scattering of single wavelength light based on Raman Effect. When a monochromatic light hits a target, this light is scattered in all directions. The major portion of this scattered light retains the same wavelength, and is called as Rayleigh scattering. As the wavelength is not changed this portion of scattered light is also called as elastic scattering. The rest of the scattered light which is just a small amount, has a different wavelength as the incident light is called as Raman scattering or ineleastic scattering. The change between final and initial vibrational state of the molecule is given by the wavelength difference and is called as Raman shift [21]. The peak positions in the Raman spectrum represent the vibrational modes of the functional groups present in the molecule; as such Raman spectroscopy forms a great aid in quantifying and detecting specific absorption bands in the sample molecule [22]. It is found that the Raman shift is same no matter which wavelength of the incoming light is used. The prominent vibrations mode of glucose are those of C-O and C-C stretching bands between 12500 nm (800 cm^{-1}) and 7692 nm (1300 cm^{-1}) and C-H stretching at around 3448 nm (2900 cm^{-1}) [23-24]. Another advantage of using Raman spectroscopy is that light travels relatively deep into the skin tissue however, Raman spectra of living tissue are complicated by background fluorescence.

2.3.3 Optical Polarimetry

Optical polarimetry is a field evolved around chiral molecules. Chiral molecules are molecules which are capable of rotating the plane of plane polarized light. Glucose, being a chiral molecule rotates the plane of plane polarized light. The angle of rotation is proportional to the glucose concentration. The wavelength of the laser beam is usually chosen between approximately 400-780 nm. The presence of other active molecules, small optical rotation due to the physiological relevant glucose concentration light, scattering in the skin tissue make optical polarimetry unfeasible for use on skin [25]. However the aqueous humor inside anterior chamber of the human eye, serves as a viable region as it possess excellent optical properties [25-26]. Before application, the light is polarized, and then allowed to pass through the aqueous humor. The emerging light is than analyzed for the amount of rotation. This technique can detect minute amounts of glucose if we can positively address the issues such as temperature sensitivity and motion artifacts.

2.3.4 Photoacoustic spectroscopy

Developed by Alexander Graham Bell in the 19^{th} century this technology has evolved to use advancements in the field of optoelectronics such as pulsed laser. The wavelength of the laser is chosen such that it is strongly absorbed by the target molecule. This absorption of laser light by the target molecule creates microscopic localized heating. The specific heat capacity of the human tissue being probed decides the amount of the localized heat generated [22]. The localized heating generates a volumetric expansion of the surrounding medium, generating a sound wave. This sound wave can be detected using an acoustic sensor. The peak to peak amplitude of the detected acoustic signal is dependent on the glucose concentration in tissue. Both continuous wave and pulsed light sources are used for non invasive glucose estimation. The use of pulsed mode involves the application of pulses with duration in the range of nanosecond, which makes to sample undergo an adiabatic thermal expansion at a fast rate. The resultant acoustic spectrum has a wide range of acoustic frequencies [27-28]. The continuous wave method involves application of a modulated continuous optical laser beam, which generates a one acoustic frequency in the detected spectrum. Lock-in detection is employed to achieve a higher signal-to-noise ratio [29].

2.3.5 Bioimpedance Spectroscopy

This technique measures the impedance levels of tissues using a minute alternating current signal less that 1MHz frequency. Researchers have modeled biological tissue as electric circuit of capacitors and resistors however, more realistic tissue electrical models have been proposed [30-32]. The Red blood cell membranes has an important role in the determining total tissue impedance as they make up the major portion of the human blood [33]. The electric characteristics of the cell membranes influence the tissue impedances. The serum osmolality increases if amount of glucose in blood increases. As a result of this, water from inside of the cell moves out via the cell membrane. Due to dilution, the levels of sodium ions plummet. Also there is a redistribution of potassium ions from the intracellular spaces to extracellular spaces due to cellular dehydration [33-35].The permittivity and conductivity of surrounding medium and cell membranes such as RBCs changes as the [Na+] and [k+] ions are balanced. These activities result in changes to the tissue impedance which can be correlated to the blood glucose concentration [36].

2.3.5 Optical Coherence Tomography

Optical Coherence Tomography (OCT) has emerged as a high resolution imaging technique in the past decades. It is a form of non destructive testing which uses a low coherence NIR light source. The coherence length of the light source is usually between 10 to 15 μm. The interference signal formed by the light coming from reference mirror and tissue sample is used for analysis. This is achieved by using interferometer optics and a photodetector. In the interferometer setup the beam from the source is split up into two beams, one is allowed to hit the target tissue and then backscattered. The second beam reflects from a reference mirror and then reaches the beam splitter [37-39]. At the beam splitter the light reaching from the reference mirror and sample interfere to form interference pattern. The interference pattern is recorded by the photodetector. The intensity of the interference pattern is dependent on the glucose concentration at varying tissue depths, and can be recorded up to a depth of 1.6 mm [40]. A scanning mirror in the reference arm is used to measure the optical coherence tomography signal at a specific depth of a tissue layer. Another moving mirror included in the tissue sample arm provides lateral movement over the tissue surface, such that a two-dimensional

image can be obtained [39,41,42]. The OCT has the potential to resolve microstructure with a high signal to noise ratio of the order of 130 dB [43].

2.3.5 Near Infrared spectroscopy

Near-Infrared **(**NIR) spectroscopy was accepted as a technique in early 1960s with the work of Karl Norris of United States in the field of agriculture [44]. After that, NIR spectroscopy expanded in many fields such as food processing, pharmaceuticals, process control, remote imaging and many others applications [45]. Tremendous research is conducted by many universities and industries to use this approach in non-invasive glucose sensing for diabetes [46-51].In our research work we have used near infrared spectroscopy which spans the wavelength range of 700-2500nm of the electromagnetic radiation. Studies have shown that Combination region (2000 – 2500 nm) of NIR region has shown better analytical utility as compared to overtone region for glucose estimation [52]. Best site in the human body for glucose detection with NIR spectroscopy is oral and lip mucosa, forearm skin, cheeks, earlobe, tongue and nasal septum [53].

M.A. Arnold et al. determined glucose concentration in an aqueous matrix having physiological ranges [54]. The absorbance at 2273 nm was linked to concentration using a univariate calibration model and found an error of prediction of 0.3 mM. Other research groups have investigated the NIR region for robust glucose estimation using human serum and whole blood in the presence of other interferences, such as glycated and total protein concentration [50,55]. Others studies have studied the result of temperature variation on glucose determination. This effect introduced by temperature can be reduced by using pre-processing of the spectra using digital Fourier filter [56,57]. Measurements in aqueous solution of glucose, glutamine, glutamate, lactate and ammonia were done and calibration models were built for simultaneous measurements of each solute in the near infrared region [58]. For glucose prediction the standard error of prediction and mean percent errors of prediction was 0.54 and 6.98 percent respectively.

Even more complex matrix such as human serum was investigated for feasibility in estimation of glucose. A total of 242 undiluted human serum samples were used, which were further divided randomly into 3 sets named as training, monitoring and test sets. The training, monitoring and test sets had 162, 40 and 40 samples respectively [59]. The

calibration process resulted in a model which gave a standard error of prediction for glucose of 23.3 mg/dl (1.29 mM). In addition, to test the stability of the calibration process, another 50 human serum samples were collected on a modifier spectrometer nineteen months later, which were used as a blind test set which resulted in a Standard Error of Prediction (SEP) of 2.91 mM.

In one study, Independent Component Regression (ICR) was investigated for estimation of glucose. They recorded NIR spectra for 30 mixtures containing triacetin, urea and glucose in a phosphate buffer solution. The training model was constructed using spectra of the 20 mixtures and the spectra of the remaining 10 mixtures were used for testing the prediction. The optimum models for PCA-ICR, ICR, PCR and PLS gave lowest SEP 24.1, 29.1, 39.56 and 35.59 respectively [60].

Scattering in human tissue can cause deviation (non-linear) from the linear relation between the absorbance and analyte concentration given by Beer-Lamberts Law. Xue et al. compared a Partial Least Squares (PLS) which is a linear regression method with Artificial Neural Network(ANN) which is a non-linear regression for glucose estimation [61]. They collected in vivo NIR spectra from normal and diabetic rats. Compared to the ANN model, the performance of the PLS model was much better, with lower root mean square error of validation of 0.419 and higher correlation coefficients (R) of 96.22%. In another study, the collection of NIR diffuse reflectance spectra (850-1300nm) on the fingers of type-1 diabetics was carried out [62]. Using partial least squares and Radial Basis Function (RBF) networks for calibration on these NIR diffuse reflectance spectra a Root Mean Square Error of Prediction (RMSEP) of 1.4 mM and 1.9 mM was obtained respectively.

The optical techniques discussed in this chapter are very popular to monitor glucose non-invasively. A tabulated literate review of the optical techniques is presented in the table 2.1.

Table 2.1: Optical techniques used for non-invasive glucose monitoring

Sr. No.	Working Principle	Salient Features	Critical remarks	Results	Ref
1	Raman spectroscopy	In vivo application of Raman spectroscopy to non- invasively quantify glucose.	The Raman spectra collected from the forearms were dominated by collagen and triglyceride.	461 Raman spectra were collected of 17 volunteers. PLS calibration was done for each subject. The R^2 of 0.83 ± 0.10 was obtained	63

				with a mean absolute error of 0.8% ± 1.8% for each subject.	
2	Raman spectroscopy	Employed Raman spectroscopy for in vivo blood glucose quantification on mice.	In the experiment no Raman signal was found at concentration below 50mmol/dl in a glucose solution.	Three mice were subjected to elevated blood glucose levels using a glucose test assay, 25 Raman spectra were recorded and a relationship was found between Raman intensity and concentration which showed a correlation coefficient of 0.91.	64
3	Raman spectroscopy	In vivo, miniature wearable fiber optic probe is designed to work with a portable Raman spectrometer.	The limit of detection of glucose by the wearable fiber optic probe based Raman system is not reported in the research work.	Wearable fiber optic probe used in conjunction with non linear partial least squares to predict glucose. This method produced coefficients of determination of 0.99, 0.893 and 0.844 for glucose solution, laboratory rats and human volunteers respectively.	65
4	Raman spectroscopy	Non-invasive glucose sensing implemented using a confocal Raman spectrophotometer	This study employs only subjects having diabetes and does not include normal healthy individuals.	It is successfully shown that the confocal Raman spectrometer can reach dept of 250 μm below skin of the thumb. The prediction resulted in 93% of measured data points in the A and B region of consensus error grid analysis.	66
5	Raman spectroscopy	Non invasive measurement was done using Raman spectroscopy of blood in the micro vessels in the nail fold of finger	In the spectra of 12 volunteers no Raman peaks were isolated which depicted a regular change with corresponding change in blood glucose in the physiological concentrations range, this is attributed due to the small Raman cross section of glucose	Raman spectroscopy is used in conjunction with an algorithm which combines PCA and BP-ANN. RMSEP of 0.27 mmol/L and R^2 of 0.98 was obtained for the total prediction performance of all volunteers.	67
6	Raman spectroscopy	Assessment of precision of calibration models based on the ratio of validation and calibration points.	Study conducted only on non diabetic patient.	17 time points of OGTT of 20 patients were used to build PLSR calibration models using 50, 30 and 18% spectra of the individuals. In each of these respective cases 71.05, 70.23 and 60.65% points were found to lie in A region of Clarke error grid	68

7	Raman spectroscopy	Used confocal Raman microscope to acquiring the Raman spectra of the anterior chamber model.	The energy density that is safe for the eye at the wavelength used is not empirically determined	The optimum standard error of prediction (SEP) obtained for glucose was 34.3 mg/dl (2.72% of full range) using a 12-factor PLS model.	69
8	NIR spectroscopy	Used an aqueous matrix with glucose in it in order to determine the physiological glucose levels in conjunction with digitally filtered Fourier transform	Not determined whether the univariate methods used provides sufficient selectivity for clinically relevant application or there is a need for multivariate analysis	The predictions resulted in a maximum error of 0.3 mM with the mean percent error of 2.5%.	54
9	NIR spectroscopy	Temperature insensitive calibration models are built using PLSR and digital Fourier filtering.	When strongly absorbing interference are present with varying concentrations, the adequacy of digital filtering is not determined.	The most optimum model provided a mean standard error for prediction across temperatures of 0.14 mM (2.52 mg/dL).	70
10	NIR spectroscopy	Calibration models are generated using PLSR to predict glucose in two separate spectral datasets with varying triacetine and bovine serum albumin	Although digital Fourier filtering reduced high frequency noise and baseline variation, but is not capable of selecting information of one analyte over another when spectral bandwidths are similar.	The triacetin and bovine-serum albumin matrices gave a SEP of 0.5 mM and 0.2 mM respectively	71
11	NIR spectroscopy	Comparisons were done between the first overtone and combination band to build calibration models when a aqueous solution of alanine, triacetin ,ascorbate, lactate, urea and glucose is used.	Urea in overtone spectral region showed a high SEP of 7.33 mM	Results show the superior nature of combination band to overtone to form calibration models. SEP values showed approximately 3 fold lower values for combination as compared to overtone band	72
12	NIR spectroscopy	Attempted to find the effect of temperature change on PLS analysis in the spectral range of 1250 to 1800 nm.	The procedure used concentration in the range of 1-3 g/dL which is not clinically relevant glucose concentrations.	The result of prediction produced an error in glucose concentration of 4.4%	73
13	NIR spectroscopy	In-vivo measurements of first overtone spectra of tongue of human subjects with type 1 diabetes were done using PLSR	The presence of tissue fat introduced significant variability	A SEP of 3.4 mM was found for the optimum calibration model.	74
14	NIR spectroscopy	Human serum samples are used to build PLSR calibration models to measure the albumin protein, globulin protein, triglycerides, cholesterol, urea,	Simultaneous lactate prediction was not accurate as it was below the detection limit in the experimental setup	SEP for glucose was reported to be 23.3 mg/dl (1.29 mM)	48

		glucose, and lactate.			
15	NIR spectroscopy	Performance of RBFNN with PLSR using diffused reflectance spectra recorded from the fingers of type 1 diabetic patient. LOOCV was used to determine the number of hidden neurons.	The tuning of the non linear technique is a complex task even though it provides a considerable improvement in prediction	RBFNN was found to perform better as compared to PLSR with RMSEP values of 1.4 mM and 1.9 mM respectively.	62
16	NIR spectroscopy	Tunable diode laser system developed to non- invasively determine glucose concentration. A diode systems gives high SNR values in the region where glucose has significant absorption signatures	The tuning range of the diode laser system does not encompass all the three absorption peaks of glucose in the spectral region of 2000-2500nm.	The paper reports the development of a diode laser system for in vivo measurement of glucose which has a tunability range from 2210–2330 nm with high brightness of 0.5mW	75
17	NIR spectroscopy	Non invasive glucose measurement using a 2300nm Vertical-Cavity Semiconductor Laser (VCSL) which is thermally tuned.	The VCSEL provides only a small spectral window of 5-6 nm around the center wavelength of 2300nm, and does not encompass all the absorption peaks of glucose.	A PLS calibration process was used to determine the glucose concentration in aqueous solution in the range of (50–300 mg/dL).	76
18	NIR spectroscopy	Novel method of building calibration model by using NIR diffuse reflectance spectra which were obtained by numerical simulation of light propagation in skin tissue. Later this calibration model was used to predict glucose by a vivo experiment.	The robustness of the calibration was not tested on multiple subject as only one subject was used in the in vivo experiment	The calibration model validated using a in vivo experiment produced a SEP of 12.3 mg/dL and a coefficient of determination (R^2) of 0.87.	77
19	Photoacoustic spectroscopy	MIR fiber coupled photoacoustic sensor employing a QCL laser	The fiber coupled sensor monitored glucose in aqueous solution in the concentration range of 0 to 5 g/dL and produced a detection limit of 140mg/dL which is not conducive for clinical relevant range of glucose.	The performance of the fiber coupled sensor is demonstrated by sensing glucose in aqueous solutions.	78
20	Photoacoustic spectroscopy	Novel “guide star” assisted photo acoustic (GSPA) system which employs a virtual photodiode to amplify the photoacoustic signal	As a result of stronger absorption and scattering in biological tissue the laser power, optical path length and sensitivity needs to be	Human blood serum in 2mm path length gave a R2 of 0.9791 and RMSE of 17.3 mg/dL.	79

		difference. Tested on aqueous glucose and Human blood serum matrices.	calibrated in order to apply for clinical setup.		
21	Photoacoustic spectroscopy	Novel method to non- invasively determine glucose using photoacoustic sensor by using fusion of both peak arrival time and peak to peak variation	For in vivo application, the interference due to temperature and movement needs to be accounted.	The accuracy found were 29.5% for the glucose concentration range of 0–7 g/dL and 33.63% for concentration range of 0–350 mg/dL	80
22	Photoacoustic spectroscopy	Deployed an external cavity QCL with a tuning range of 9132 - 9900nm (1010-1095 cm^{-1}) and photoacoustic sensor to monitor epidermal skin sample in contact with glucose solution	The glucose detection limit was found to be 100mg/dL which is not appropriate for clinical deployment.	Detection of glucose resulted with R^2 value of 0.998	81
23	MIR spectroscopy	Employed Fourier transform IR spectroscopy with a ATR prism to implement glucose detection on oral mucosa	It was found that the glucose specific peaks varied with the pressure variation of ATR prism setup to mucous membrane. Also the oral measurement may be affected by saliva and other residual food materials	Good correlation (r = 0.91) was found for the calibration curves constructed.	82
24	MIR spectroscopy	Used Integration sphere in conjunction with a quantum cascade laser to implement a non-invasive glucose sensor on human subjects	Hypoglycemia range not included in the study of the three subjects	It is observed that for all the subject 78% predictions fell in the zone A of the Clarke error grid. The constructed models for subjects 1 and subject 2 gave an accuracy of 91% whereas the 86% accuracy was observed for subject 3.	83
25	MIR spectroscopy	ATR spectroscopy employed along with hollow optical fibers to enhance sensitivity for a in-vivo measurement on human inner lip mucosa	Faced with fluctuation in the pressure applied by the lips and this contact pressure causes variation in the measured depth	Applied least square fitting and obtained calibration plots measurements errors of <20%	84
26	MIR spectroscopy	In vivo non- invasive glucose monitoring using few wavelengths with an ATR prism. Three wavelengths were determined using series cross validation method and regression realized accuracies comparable to those with greater number of wavelengths	A delay of 20min was found to exist between the actual and observed readings.	When MLR is used with three wavelengths it results with the correlation coefficient of 0.36, and all the samples lie in the A and B region of Clarke error grid, whereas for PLS with higher number of wavelengths give a correlation coefficient of 0.25, and 98.8% of the samples are in the area A	85

				and B.	
27	Polarimetry	In vivo polarimetric monitoring of glucose in the physiological range inside the anterior chamber of the eye of the New Zealand rabbit.	The movement of the rabbits during procedure cause corneal birefregence. It is also found There is a lag time is present between glucose reading in the anterior chamber and blood plasma of 2.9-5.4 seconds	A dataset of 41 points on the Clarke error grid gave a result of 93% in the zone A, 7% in zone B and none in the C and D.	86
28	Polarimetry	A setup is constructed to measure the corneal birefringence by spectrally resolved Mueller matrix ellipsometry on porcine corneas. The research discussed the implication for non invasive glucose monitoring.	A mathematical model was used to determine the amount of delay or lag in the estimated glucose measurement and was found to be 4 – 7 minutes	In vitro 16 element Mueller matrices were obtained in the optical range of 300-1000 nm.	87
29	OCT	In vivo and in vitro OCT used to find the glucose induced changes in the optical properties of different tissues.	Motion artifacts, temperatures, humidity and CO_2 impacted the results.	The study shows that the OCT backscattered signals is stronger in the skin tissue for the in vivo setup as compared to the in vitro setup. A prominent effect of glucose is found in the in vivo condition with the least effect in 2% intralipid	88
30	OCT	OCT was used to determine the specificity of blood glucose for non invasive monitoring.OCT signals were isolated from skin of New Zealand rabbits and Yucatan micro pigs for the study.	Time lag is observed in the change in OCT signal slope and the actual blood glucose change.	It was found that a change in glucose concentration in the interstitial fluid within the physiological range (3-30mM) gave a reduction in scattering coefficient by 0.22% mM^{-1}. The OCT signal slope was found to be resilient to temperature change of ±1 ◦C	41

2.4 Non Invasive Glucometer, Need of the hour!!!

As self monitoring blood glucose monitoring became a more common place from the early1980s through the early 21st century, it still has encountered hindrance to its acceptance. It was largely due to the reason that, no matter how fast the test or how small the blood drop was, blood withdrawal is a must by a sharp lancing device from a body part. For all but a few, this causes pain, fear, apprehension, revulsion and many people just take the easy way out of complete avoidance.

Before blood glucose testing at home became common, the only lancing device available was a sharp piece of stamped steel that made a painful and fairly deep cut in the fingertip. In parallel with the development of blood glucose meters, lancing devices also evolved. Both small, disposable units and reusable "pens" with replaceable tips became commercially available, and they had the added advantage of sharp point being hidden from the view. Even though the lancing device used by a diabetic patient has evolved the reluctance due to pain involved has still persisted.

In this industry it is well understood that cost, comfort and convenience drives the overall acceptance of the method. Non-invasive monitoring of glucose has been of particular interest because it particularly highlights the comfort in the above statement. Ease of use and reduction of pain can encourage more frequent testing and hence tighter control of the glucose concentration. Recently several reviews have discussed the importance of non-invasive glucose testing [89-92]. The limits of detection and quantification, the standard deviation of the measurement, the accuracy, and the total error of non-invasive measurement need to correlate with self-monitoring devices and with measurements in the laboratory if it has to be considered a viable option for blood glucose monitoring.

The use of NIR spectroscopy being non-invasive circumvents all the problems and issues posed by all the other methods. Present day requirements in medical field are that patients demand quick treatment for which fast diagnosis is important. Current pathological tests which are available to analyze blood glucose, though being very accurate have long waiting time. In addition to long waiting time, there are possibilities of infection of the wound, which has resulted due to pricking of the finger during the withdrawal of blood. The same can be said of self-monitoring home devices. The self monitoring device require a test strip for each new reading which involves a recurring cost every time you decide to measure your blood glucose.

References

[1] J. M. McMillin, "Blood Glucose" In Clinical Methods: The History, Physical and Laboratory Examinations, H.K. Walker (Ed.), W.D. Hall (Ed.), J.W. Hurst (Ed.), Butterworth-Heinemann, 1990.

[2] M. E. Delost, "Blood Gas and Critical Care Analyte Analysis" In Equipment for Respiratory Care, T.A.Volsko (Ed.), R.L. Chatburn (Ed.), M.F El-Khatib (Ed.), Jones and Bartlett Publishers Inc., 2014.

[3] M.W Slein, “D-glucose: Determination with hexokinase and glucose-6-phosphate dehydrogenase” In Methods of Enzymatic Analysis,H.U. Bergmeyer (Ed.), Academic Press, 1965.

[4] J.M Burrin, C.P. Price, “Measurement of Blood Glucose”. Ann. Clin. Biochem.Vol. 2,1985, pp.327–342.

[5] N. Dalvi, “Glucose meter reference design” In Application Note Nr. 1560, Microchip Technology Inc.,2013.

[6] A. Rebel, M.A. Rice, B.G. Fahy, “The Accuracy of Point-of-Care GlucoseMeasurements”, J. Diabetes Sci. Technol.,Vol. 6, 2012, pp.396–411.

[7] P.P. Chakraborty, S. Patra, R. Bhattacharjee, S. Chowdhury, “Erroneously elevated glucose values due to maltose interference in mutant glucose dehydrogenase pyrroloquinolinequinone (mutant GDH-PQQ) based glucometer”, BMJ Case Rep.,2017.

[8] D.G. Schultz, “FDA Public Health Notification: Potentially Fatal Errors with GDH-PQQ Glucose Monitoring Technology”, [Online] Available at: http://labmed.ucsf.edu/labmanual/db/resource/FDA_glucometer_warning_Aug_2009.pdf

[9] C.F. So, K.S. Choi, T.K.S Wong, J.W.Y. Chung, “Recent advances in noninvasive glucose monitoring”, Med. Dev. (Auckl.)Vol. 5, 2012, pp.45–52.

[10] J. Kost, “Ultrasound-Assisted Insulin Delivery and Noninvasive Glucose Sensing”, Diabetes Technol. Ther, Vol. 4,2002, pp.489–497.

[11] T.J Dubinsky, C. Cuevas, M.K. Dighe, O. Kolokythas, J.H. Hwang, “High-Intensity Focused Ultrasound: Current Potential and Oncologic Applications”, Am. J. Roentgenol., Vol. 190, 2008, pp.191–199.

[12] S. Gebhardt, M. Faupel, R. Fowler, C. Kapsner, et. al. “Glucose sensing in transdermal body fluid collected under continuous vacuum pressure via micropores in the stratum corneum”, Diabetes Technol. Ther. Vol. 5, 2003, pp.159–166.

[13] A. Sieg, R. H. Guy, M. B. Delgado-Charro, “Noninvasive and minimally invasive methods for transdermal glucose monitoring”, Diabetes Technology & Therapeutics. Vol. 7(1), 2005, pp.174-197.

[14] O.S. Khalil, “Non-Invasive Glucose Measurement Technologies: An Update from 1999 to the Dawn of the New Millennium”, Diabetes Technol. Ther., Vol. 6,2004, pp.660–697.

[15] J. Coates, “Vibrational Spectroscopy: Instrumentation for Infrared and Raman Spectroscopy”, Appl. Spectr. Rev., Vol. 33,1998, pp, 267–425.

[16] A. Tura, A. Maran, G. Pacini, “Non-invasive glucose monitoring: Assessment of technologies and devices according to quantitative criteria”, Diabetes Res. Clin. Prac, Vol.77, 2007, pp.16–40.

[17] S. Liakat, K.A. Bors, T.Y. Huang, A.P.M Michel, et. al. “ In vitro measurements ofphysiological glucose concentrations in biological fluids using mid-infrared light”, Biomed. Opt. Exp., Vol. 4, 2013, pp.1083–1090.

[18] H.A. MacKenzie, H.S. Ashton, S. Spiers, Y. Shen, et. al. “ Advances in Photoacoustic Noninvasive Glucose Testing”, Clin. Chem., Vol. 45, 1999, p.1587.

[19] S. Liakat, K.A. Bors, L. Xu, C.M. Woods, et al. " Noninvasive in vivo glucose sensing on human subjects using mid-infrared light", Biomed. Opt. Exp.,Vol. 5, 2014, pp.2397–2404.

[20] H. V. Lilienfeld-Toal, M. Weidenmüller, A. Xhelaj, W.A. Mäntele, "Novel approach to non-invasive glucose measurement by mid-infrared spectroscopy: The combination of quantum cascade lasers (QCL) and photoacoustic detection", Vib. Spectr., Vol. 38, 2005, pp.209–215.

[21] G.S. Bumbrah, R.M. Sharma, "Raman spectroscopy–Basic principle, instrumentation and selected applications for the characterization of drugs of abuse", Eg. J. Forensic Sci., Vol.6, 2016, pp.209–215.

[22] N.S. Oliver, C. Toumazou, A.E.G. Cass, D.G. Johnston, "Glucose sensors: a review of current and emerging technology", Diabet. Med., Vol. 26, 2009, pp.197–210.

[23] E. Wiercigroch, E. Szafraniec, K. Czamara, M.Z. Pacia, et al. "Raman and infrared spectroscopy of carbohydrates: A review", Spectrochim. Acta Part A Mol. Biomol. Spectr., Vol. 185, 2017, pp.317–335.

[24] Y. Xu, J.F. Ford, C.K. Mann, T.J. Vickers, J.M. Brackett, et al. "Raman measurement of glucose in bioreactor materials", Proc. SPIE,1997, p.2976.

[25] B.H. Malik, G.L. Coté, "Real-time, closed-loop dual-wavelength optical polarimetry for glucose monitoring", J. Biomed. Opt., Vol. 15, 2010, p.017002.

[26] R. Rawer, W. Stork, C.F. Kreiner, "Non-invasive polarimetric measurement of glucose concentration in the anterior chamber of the eye", Graefe's Arch. Clin. Exp. Ophthalmol., Vol. 242, 2004, pp.1017–1023.

[27] G. Purvinis, B.D. Cameron, D.M. Altrogge, "Noninvasive polarimetric-based glucose monitoring: an in vivo study", J Diabetes Sci Technol.,Vol. 5(2), 2011, pp.380-387.

[28] P. Patel, M. Hardik, P. Patel, "A Review on Photoacoustic Spectroscopy", Int. J. Pharm. Erud.,Vol. 3, 2013, pp.41–56.

[29] Y. Tanaka, T. Tajima, M. Seyama, "Differential photoacoustic spectroscopy with continuous wave lasers for non-invasive blood glucose monitoring" In Proceedings of the Photons Plus Ultrasound: Imaging and Sensing 2018, San Francisco,USA, 2018, p. 104945A.

[30] D.A. Dean, T. Ramanathan, D. Machado, R. Sundararajan, "Electrical impedance spectroscopy study of biological tissues", J. Electrost.,Vol. 66,2008, pp.165–177.

[31] K. Chinen, I. Kinjo, A. Zamami, K. Irei, "Nagayama, K. New equivalent-electrical circuit model and a practical measurement method for human body impedance", Biomed. Mater. Eng., Vol. 26, 2015, pp.S779–S786.

[32] E. Hernández-Balaguera, E. López-Dolado, J.L. Polo, "Obtaining electrical equivalent circuits of biological tissues using the current interruption method, circuit theory and fractional calculus", RSC Adv., Vol. 6, 2016, p. 22312–22319.

[33] T. Saito, S. Ishikawa, M. Higashiyama, T. Nakamura, et. al. " Inverse distribution of serum sodium and potassium in uncontrolled in patients with diabetes mellitus", Endocr. J.,Vol. *46*, 1999, pp.75–80.

[34] G. Liamis, E. Liberopoulos, F. Barkas, M. Elisaf, "Diabetes mellitus and electrolyte disorders", World J. Clin.Cases, Vol. 2, 2014, pp. 488–496.

[35] Y. Hayashi, L. Livshits, A. Cadu, “Feldman, Y. Dielectric spectroscopy study of specific glucose influence on human erythrocyte membranes”, J. Phys. Appl. Phys., Vol. 36, 2003, pp.369–374.

[36] W. V. Gonzales, A. Mobashsher, A. Abbosh, “The progress of glucose monitoring—A review of invasive to minimally and non-invasive techniques, devices and sensors”, Sensors,Vol. 19, 2019,p.800.

[37] C.F.; Choi, K.S.; Wong, T.K.; Chung, J.W. Recent advances in noninvasive glucose monitoring. Med. Devices Evid. Res. 2012, 5, 45–52.

[38] J,Rogers, A.J. Radosevich, Y. Ji, V. Backman, “Modeling light scattering in tissue as continuous random media using a versatile refractive index correlation function”, IEEE J. Sel. Top. Quantum Electron. Vol. 20, 2014, pp173–186.

[39] K.V. Larin, M.S. Eledrisi, M. Motamedi, R.O. Esenaliev, “Noninvasive blood glucose monitoring with optical coherence tomography: A pilot study in human subjects”, Diabetes Care, Vol. 25, 2002, pp.2263–2267.

[40] Y.T. Lan, Y.P. Kuang, L.P. Zhou, G.Y.Wu, et. al.“Noninvasive monitoring of blood glucose concentration in diabetic patients with optical coherence tomography”, Laser Phys. Lett., Vol. 14, 2017, p.035603.

[41] K.V. Larin, M. Motamedi, T.V. Ashitkov, R.O. Esenaliev, “Specificity of noninvasive blood glucose sensing using optical coherence tomography technique: A pilot study”, Phys. Med. Biol., Vol. 48, 2003, pp.1371–1390.

[42] A.I. Kholodnykh, I.Y. Petrova, K.V. Larin, M. Motamedi, et. al. “Precision of measurement of tissue optical properties with optical coherence tomography”, Appl. Opt., Vol. 42, 2003, p.3027.

[43] M.G. Ghosn, N. Sudheendran, M. Wendt, A. Glasser, et. al. “Monitoring of glucose permeability in monkey skin in vivo using Optical Coherence Tomography”, J. Biophotonics, Vol 3, 2009, pp.25–33.

[44] I. Barton, “FE Theory and principles of near infrared spectroscopy”, Spectroscopy Europe, Vol. 14, 2002, pp. 12-18.

[45] M.Schwanninger, J. C. Rodrigues, K. Facklers, “A review of band assignments in near infrared spectra of wood and wood components", J. Near Infrared Spectrocopy, Vol. 19(5), 2011, pp.287-308.

[46] G. L. Coté, “Noninvasive and Minimally-Invasive Optical Monitoring Technologies”, The Journal of Nutrition, Vol. 131(5), 2001,pp. 1596S-1604S.

[47] C. Bai, “Noninvasive Near Infrared Spectroscopy on Living Tissue with Multivariate Calibration Approaches”, Doctoral Thesis, The University of Iowa, 2010.

[48] K.H. Hazen, M.A. Arnold, G.W. Small, “Measurement of Glucose and Other Analytes in Undiluted Human Serum with Near-infrared Transmission Spectroscopy”, Analytical Chimica Acta, Vol. 371, 1998, pp. 255-267.

[49] J. T. Olesberg, L.Z. Liu, V. Van Zee, M.A. Arnold, “ In Vivo Near-infrared Spectroscopy of Rat Skin Tissue with Varying Blood Glucose Levels”, Analytical Chemistry, Vol. 78, 2006, pp.215-223.

[50] Y.C. Shen, A.G. Davies, E.H. Linfield, T.S. Elsey, et al. “The Use of Fourier-transform Infrared Spectroscopy for The Quantitative Determination of Glucose Concentration in Whole Blood”, Physics in Medicine & Biology,Vol. 48, 2003, pp.2023-2032.

[51] M.A. Arnold, L.Z. Liu, J.T. Olesberg, “Selectivity Assessment of Noninvasive Glucose Measurements Based on Analysis of Multivariate Calibration Vectors”, Journal of Diabetes Science and Technology, Vol. 1, 2007, pp. 454-462.

[52] J.Chen, M.A. Arnold, G.W. Small, “Comparison of Combination and First Overtone Spectral Regions for Near Infrared Calibration Models for Glucose and Other Biomolecules in Aqueous Solutions”, Analytical Chemistry, Vol. 76, 2004, pp. 5405- 5413.

[53] A. Losoya-Leal , S. Camacho-León, G. Dieck-Assad, et al. “State of the art and new perspectives in non-invasive glucose sensors”, Rev Mex Ing Biomed., Vol 33, 2012, pp. 41-52

[54] M.A. Arnold, G.W. Small, “Determination of physiological levels of glucose in an aqueous matrix with igitally filtered Fourier transform near-infrared spectra”, Anal. Chem., Vol. 62, 1990, pp. 1457–1464.

[55] S. Sharma, M. Goodarzi, J. Delanghe, H. Ramon, et. al. “Using experimental data designs and multivariate modelling to assess the effect of glycated serum protein concentration on glucose prediction from near infrared spectra of human serum”, Appl. Spectrosc., Vol. 68,2014, pp. 398–405.

[56] L.A.Marquardt, M.A. Arnold, G.W. Small, “Near-infrared spectroscopic measurement of glucose in a protein matrix”, Anal. Chem., Vol. 65, 1993, pp. 3271–3278.

[57] R. S. Gad, “Instrumentation design for non-invasive blood analysis based on optical sensors”, Doctoral Thesis, Goa University, 2008.

[58] H. Chung, M.A. Arnold, M. Rhiel, D.W. Murhammer, “Simultaneous measurements of glucose, glutamine, ammonia, lactate, and glutamate in aqueous solutions by near-infrared spectroscopy”, Appl. Spectrosc., Vol. 50, 1996, pp. 270–276.

[59] K.H. Hazen, M.A. Amold, G.W. Small, “Measurement of glucose and other analytes in undiluted human serum with near-infrared transmission spectroscopy”, Anal. Chim. Acta, Vol. 371, 1998, pp.255–267.

[60] A. Al-Mbaideen, M. Benaissa, “Determination of glucose concentration from NIR spectra using independent component regression”, Chemom. Intell. Lab. Syst., Vol. 105, 2011, pp. 131–135.

[61] X Jintao, L. Ye, Y. Liu, C. Li, H. Chen, “Noninvasive and Fast Measurement of Blood Glucose in Vivo by near Infrared (NIR) Spectroscopy”, Spectrochim. Acta Part A: Mol. Biomol. Spectrosc., Vol. 179, 2017, pp. 250–254.

[62] C. Fischbacher, K.U. Jagemann, K. Danzer, U.A. Muller, et al. “Enhancing calibration models for non-invasive near-infrared spectroscopical blood glucose determination”, Fresenius. J. Anal. Chem., Vol. 359, 1997, pp. 78–82.

[63] A.M. Enejder, T.G. Scecina, J O, M.Hunter, W.C. Shih, et al. “Raman spectroscopy for noninvasive glucose measurements”, J Biomed Opt., Vol. 10, 2005, p.031114.

[64] J. Shao, M. Lin, Y. Li, X. Li, et al. “In Vivo Blood Glucose Quantification Using Raman Spectroscopy”, PLoS ONE, Vol. 7, 2012, p. e48127.

[65] Y. Zheng, X. Zhu, Z. Wang, Z. Hou, et al. " Noninvasive Blood Glucose Detection Using a Miniature Wearable Raman Spectroscopy System", Chin. Opt. Lett., Vol. 15, 2017, p.083001.

[66] S.M. Lundsgaard-Nielsen, A. Pors, S.O. Banke, J.E. Henriksen, et al. "Critical-depth Raman spectroscopy enables home-use non-invasive glucose monitoring", PLoS ONE, Vol. 13, 2018, p. e0197134

[67] N. Li, H. Zang, H. Sun, X. Jiao, et al. "A noninvasive accurate measurement of blood glucose levels with raman spectroscopy of blood in microvessels", Molecules, Vol. 24, 2019, p. 1500.

[68] S.P. Singh, S. Mukherjee, L.H. Galindo, P.T.C. So, et al. "Evaluation of accuracy dependence of Raman spectroscopic models on the ratio of calibration and validation points for non-invasive glucose sensing", Anal. Bioanal. Chem., Vol. 410, 2018, pp. 6469–6475.

[69] J.L. Lambert, J.M. Morookian, S.J. Sirk, M.S. Borchert, "Measurement of aqueous glucose in a model anterior chamber using Raman spectroscopy", J. Raman Spectrosc., Vol. 33, 2002, pp.524–529.

[70] K. H. Hazen, M.A. Arnold, G. W. Small, "Temperature-Insensitive Near-Infrared Spectroscopic Measurement of Glucose in Aqueous Solutions", Appl. Spectrosc., Vol. 48, 1994, pp. 477-483.

[71] S. Pan, H. Chung, M. A. Arnold, G. W. Small, "Near-Infrared Spectroscopic Measurement of Physiological Glucose Levels in Variable Matrices of Protein and Triglycerides",Analytical Chemistry, Vol. 68, 1996, pp. 1124-1135.

[72] J. Chen, M. A. Arnold, G. W. Small, "Comparison of Combination and First Overtone Spectral Regions for Near-Infrared Calibration Models for Glucose and Other Biomolecules in Aqueous Solutions", Analytical Chemistry, Vol. 76, 2004 , pp. 5405-5413.

[73] H. Arimoto, M. Tarumi, Y. Yamada, "Temperature-Insensitive Measurement of Glucose Concentration Based on Near Infrared Spectroscopy and Partial Least Squares Analysis", OPT REV , Vol. 10, 2003, pp.74–76.

[74] J.J. Burmeister, M.A. Arnold, G.W. SmalL, "Non-invasive blood glucose measurements by near-infrared transmission spectroscopy across human tongues", Diabetes Technol. Ther., Vol. 2, 2000; pp.5–16.

[75] J.T. Olesberg, M. A. Arnold, C. Mermelstein, J. Schmitz, et al. "Tunable Laser Diode System for Noninvasive Blood Glucose Measurements", Appl. Spectrosc., Vol. 59, 2005, pp. 1480-1484.

[76] S. T. Fard , W. Hofmann , P.T. Fard, G. Bohm, et al. "Optical Absorption Glucose Measurements Using 2.3μm Vertical-Cavity Semiconductor Lasers", IEEE Photonics Technology Letters, Vol. 20, 2008, pp. 930-932.

[77] K. Maruo, T. Oota, M. Tsurug, T. Nakagawa, et al. "New methodology to obtain a calibration model for noninvasive near-infrared blood glucose monitoring", Appl Spectrosc., Vol. 60, 2006, pp. 441-449.

[78] J. Kottmann, U. Grob, J. M. Rey, M. W. Sigrist, "Mid-Infrared Fiber-Coupled Photoacoustic Sensor for Biomedical Applications", Sensors, Vol. 13, 2013, pp. 535-549.

[79] R. Zhang, F. Gao, X. Feng, H. Jin, et al. "Guide Star Assisted Noninvasive Photoacoustic Measurement of Glucose", ACS Sens., Vol. 3, 2018, pp. 2550-2557

[80] R. Zhang, F. Gao, X. Feng, S. Liu, et al. "Noninvasive Photoacoustic Measurement of Glucose by Data Fusion", Analyst., Vol.142, 2017, pp. 2892–2896.

[81] J. Kottmann, J.M. Rey, J. Luginbühl, E. Reichmann, “Glucose sensing in human epidermis using mid-infrared photoacoustic detection”, Biomedical optics express, Vol. 3, 2012, pp. 667-680.

[82] K. Kajiwara, T. Uemara, H. Kishikawa, K. Nishida, et al. “Non-invasive measurement of blood glucose concentrations by analysing Fourier transform infra-red absorbance spectra through oral mucosa”, Med Biol Eng Comput, Vol.31, 1993, pp. S17–S22.

[83] A. Werth, S. Liakat, A. Dong, C. M. Woods, et al. “Implementation of an integrating sphere for the enhancement of noninvasive glucose detection using quantum cascade laser spectroscopy”, Appl. Phys. B, Vol. 124, 2018, p. 75.

[84] S. Kino, S. Omori, T. Katagiri, Y. Matsuura, “Hollow optical-fiber based infrared spectroscopy for measurement of blood glucose level by using multi-reflection prism”, Biomedical optics express, Vol. 7, 2016, pp. 701–708.

[85] R. Kasahara, S. Kino, S. Soyama, Y. Matsuura, “Noninvasive glucose monitoring using mid-infrared absorption spectroscopy based on a few wavenumbers”, Biomedical optics express, Vol. 9, 2017, pp.289–302.

[86] G. Purvinis, B.D. Cameron, D.M. Altrogge, “Noninvasive polarimetric-based glucose monitoring: an in vivo study”, J. Diabetes Sci. Technol., Vol. 5, 2011, pp. 380-38.

[87] P. Westphal, J.M. Kaltenbach, K. Wicker, “Corneal birefringence measured by spectrally resolved Mueller matrix ellipsometry and implications for non-invasive glucose monitoring”, Biomed. Opt. Express., Vol. 7, 2016, pp.1160-1174.

[88] M. Kinnunen, R. Myllylä, S. Vainio, “Detecting glucose-induced changes in in vitro and in vivo experiments with optical coherence tomography”, J. Biomed Opt., Vol. 13, 2008, p. 021111.

[89] J. Lin, C.W. Brown, “Spectroscopic measurement of NaCl and sea water salinity in the near-IR region of 680–1230 nm”, Appl. Spectrosc., Vol. 47, 1993, pp.239-241.

[90] J.J. Kelley, K.A. Kelley, C.H. Barlow, “Tissue temperature by near-infrared spectroscopy”, SPIE Proc. Vol. 2389, 1995, pp.818–828.

[91] S. Haddad, P. Poulin, K. Krishnan, “Relative lipid content as the sole mechanistic determinant of the adipose tissue:blood partition coefficients of highly lipophilic organic chemicals”, Chemosphere, Vol. 40, 2000, pp. 839-843.

[92] V. Tuchin, “Tissue Optics: light scattering methods and instruments for medical diagnosis”, SPIE Press, 2000.

Near infrared radiation was discovered by German born English scientist Sir Frederick William Herschel. He was a musician and an astronomer who is also credited to discover the planet Uranus. He discovered the invisible radiation while performing an experiment to investigate the rise in temperature due to each of the colors present in sunlight. To his amazement, he found that the temperature rose even when he went beyond the visible red color region. He termed them as calorific rays. Later on this region of the electromagnetic radiation was named as Infrared [1- 4].

Near infrared light occupies the spectral range of 700 – 2500 nm. The energy possessed by these photons is in the range of 2.471 x 10^{-19} to 7.96 x 10^{-20} Joules. This energy of photon is more than sufficient to transfer a molecule to fundamental vibrational states, but is lower than the energy required for electron transitions.

The near infrared region is used in many present day analytical techniques and it presents user with many advantages. Near infrared analysis is non-destructive in nature and the sampling is fast. Any sample molecule containing C-H, N-H, S-H and O-H bonds can be analyzed using this radiation with a added advantage of relatively deep penetration in the probed sample.

3.1 Theory

In a chemical bond, there are participating atoms. These atoms are displacing themselves relative to each other with a specific frequency. These displacement or vibrations are of the order of a few nanometers. If external energy is transferred to them, the amplitude of vibration can increase. A photon can transfer energy to the molecule; the energy of the photon is given by,

$$\mathbf{E_p = h\nu = h\frac{c}{\lambda}} \qquad (3.1)$$

Where h is the Planck constant, ν is the frequency of the photon, c is the speed of light and λ is wavelength of photon.

3.1.1 The Diatomic Molecule

The interaction of near infrared radiation with matter can be understood by a simplified classical model of a diatomic molecule. This entire system of two atoms in a bond can be regarded as a simple harmonic oscillator where a spring with force constant k

connects the two spherical masses m_1 and m_2. One finds that the bond strength in molecules and their mass determines the energy of the system given by the Hook's law.

$$\mathbf{E} = \frac{\mathbf{h}}{\mathbf{2\pi}}\sqrt{\frac{\mathbf{k}}{\mathbf{u}}} \qquad (\mathbf{3.2})$$

Where h is Planck constant, k is force constant and the reduced mass μ is given by

$$\boldsymbol{\mu} = \frac{\mathbf{m_1 m_2}}{\mathbf{m_1 + m_2}} \qquad (\mathbf{3.3})$$

The potential energy V of the harmonic oscillator system is given by

$$\mathbf{V} = \frac{\mathbf{1}}{\mathbf{2}}\mathbf{kx^2} \qquad (\mathbf{3.4})$$

where x is the dispalacement of the atoms.

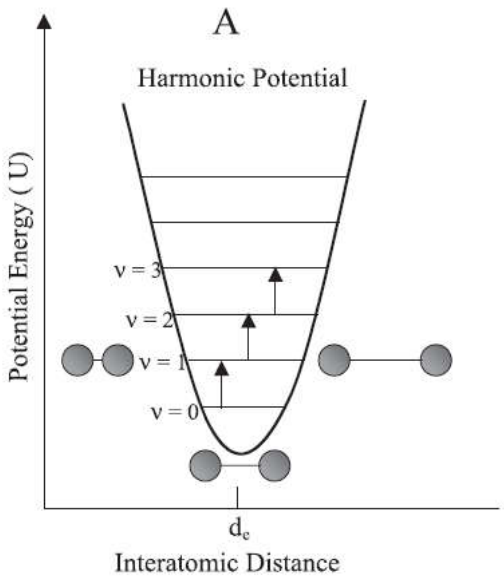

Figure 3.1: The potential energy of harmonic oscillator [1]

The plot in figure 3.1 shows the potential energy of the harmonic oscillator versus the interatomic distance. To understand the concept of vibrational energy the above approach suffices, however when we consider micorsocopic system like the molecules it fails. The molecular system cannot have a continous energy profile given by the classical model elucidated above.The molecular system is only allowed to have a few

discrete energy levels given by quantum mechanical treatment and is given by the equation

$$\mathbf{E_\upsilon = \left(\upsilon + \frac{1}{2}\right) h\nu} \qquad (\mathbf{3.6})$$

E_υ is the energy of the υth quantum level, υ is the vibrational quantum number and ν represents the is the fundamental vibrational frequency. The frequency of vibration in the classical model is given by

$$\mathbf{\nu = \frac{1}{2\pi}\sqrt{\frac{k}{\mu}}} \qquad (\mathbf{3.5})$$

The energy differnce between adjacent states has to be always the same. Also, it must be noted that in the harmonic quantum model the transion can take place only between adjacent levels and therefore $\Delta\upsilon = \pm 1$. The energy of the photon, which is imparted to the molecule to reach the excited state, must exactly match the difference between adjacent energy levels. The effect of absorption on the vibration amplitude is depicted in figure 3.2. The energy of the photon must be

$$\mathbf{\Delta E = E_{\upsilon 2} - E_{\upsilon 1} = \Delta\upsilon h\nu} \qquad (\mathbf{3.7})$$

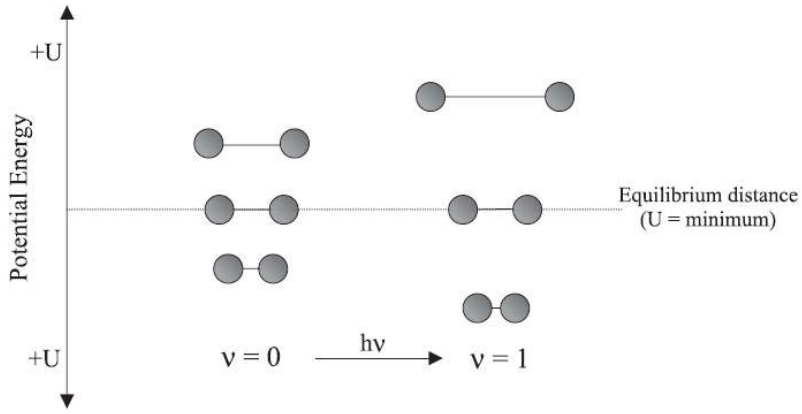

Figure 3.2: Photon absorption by a molecule [1]

Harmonic oscillator proves to be a promising aid in understanding vibrational spectroscopy. Even then it has significant restrictions, transition with $\Delta\upsilon = 2$ and above are not allowed in the harmonic/quantum model and hence this model fails to explain the overtones and combination bands which are observed in the near infrared region.

The anharmonic model which is presented in the following section is able to explain the observed overtone and combination band.

3.1.2 The Anharmonic Model

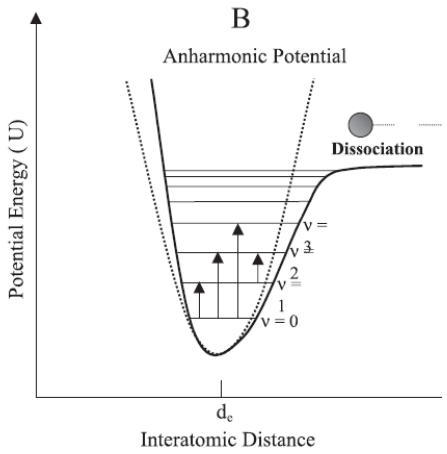

Figure 3.3: the potential energy of an anharmonic oscillator

The anharmonic model was a result of developing a more realistic model, it develops on the earlier harmonic model, which contains two masses and spring, but includes some non-ideal behaviors. These non-ideal behaviors include varying bond force due to the movements of the atoms and the repulsions experienced by the electronic clouds when nuclei approach each other. Higher order terms are used in the potential energy equation.

$$\mathbf{V = k_1 x^2 + k_2 x^3 + k_3 x^3} \qquad \mathbf{(3.8)}$$

The potential energy is approximated by the Morse function 'V' in equation 3.9. This function approximates the anharmonic behaviors of diatomic molecule.

$$\mathbf{V = D_e(1 - e^{-a(r-r_e)})^2} \qquad \mathbf{(3.9)}$$

Here, r is the instantaneous distance between the atoms, r_e is the equilibrium distance between the two atoms, D_e is the spectral dissociation energy and a is the constant for the said molecule. The Morse function after quantum mechanics treatment results in the following equation.

$$\mathbf{E} = \mathbf{h\nu}\left(\upsilon + \frac{1}{2}\right) - \mathbf{x_m h\nu}\left(\upsilon + \frac{1}{2}\right)^2 \qquad \textbf{(3.10)}$$

The anharmonicity constant of vibration x_m lies in the range of 5 x 10^{-3} and 5 x 10^{-2}. The anharmonic model allows for transition with $\Delta\upsilon = 2$ or greater and also allows for the existence of combination band of fundamentals vibrations. A detailed consideration of the theory underlying the near infrared vibrational spectroscopy is elucidated in several references [1-2].

3.2 Near Infrared for Absorption Analysis

The first near infrared spectrum was obtained in 1881 by Abney and Festing in the range of 1000–1200nm [5]. But it was not until the 1980s Near Infrared spectroscopy encountered steady growth mainly due to development in the instrument design, application of chemometric techniques and advancement in processing devices. Near infrared spectrum covers several optical windows where photons have less interactions with interfering tissue compounds, such as water, hemoglobin, and lipids, so that the penetration depth can achieve several millimeters [6-7]. In near infrared region, the absorption property of tissue is greatly affected by its constituents such as collagen, fat and water. This spectral region is known as a "tissue optical window" or "therapeutic window"[8].

As near infrared analysis is non-destructive, it is viable for online monitoring. It can be used for analysis of various biomolecules hence, near infrared spectroscopy has found its application in many fields such as agriculture, food, petroleum and pharmaceutical industries [9-16]. Within the biomedical field, near infrared spectroscopy is emerging as a potential diagnostic tool with many diverse applications [17].The increasingly prevalent disease diabetes mellitus has created a demand for continuous non-invasive monitoring of blood glucose concentration. Therefore, methods to do so based on a variety of techniques, including near and mid infrared spectroscopy, has been sought intensively in recent years[18-27].Absorption spectroscopy quantifies the concentrations of substances through the detection of transmitted photons which have the same wavelength as the incident beam.

3.2.1 Beer-Lambert Law

The Beer-Lambert law describes the attenuation of intensity of incident light (I_0) crossing a material with absorbing properties, as seen in figure 3.4 when an incident beam (I_0) enters the sample, the intensity of transmitted light (I) decreases exponentially as shown in equation [28].

$$\mathbf{I = I_0 e^{-\varepsilon(\lambda).c.L}} \qquad \mathbf{(3.11)}$$

Where I is intensity of transmitted light, $I_0$is the intensity of incident light, ε is the absorptivity (extinction coefficient) of the substance at a specific wavelength in mol^{-1} cm^{-1} (1/mol centimeters), c is the concentration of absorbent in mol and L is the optical path length in the medium in cm (centimeters).

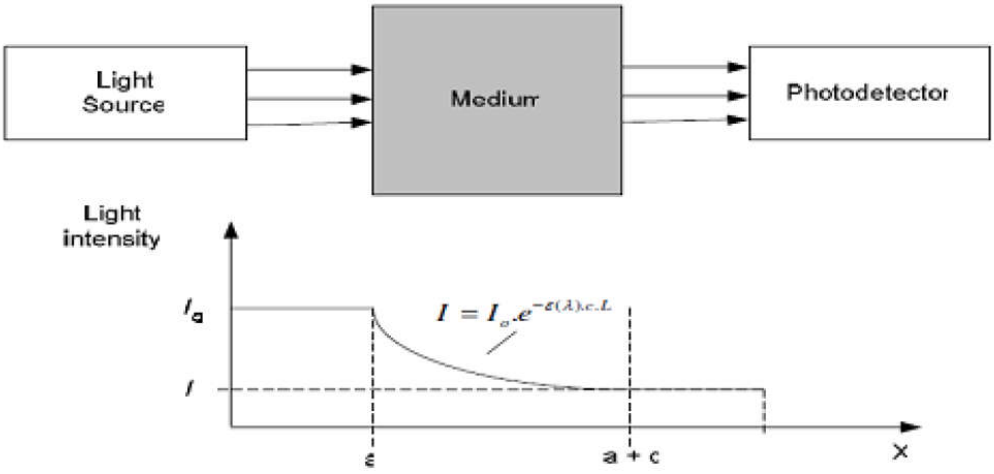

Figure 3.4: Absorption of light in a material

The transmittance (T) of light crossing a medium with absorbing properties is the ratio of intensity of transmitted light (I) to the intensity of incident light (I_0), and absorbance is equal to the negative natural logarithm of the transmittance, as shown in Equation.

$$\mathbf{A = -\ln T = -\ln \frac{I}{I_0} = -\varepsilon(\lambda).c.L} \qquad \mathbf{(3.12)}$$

Where A is the absorbance, T is the transmittance (no units). Even if absorption of light in a medium occurs in different sections of the medium of lengths L_1, L_2, ….L_n, the Beer-Lambert law is still valid and is given by,

$$\mathbf{A_t} = \boldsymbol{\varepsilon_1(\lambda).c_1.L_1} + \boldsymbol{\varepsilon_2(\lambda).c_2.L_2} + \ldots . + \boldsymbol{\varepsilon_n(\lambda).c_n.L_n} \quad (3.13)$$

3.2.2 Glucose Absorption

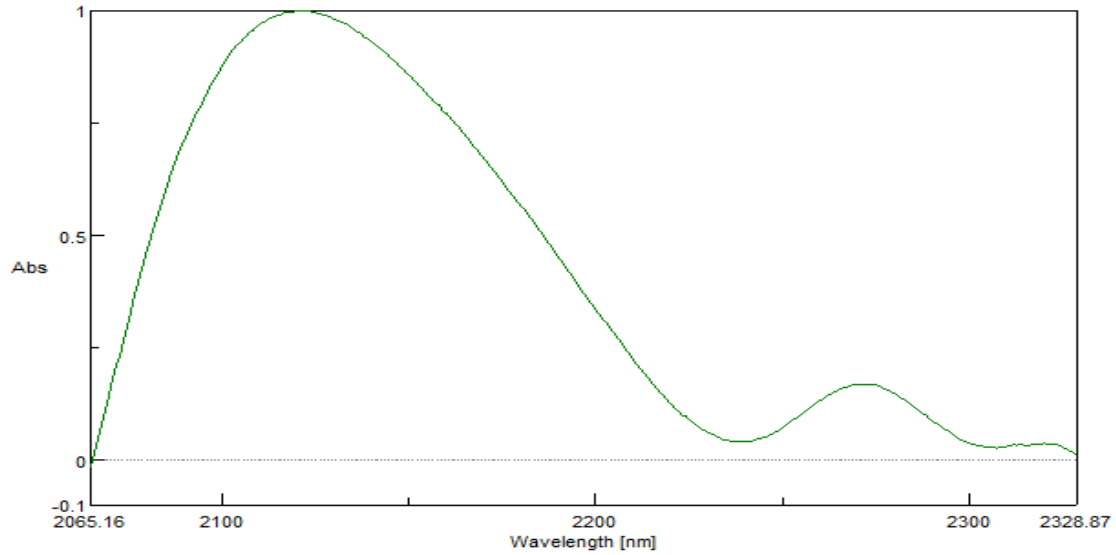

Figure 3.5: Normalized glucose absorbance spectra recorded on Jasco V-770

Glucose absorption spectra has three regions, the short wavelength near infrared region from 700 – 1330 nm, the first overtone region from 1540 – 1820 nm and the combination region from 2000 – 2500 nm.. Glucose is reported to have absorption peaks at 939nm, 970nm, 1197nm in the higher overtone region, 1408nm, 1536nm and 1688, 1925nm in the first overtone region and 2100nm, 2261nm, 2326nm in the combination region [29]. Absorbance spectrum of glucose in combination region as recorded on Jasco V-770 spectrophotometer shows three peaks centered at 2120, 2,270, and 2,320 nm as shown in figure 3.5.

3.3 Major Interferents in Human Tissue

3.3.1 Water Absorption

Water makes up 60 to 80% of the total body mass and as such is major component of the human body. The water content varies with tissue type and it is also age and gender-dependent. For instance, water content in adult skeletal muscle is around 74%, whereas the newborn brain comprises 90% water by mass. Water is considered one of the most important chromophores in tissue spectroscopy measurements because of its high concentration in most biological tissue. Corresponding to the various types of the

excited molecular vibrations there are three different regions associated with the near infrared spectrum, namely the combination band region, the first overtone region and the higher-order overtone region. It can be seen in the figure 3.6 that water has very low absorption below 1300 nm, thus leaving the higher-order overtone region highly accessible. What this means is that based on the water absorption characteristics alone, centimeter-thick samples can be measured between 800 nm and 1300 nm. Unfortunately, glucose absorption in this region is extremely weak for clinically accurate measurements. In the first overtone region is there is window between 1600 nm and 1850 nm. In the combination band region, there is a window around the absorption minimum at 2200 nm. The below spectra shows the three windows which water offers. The absorption spectrum of water shown in figure 3.6 is recorded on a Jasco- V770 spectrophotometer using a cuvette with a path length of 1mm.

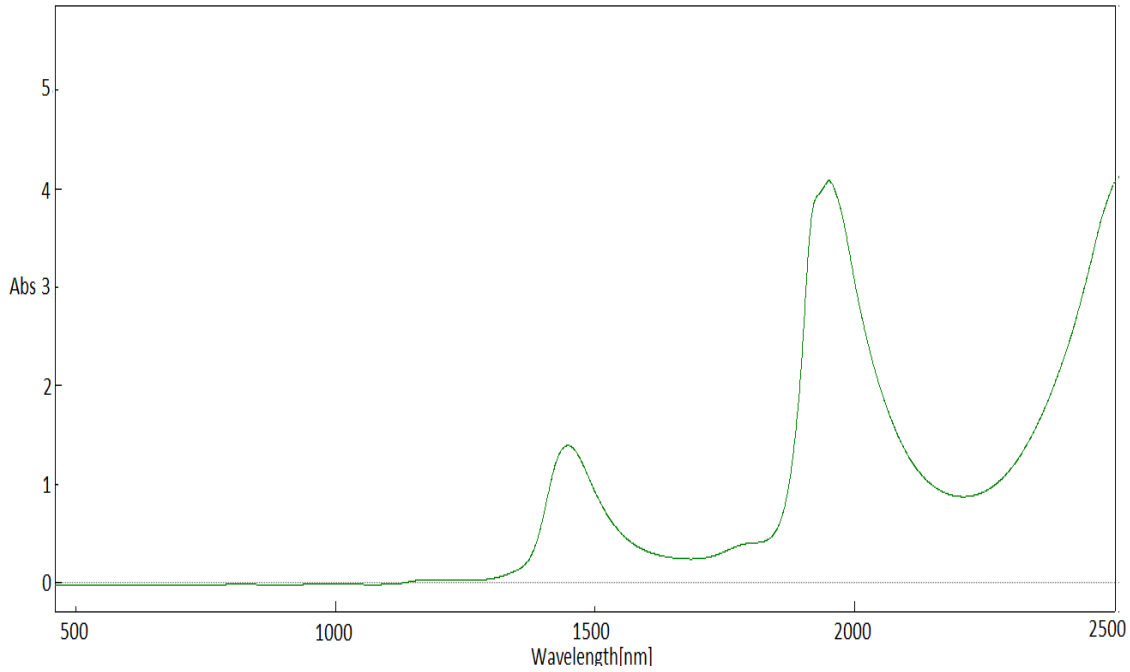

Figure 3.6: Water absorption spectra

The intensity of the near infrared absorption bands for water is sensitive to solute concentration and temperature [30-32]. It decreases as solute concentration increases because of the change in the molar ratio of water. This is referred to as water displacement. Temperature sensitivity of the near infrared absorption of water is also observed in the tissue [33].

3.3.2 Hemoglobin Determination

Hemoglobin is the most dominant absorber of near infrared light in the window where water has good transparency. Hemoglobin is carried in red blood cells also called erythrocytes, and constitutes approximately 40 – 45 % of whole blood. It is responsible for supplying oxygen from the lungs to the body tissues and returning waste gases, such as carbon dioxide, to the lungs to be exhaled. Four 'heme' groups bind to the protein globin to from Hemoglobin. A 'heme' group consists of a ring structure with iron atom at the centre. In the oxygenated state hemoglobin binds to oxygen and is known as oxyhemoglobin (HbO_2). The de-oxygenated form, with no oxygen molecules attached, is known as deoxyhemoglobin(Hb).

3.3.3 Lipids

Lipids in the body exist in the form of triglycerides (neutral fats). They are mostly found in subcutaneous tissues and around internal organs. In the brain, the lipids exist as steroidal lipids and the percentage varies with age from 2.6 % in the new-born to 11.6 % in the adult. In adipose tissue, found in the sub-dermis, the lipid concentration is again age and gender dependent, in the range 23 – 47 % for new-born infants and 68 – 87 % for adults. The importance of lipid as an absorber in near infrared spectroscopy depends upon the tissue in question. Since the water content is much greater than the lipid content in the brain, absorption due to lipid may be insignificant. The lipid content in the forearm varies depending on the fat to muscle tissue ratio as a result of which the absorption may be significant in any spectroscopic application [34].

3.3.4 Melanin

Melanin, the pigment found in the epidermal layer of human skin, has a large scattering coefficient in the ultraviolet region, which protects the skin damaging due to UV radiation from the sun, and a significant absorption coefficient in the MIR. In the human skin, exposure to UV radiation initiates melanogenesis, the process by which melanin created gives the skin a dark look. Melanin is capable of dissipating over 99 % of the absorbed UV radiation [35]. Because of this property, melanin is thought to protect skin cells from UV radiation damage, reducing the risk of folate depletion and dermal degradation.

3.4 Optical Properties of Human Tissue

Light can penetrate deep enough into the tissue to allow a spectral measurement or a therapeutic procedure. Optical imaging and non-invasive diagnosis of the human body strongly requires the study of optical and physical properties of skin tissue in general.

3.4.1 Properties of Skin Tissue

The skin structure and properties in different parts of the body vary considerably. The skin is divided into three layers, namely, the epidermis, dermis, and subcutaneous fat, each is divided into their own sub-layers. The outermost layer of the epidermis is composed of a relatively thin protective top layer of rough, dead and dry skin cells known as the stratum corneum or horny layer. The remainder of the epidermis, including the stratum lucidum, stratum granulosum and stratum spinosum, is made up of cells called keratinocytes as well as melanocytes, which are pigment cells responsible for skin pigmentation. Epidermal thickness varies from 0.1 mm in the eyelids to approximately 1 mm on the palms and soles. The dermis consists of a variety of cells, fibers, amorphous ground substance, nerves, oil glands, sweat glands, blood vessels and hair roots. Its upper layer is called the papillary dermis and contains the vascular network and sensory nerve endings, whereas the deeper layer, referred to as reticular dermis, consists mainly of a loose connective structure and epithelial-derived structures such as glands and follicles. The thickness of the dermis varies from 0.3 mm in the eyelids to about 3 mm in the palm and soles. Subcutaneous fat is made up of fat cells, which act as a cushioning layer between the deeper muscles and the skin. It also has abundant blood content. A typical structure of skin is shown in Fig 3.7. Table 3.1 gives the average elemental composition of the skin [36].

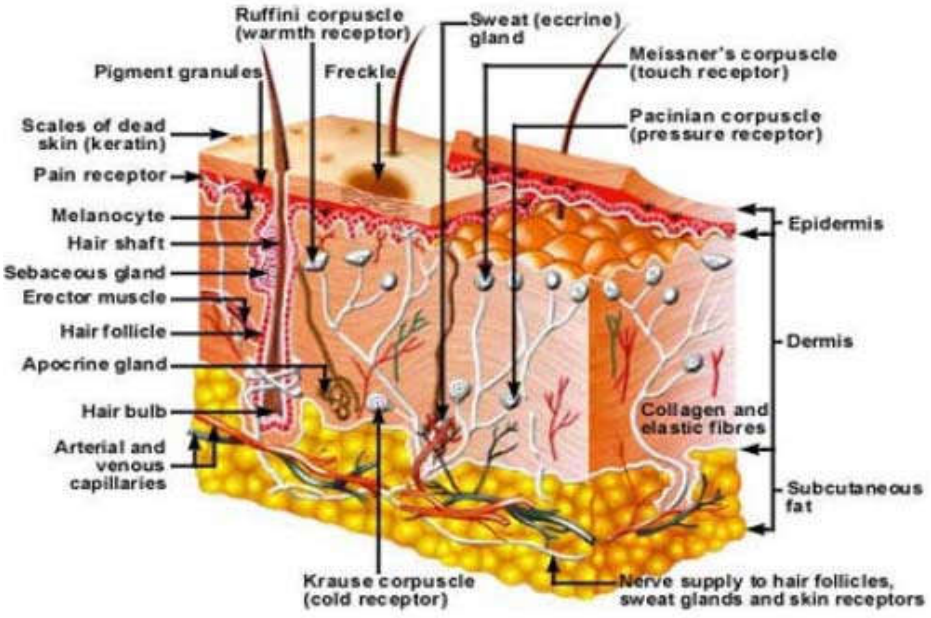

Figure 3.7: Anatomy of the skin

Table 3.1: Average elemental composition of the skin, percentage by mass

C	O	H	N	Na	Mg	P	Cl	K
25 ~ 15.8	59.4-69.5	10-10.1	4.6 - 3.7	0.2	0.1	0.2	0.3	0.1

3.4.2 Optical Absorption by Skin Tissue

As skin is composed of constituents such as water, lipids and proteins the chemical makeup of the skin influences its optical absorption properties. Water absorbs photons at wavelengths longer than the MIR range, while proteins are strongly absorbed in the UV and Violet region. Luckily, the optical absorption capacity of water, proteins and lipids is small in the red and near infrared region. This region, known as the “tissue optical window”, has a range 600 nm to 2,300 nm and the light can penetrate to a depth of a few hundreds of micrometers to a few mm into the skin tissue [37]. As such this region is exploited for a variety of purposes, including diagnosis, imaging or therapy. At the shorter wavelengths of the tissue optical window, from 600 nm to 1100 nm, the most important photon absorbing chromophores are blood and melanin. Water becomes dominant at incident wavelengths longer than 1150 nm. The epidermis does not contain any blood and its water content is also much lower that of the dermis. However, the stratum granulosum and stratum spinosum comprises of some melanocytes, including

melanin, which is involved in skin pigmentation. Because the absorption capacity of melanin is stronger than that of blood and water, it is the dominant source of absorption in the epidermis at shorter near infrared wavelengths. The volume fraction of melanosomes in the epidermis can vary from 1.3 - 6.3 % for light-skinned adults, 11 - 16% for well-tanned adults and 18 - 43 % for darkly pigmented Africans. The blood content of the dermis is about 0.2 - 5 %, representing the main source of absorption at wavelengths shorter than 1100 nm. If the optical wavelength exceeds the near infrared range, water content becomes an important consideration in terms of optical absorption. It is a well-known fact that the measured values of absorption coefficient of a tissue are different *in-vitro* and *in-vivo* measurements. This can be explained on a number of grounds such as soaking the tissue sample in saline prior to an in-vitro measurement may alter its optical properties, and increase the amount of reflectance. In addition, other kinds of tissue treatments, including drying, freezing, deforming or heating, may change the optical properties of the sample. Also measuring and calibration procedures may introduce an error into the determined values for diffuse reflectance and total transmittance.

References

[1] C. Pasquini, "Near infrared spectroscopy: fundamentals, practical aspects and analytical applications", J. Braz. Chem. Soc., Vol. 14 (2), 2003, pp. 198-219.

[2] D.A. Burns (Ed.), E.W. Ciurczak (Ed.), "Handbook of near-Infrared Analysis", CRC Press, 2007.

[3] W. Herschel, "Investigation of the powers of the prismatic colours to heat and illuminate objects; with remarks, that prove the different refrangibility of radiant heat", Phil. Trans. Roy. Soc. London, Vol. 90, 1800, pp. 255-283.

[4] W. Herschel, "Experiments on the refrangibility of the invisible rays of the sun", Phil. Trans. Roy. Soc. London, Vol. 90, 1800, pp. 284-292.

[5] W. Abney, E.R. Festing, "Near Infrared Spectral of Organic Liquids", Phil. Trans. Roy. Soc., Vol. 172, 1881, p 887.

[6] S.K. Vashist, "Non-Invasive Glucose Monitoring Technology in Diabetes Management: A Review", Analytica Chim. Acta, Vol. 750, 2012, pp. 16–27.

[7] S. Perrey, "Non-Invasive Nir Spectroscopy of Human Brain Function During Exercise", Methods, Vol. 45 (4), 2008, pp. 289–299.

[8] R. R. Anderson, J. A. Parrish, "The optics of human skin", J. Invest. Dermatol., vol. 77 (1), 1981, pp. 13- 19.

[9] E. K. Kemsley, H. S. Tapp, R. Binns, R. O. Mackin, et al., “Feasibility study of NIR diffuse optical tomography on agricultural produce”, Postharvest Biology And Technology, Vol. 48 (2), 2008, pp. 223-230.

[10] P. Williams (Ed.), K. Norris (Ed.), “Near-Infrared Technology in the Agricultural and Food Industries”, American Association of Cereal Chemists Inc., 1987.

[11] P. Pallav, G. G. Diamond, D. A. Hutchins, R. J. Green, et al. “A Near infrared (NIR) technique for imaging food materials”, J. of Food Science, Vol. 74, 2009, pp. E23-E33.

[12] K. Kaffka, “How the NIR technology came to and spread in Europe for quality assessment and control in the food industry”, Acta Alimentaria, Vol. 37, 2008, pp. 141-145.

[13] R. Z. Syunyaev, R. M. Balabin, I. S. Akhatov, J. O. Safieva, “Adsorption of petroleum asphaltenes onto reservoir rock sands studied by Near-infrared (NIR) spectroscopy”, Energy & Fuels, Vol. 23, 2009, pp. 1230-1236.

[14] R. A. Balabin, R. Z. Syunyaev, “Petroleum resins adsorption onto quartz sand: Near infrared (NIR) spectroscopy study”, J. of Colloid and Interface Science, Vol. 318 (2), 2008, pp. 167-174.

[15] G. Sando, J. Dubois, “Seeing the chemicals in pharmaceutical tablets with NIR chemical imaging”, Chimica Oggi-Chemistry Today, Vol. 28, 2010, pp. 40-42.

[16] D. Xiang, J. Berry, S. Buntz, P. Gargiulo, et al., “Robust calibration design in the Pharmaceutical Quantitative Measurements with Near-Infrared (NIR) spectroscopy: Avoiding the chemometric pitfalls”, J. of Pharmaceutical Sciences, Vol. 98, 2009, pp. 1155-1166.

[17] H.U. Gremlich, B. Yan, “ Infrared and Raman Spectroscopy of Biological Materials”, CRC Press, 2000.

[18] H. Zeller, P. Novak, P. Landgraf, “Blood glucose measurement by infrared spectroscopy”, Int. J. Artif. Organs, Vol. 12(2), 1989, pp. 129-135.

[19] P. Bhandare, Y. Mendelson, A. Robert, G. Janantsch, et al., “Multivariate Determination of Glucose in Whole Blood Using Partial Least-Squares and Artificial Neural Networks Based on Mid-Infrared Spectroscopy”, Appl. Spectrosc., Vol. 47(8), 1993, pp. 1214-1221.

[20] H. M. Heise , A. Bittner, “Investigation of Experimental Errors in the Quantitative Analysis of Glucose in Human Blood Plasma by ATR-IR Spectroscopy”, J. Mol. Struct., Vol. 348, 1995, pp. 21-24.

[21] K. J. Ward, D. M. Haaland, M. R. Robinson, R. P. Eaton, “Post-Prandial Blood Glucose Determination by Quantitative Mid- Infrared Spectroscopy”, Appl. Spectrosc., Vol. 46 (6), 1992, pp. 959- 965.

[22] J. J. Burmeister and M. A. Arnold, “Evaluation of Measurement Sites for Noninvasive Blood Glucose Sensing with Near-Infrared Transmission Spectroscopy”, Clin. Chem., Vol. 45(9), 1999, pp. 1621-1627.

[23] H. Chung, M. A. Arnold, M. Rhiel, D. W. Murhammer, “Simultaneous Measurements of Glucose, Glutamina, Ammonia, Lactate, and Glutamate in Aqueous Solutions by Near-Infrared Spectroscopy”, Appl. Spectrosc., Vol. 50(2), 1996, pp. 270-276.

[24] K. H. Hazen, M. A. Arnold, and G. W. Small, “Temperature- Insensitive Near-Infrared Spectroscopic Measurement of Glucose in Aqueous Solutions”, Appl. Spectrosc., Vol. 48(4), 1994, pp. 477-483.

[25] R. Vonach, J. Buschmann, R. Falkowski, R. Schindler, et al., “Application of MidInfrared Transmission Spectrometry to the Direct Determination of Glucose in Whole Blood”, Appl. Spectrosc., Vol. 52(6), 1999, pp. 820-822.

[26] T. Yano, T. Funats,K. Suehara, Y. Nakano, “Measurement of the concentrations of glucose and citric acid in the aqueous solution of a blood anticoagulant using near infrared spectroscopy”, J. Near Infrared Spectrosc., Vol. 9, 2001, pp. 43-48.

[27] G. Yoon, Y. J. Kim, and S. Hahn, “Determination of glucose in whole blood samples by mid-infrared spectroscopy”, Appl. Opt., Vol. 42(4), 2003.

[28] C.G. Lee, “Calculation of light penetration depth in photobioreactors”, Biotechnology and Bioprocess Engineering, springer, Vol. 4, 1999, pp. 78-81.

[29] O.S. Khalil, “Spectroscopic and clinical aspects of non-invasive glucose measurements”, Clinical Chemistry, Vol. 45 (2), 1999, pp. 165- 177.

[30] M.K. Phelan, C.H. Barlow, J.J. Kelley, T.M. Jinguji, et al., “Measurement of caustic and caustic brine solutions by spectroscopic detection of the hydroxide ion in the near-infrared region 700–1150 nm”, Anal. Chem, Vol.61, 1989, pp. 1419-1424.

[31] J. Lin, C.W. Brown, “Near-IR spectroscopic determination of NaCl in aqueous solutions”, Appl. Spectrosc, Vol.46, 1992, pp1809–1815.

[32] J. Lin, C.W. Brown, “ Spectroscopic measurement of NaCl and sea water salinity in the near-IR region of 680–1230 nm”, Appl. Spectrosc, Vol.47, 1993, pp. 239-241.

[33] J.J. Kelley, K.A. Kelley, C.H. Barlow, “Tissue temperature by near-infrared spectroscopy”, SPIE Proc., Vol.2389, 1995, pp. 818–828.

[34] S. Haddad, P. Poulin and K. Krishnan “Relative lipid content as the sole mechanistic determinant of the adipose tissue:blood partition coefficients of highly lipophilic organic chemicals”, Chemosphere, Vol.40(8), 2000, pp. 839-843.

[35] P. Meredith, J. Ries, "Radiative relaxation quantum yields for synthetic eumelanin", Photochemistry and Photobiology, Vol. 79 (2), 2004, pp. 211–216.

[36] V. Tuchin “Tissue Optics: light scattering methods and instruments for medical diagnosis”, SPIE Press, 2000.

[37] S.L. Jacques, “Origins of tissue optical properties in the UVA, visible and NIR regions”, OSA TOPS on advances in optical imaging and photon migration , Vol.2, 1996, pp. 364-371.

In our research work the fundamental quantity which we are determining is glucose absorption of near infrared light. This absorption signal which we measure is passed through a multivariate algorithm in order to estimate the glucose concentration present in the sample. This chapter details the methodology used to measure the glucose absorption signal.

4.1 Spectroscopic Measurements for Glucose Estimation

We have used standard spectroscopic techniques to measure the glucose absorption signal. The instrumentation required to effect such a measurement must be in a position to measure the absorbed light intensity at the desired wavelength. Instruments for spectroscopic measurements necessitate a radiation source, a wavelength selection device such as a monochromator, a sample holder which is transparent to the radiation, a detector to measure the intensity of the radiation and some means of digitizing, processing and then displaying the signal from the detector. The most popular instrument used for such a measurement is called a spectrophotometer.

The optical components and the sample holder used in such and spectroscopic measurement need to be transparent to infrared radiation. Also these materials must be soft enough to be polished to make lenses and sample holders.

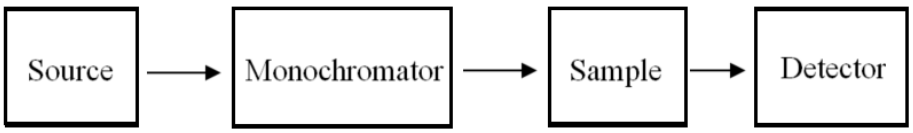

Figure 4.1 Block diagram for a spectroscopic measurement

4.1.1 Sources for Infrared

In spectroscopy two types of light sources are predominantly used, namely continuum sources and line sources. The continuum sources emit light over a board range of wavelengths, whereas line sources emit discrete wavelengths of light. Examples of continuum sources are xenon arc lamps, tungsten filament lamp etc. Infrared lasers, sodium vapour lamps are examples of line sources.

These sources have the intensity of radiation over the range of interest constant for a long period of time. Nernst glowers, Globars, and heated wires are the most commonly used mid infrared sources. Their emission spectrum is continuous and is similar to the one emitted by black body radiators when heated.

For work in the near infrared region, a quartz tungsten halogen (QTH) lamp is the most popular source. A QTH lamp contains a filament made up of tungsten, filled with iodine gas sealed inside a quartz bulb. The tungsten starts evaporating from the filament over the lifetime of the lamp and starts depositing on the wall of the lamp. Hence there is a reduction of light output due to the etching of tungsten form filament and the formation of black deposit on the inner wall of the bulb. The evaporated tungsten is removed and redeposited on the tungsten filament by the halogen gas present inside the bulb of the QTH lamp. The intensity of this source is very high compared to a standard tungsten filament incandescent lamp [1]. The range of light put out by this source is from 400nm – 5000nm (25,000 to 2000 cm^{-1}). Figure 4.2 shows spectral output of a popular commercial quartz tungsten-halogen lamps with model number 6315 from Newport (1000 W, 120 VDC operation, flux output of 27500 Lumens, 3200 K color temperature, 300 hour average life) [2].

While some of the mid infrared sources emit light above 25000nm, the intensity drops off for higher wavelengths. High pressure mercury discharge lamp is a very useful source in the far infrared region. Elemental Hg, a small amount of inert gas, and two electrodes are included inside a quartz bulb. Mercury is vaporized, exited and ionized on passage of a current, forming a plasma discharge at high pressure.

Solid-state diode lasers with wavelengths in the near infrared region are available which are capable of emitting a very intense monochromatic radiation. Laser have high intensity and narrow line width, hence they offer high signal to noise ratio for many application. These diode lasers have found application in near infrared food and fuels analysis.

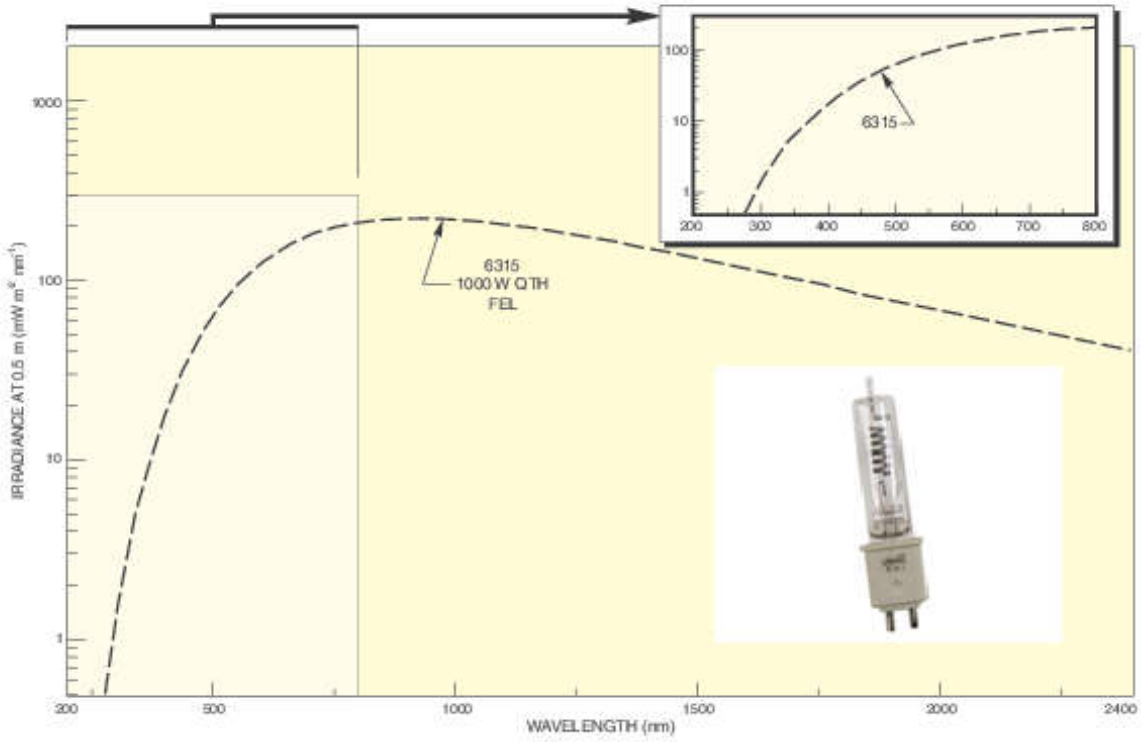

Figure 4.2: Spectral output of a 6315 quartz tungsten-halogen lamp (Courtesy of Newport Corporation, Irvine, USA)

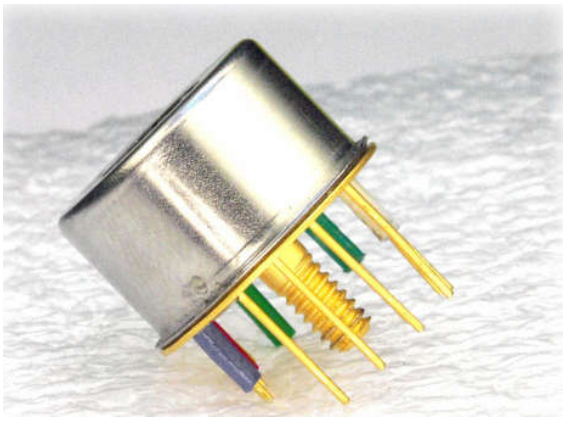

Figure 4.3: Febry perot laser diode LD200 in TO-8 package (Courtesy of IBSG Co. Ltd, Russia)

4.1.2 Monochromator for Spectroscopic Measurement

Much versatile optical instruments can be designed with a monochromator, the primary function of a monochromator is to provide a beam of radiant energy of a specific wavelength and spectral bandwidth. A Monochromator generally consists of following

components namely entrance slit, collimator lens, dispersive elements and exit slits. Lenses are used to collect radiation from a source and direct it to the monochromator entrance slit. Entrance Slit provides narrow path for the radiation to pass. Collimator lens makes parallel the light spreading from the entrance slit. Exit slit separates the desired spectral band by blocking all other dispersed radiation except that within a given resolution element. Gratings or prisms are the usual choice used to disperse the incident light. Many near infrared instruments utilize a reflective diffraction grating for dispersal of light. Diffraction Gratings consist of a series of closely spaced parallel grooves cut (or ruled) into a hard glass, metallic, or ceramic surface. Both flat and concave surfaces are used, and are coated on the ruled surface with a reflective coating. A grating for UV and visible regions will contain 500 - 5000 grooves/mm, while a grating for the IR region will have 50 - 200 grooves/mm. The dispersion of light is the result of diffraction of light at the surface of a grating. Diffraction of light occurs because of constructive interference between reflected light waves. The path of one wave is shown in figure 4.4. Parallel waves can be visualized on adjacent grooves. Constructive interference or diffraction of light occurs when,

$$\mathbf{n\lambda = d(\sin i \pm \sin \theta)} \qquad \mathbf{(4.1)}$$

where n is the order of diffraction (n is a integer 1, 2, 3. . .), λ is the wavelength of the radiation, d is the distance between adjacent grooves, i is the angle of incidence of the beam of light and θ the angle of dispersion of light of wavelength λ made with the normal to the grating. For a particular value of n, but different values of λ, the angle of dispersion θ is different thus separation of light occurs because light of different wavelengths is diffracted at different angles.

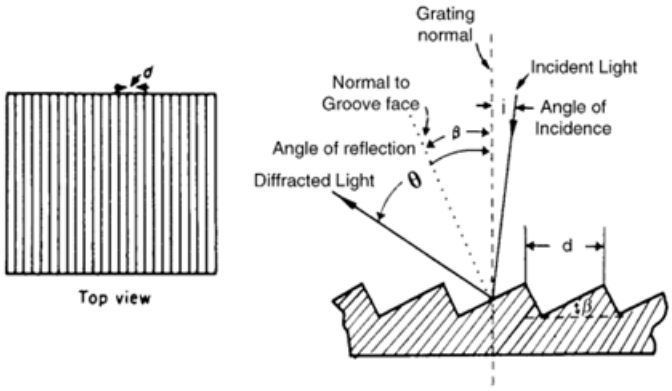

Figure 4.4: Reflective Grating

4.1.3 Sample Holder for the Infrared Region

First and foremost, the material used in the infrared instrument must be transparent to the infrared radiation. Secondly these materials must be strong enough for polishing and shaping into windows, samples cells, lenses etc. Common compounds used are potassium bromide, calcium fluoride, sodium chloride, and zinc selenide. The choice of which material to use for the above is determined by wavelength range of interest, as sodium chloride is transparent in the wavelength range 0.25 - 16μm it can be used over this range as a sample holder. Potassium bromide can be used over the range of 0.25–26 μm. The wavelength ranges of some materials used for IR optics and sample holders are given in table 4.1.

Table 4.1: IR sample holders

Material	Transmission range (μm)	Solubility (g/100 g water)	Refractive index
Sodium chloride (NaCl)	0.25–16	36	1.49
Potassium chloride (KCl)	0.30–20	35	1.46
Potassium bromide (KBr)	0.25–26	65	1.52
Barium fluoride (BaF2)	0.2–11	0.1	1.39
Cesium iodide (CsI)	0.3–60	160	1.74
Cesium bromide (CsBr)	0.3–45	125	1.66
Thallium bromide/iodide eutectic (KRS-5)	0.6–40	< 0.05	2.4
Silver chloride (AgCl)	0.4–25	1.5 x 10-4	2
Silver bromide (AgBr)	0.5–35	1.2 x 10-5	2.2
Germanium	2–11	Insoluble	4
Fused silica	0.2–4.5	Insoluble	1.47
Magnesium fluoride (MgF2)	0.5–9	Insoluble	1.34
Zinc sulfide (ZnS)	0.4–14.5	Insoluble	2.2
Calcium fluoride (CaF2)	0.4–11.5	Insoluble	1.3

Zinc selenide (ZnSe)	0.5–22	Insoluble	2.4
Magnesium oxide (MgO)	0.4–9.5	Insoluble	1.6
Cadmium telluride (CdTe)	0.9–31	Insoluble	2.7

NaCl and KBr are very popular for use as sample holder in the infrared range. As these are water soluble any moisture in the atmosphere can dissovle the polished surfaces, which makes the surface opaque and scatter light. Therefor these materials are stored in a desiccator. Sample provision is made for inserting the sample solution and is usually located immediately in front of the detector and after the monochromator. Cuvettes made of above materials with different optical path length are used. The sample holder section is a completely covered enclosure with the inner walls painted in black, this is done to block the ambient light.

4.1.4 Detectors for Infrared

Detectors in the infrared fall in two categories namely thermal detectors and photon sensitive detectors. The advantage of thermal detectors is that they have a flat spectral response but have a slow response time and low detection capability. Examples of thermal detectors include thermocouples, bolometers, thermistors and pyroelectric. The photon sensitive detectors have faster response times and higher detection capability but their spectral response are not flat.

Semiconductor materials are used for photon sensitive detectors. When an infrared photon is absorbed by a semiconductor material, an electron form the valence band is raised to the conduction band, which changes its conductivity greatly. This photon which is absorbed must have sufficient energy to raise an electron to the conduction band and hence the band gap determines the lowest wavelength which can be detected. Materials such as lead selenide (PbSe), lead sulfide (PbS), indium antimonide (InSb), indium gallium arsenide (InGaAs), and mercury cadmium telluride (HgCdTe/ MCT) are intrinsic semiconductors commonly used as detectors in the near and mid infrared regions. PbS photoconductor detectors are infrared detectors which make use of photoconductive effect i.e. the resistance is reduced when infrared light falls on it. PbS detector gives improved results if used with cooling but can also be used at room

temperature. This detector has faster response and superior detection capability in comparison to other detector of the same spectral range.

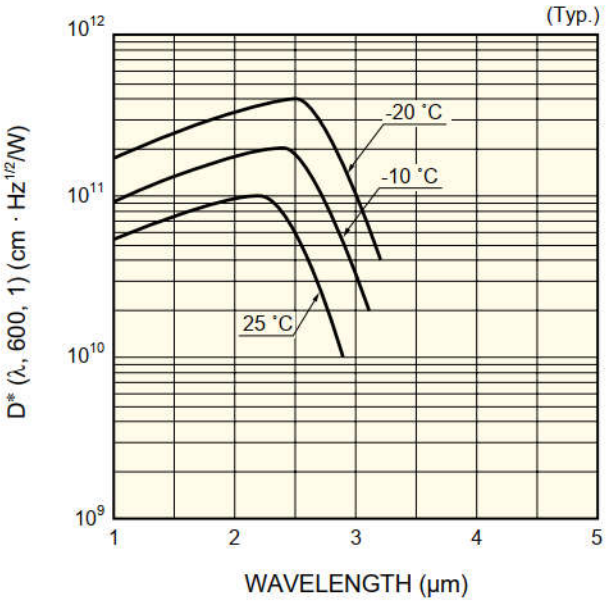

Figure 4.5: Typical spectral response of PbS detector (Courtesy of Hamamatsu photonics K.K.)[3]

Table 4.2: Infrared detectors (Courtesy of Hamamatsu Photonics K.K.)[3]

Detector	**Spectral response(µm)**	**Operating temperature(K)**
Thermocouple/Thermopile	Flat response	300
Bolometer	Flat response	300
Pyroelectric detector	Flat response	300
PbS	1 to 3.6	300
PbSe	1.5 to 5.8	300
InSb	2 to 6	213
HgCdTe (photoconductive type)	2 to 16	77
Ge	0.8 to 1.8	300
InGaAs	0.7 to 1.7	300
Ex. InGaAs	1.2 to 2.55	253

InAs	1 to 3.1	77
HgCdTe (photovoltaic type)	2 to 16	77

4.2 Measurement of Glucose Absorption

For our study we have used the Jasco V-770 spectrophotometer with extended range. It is a dual beam spectrophotometer with a Czerny-Turner grating mount. It houses two radiation sources namely Halogen lamp and a Deuterium lamp and can be operated in the wavelength range of 190 to 3200 nm. Key features are outline in the table 4.3.

Table 4.3: V-770 UV-Visible Spectrophotometer specifications

Optical System	Fully symmetrical double-beam Single monochromator Czerny-Turner grating mount
Wavelength range	190 to 3200 nm*
Wavelength accuracy	+/-0.3 nm (at 656.1 nm) +/-1.5 nm (at 1312.2 nm)
Wavelength repeatability	+/-0.05 nm (UV-Vis), +/-0.2 nm (NIR)
Light Source	Halogen lamp, Deuterium lamp
Spectral bandwidth (BW)	NIR: 0.4, 0.8, 1, 2, 4, 8, 20, 40 UV-Visible: 0.1, 0.2, 0.5, 1, 2, 5, 10 nm
Photometric range	NIR: -3~3 Abs UV-Visible: -4~4 Abs
Baseline flatness	+/-0.0002 Abs (200 - 2500 nm)
Baseline stability	0.0003 Abs/hr (Wavelength: 250nm response: slow and BW: 2nm)
Scanning speed	10-4000 nm/min (8000 nm/min in preview mode)
RMS noise	0.00003 Abs (0 Abs, wavelength: 500 nm, measurement time: 60sec, BW:2nm)

Power requirements	150 VA
Detector	PMT, Peltier cooled PbS
Installation requirements	Temperature required: 15-30 °C, humidity: below 85%

* Specially ordered JASCO V770 spectrophotometer with extended range for our application.

The absorbance and transmission recording is done on the spectrophotometer using spectra manager software provided by Jasco [4]. To start we select the spectra measurement utility under the spectra manager. Starting the spectra measurement displays the window as shown in figure 4.6. We need to specify the parameters for the spectrophotometer operation. The photometric mode can be choosing between absorbance, transmittance and reflectance using the corresponding drop down menu in the parameters panel as shown in figure 4.7.

The operation range is set using the start and end wavelength field anywhere between 190nm to 3200nm. Desired scan speed, bandwidth and response time can be selected using the corresponding drop down menu. Spectra analysis utility also bundled in the spectra manger allows smoothening of noisy spectra as shown in figure 4.8.

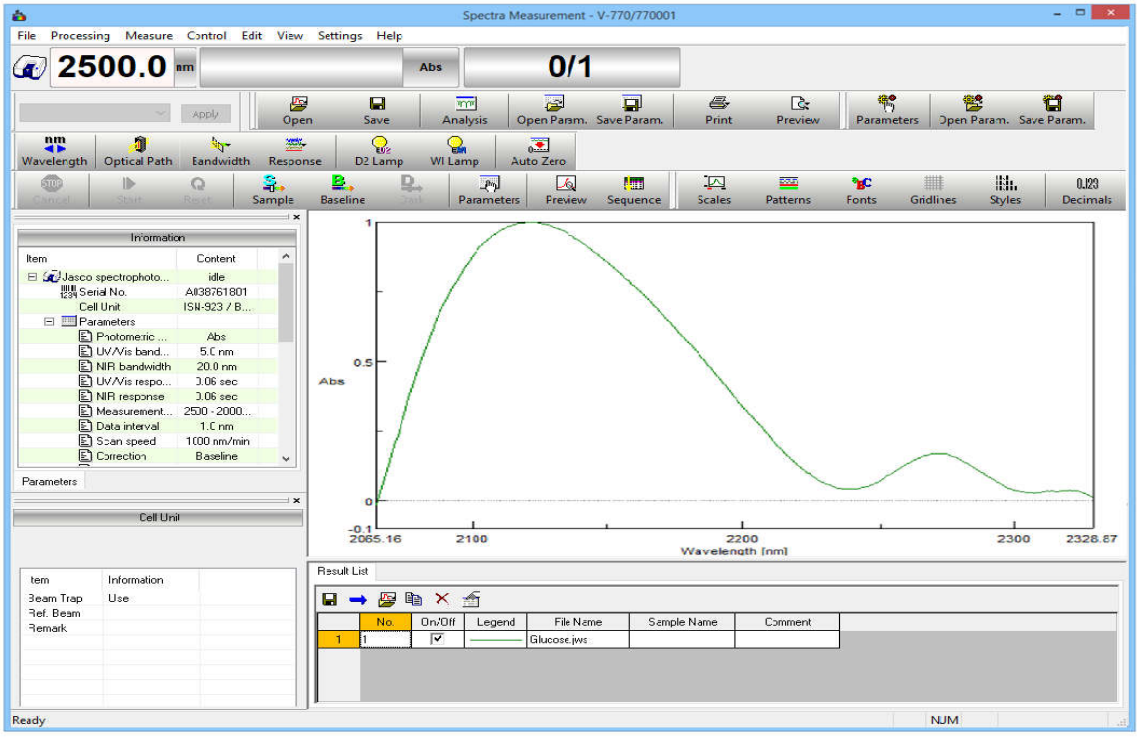

Figure 4.6: Spectra Measurement utility

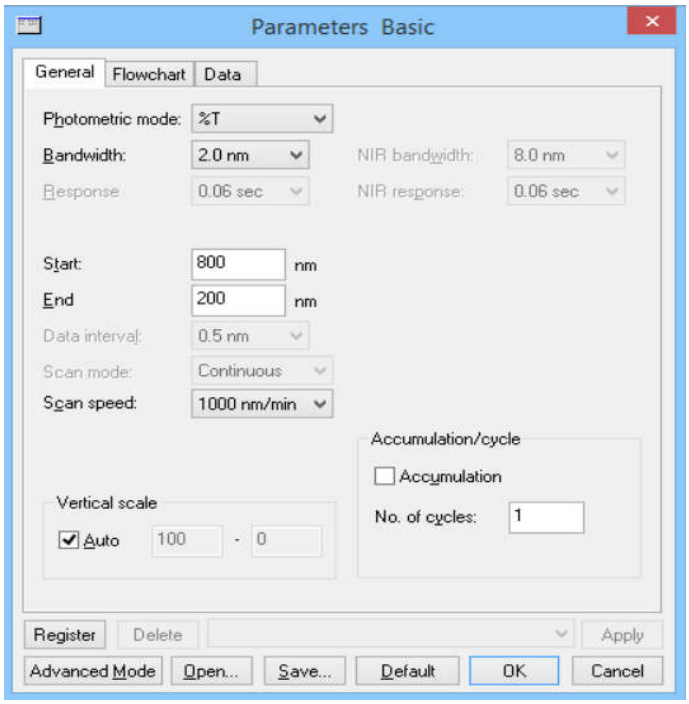

Figure 4.7: Parameters Panel

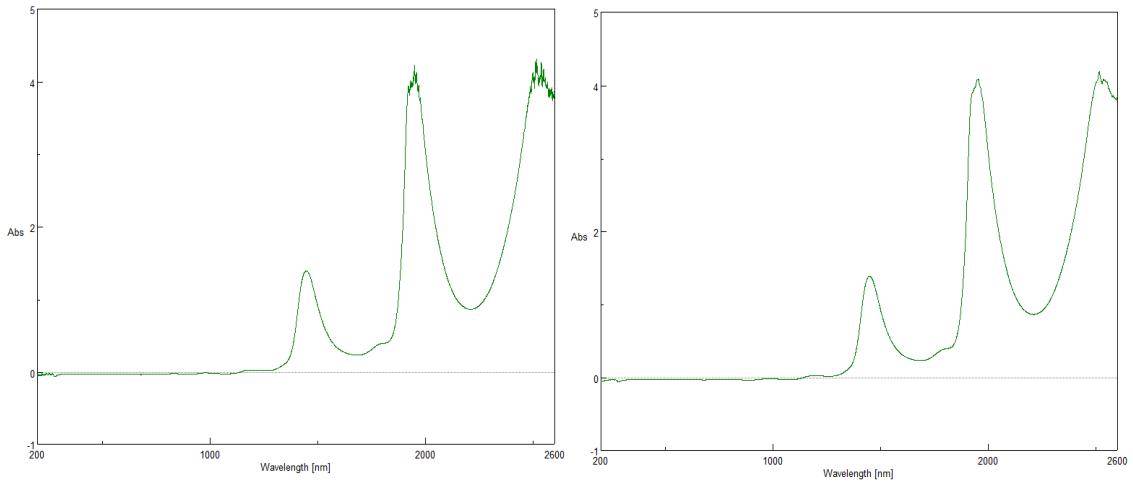

Figure 4.8: Smoothening of water spectra using spectra analysis

4.3 Sample Preparation

To simulate the blood matrix we prepared laboratory samples containing five of the major blood constituents namely glucose, urea, lactate, ascorbate and analine. Each aqueous sample contained all the above constituents in varying composition. The physiological relevant ranges of the above constituents were chosen for our experiment. Glucose ranges 70–280 mg/dL, analine ranges 10–28 mg/dL, urea ranges 11–20 mg/dL, lactate ranges 12–22 mg/dL and ascorbate 2–5 mg/dL. Instead of preparing deciliter of

solution we prepared 10ml of solution and the concentration was scaled proportionally to reflect the above physiological ranges. The above constituents are measured, using a precision weighing machine having an error accuracy of 0.01mg. A total of 64 samples were prepared for the purpose of experiment. Typical 15 of the 64 samples are shown in the table 4.4 below.

Table 4.4: Laboratory samples

Sample No	All above reading are in mg/dL				
	Urea	Lactate	Ascorbate	Analine	Glucose
1	11	12	2	10	70
2	11	22	2	10	70
3	20	12	2	10	70
4	20	22	5	28	70
5	11	12	5	10	100
6	11	22	5	10	100
7	20	22	2	28	100
8	11	12	2	28	200
9	11	22	2	10	200
10	20	12	5	28	200
11	20	22	5	28	200
12	11	12	5	28	280
13	11	22	5	10	280
14	20	12	5	10	280
15	20	22	5	28	280

4.4 Path length consideration

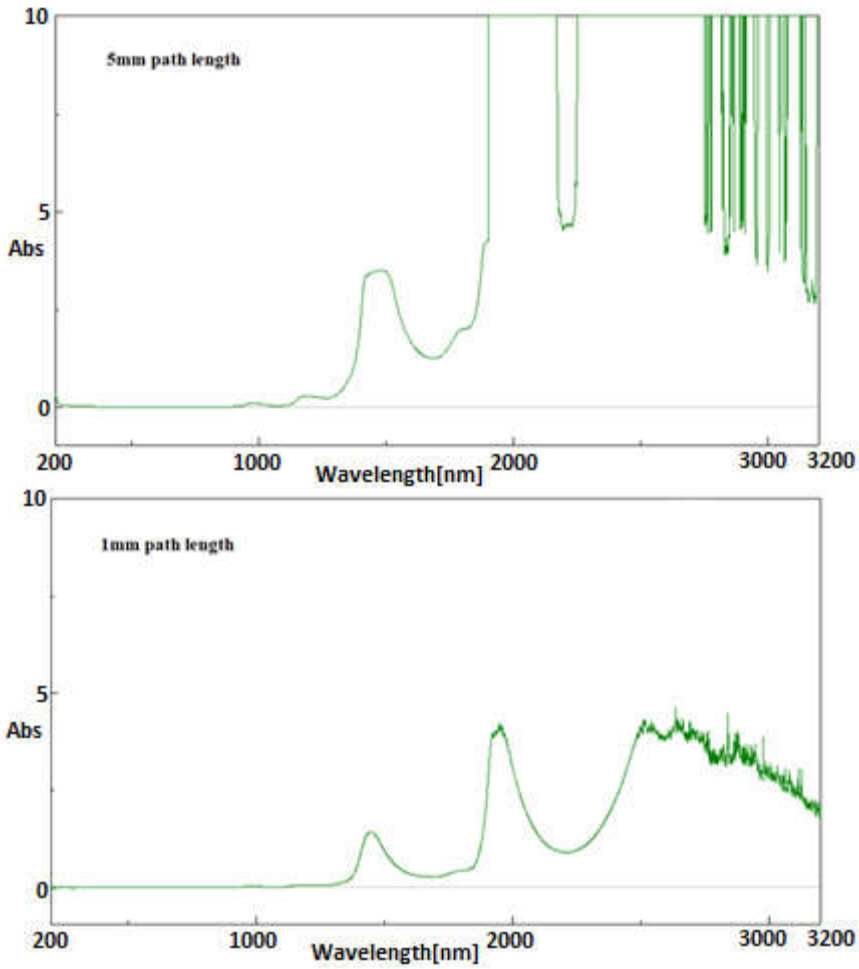

Figure 4.9: Absorbance spectra for 5mm and 1mm path length cuvette

Water exhibits absorption peaks in the infrared region, and the overall absorption of water shows a rising trend from the near infrared to mid infrared region. As water is the major component of human tissue, it is impractical to use mid infrared region for glucose estimation. The water absorption in near infrared region is relatively lower as compared to mid infrared region, but the path length of the sample holder plays a significant role in our studies. Figure 4.9 show the absorbance spectrum of water recorded in quartz cuvette of path length 5mm and 1mm. We can clearly see higher noise in the spectrum for water in 5mm path length. In the 5mm cuvette the noise is so large above 1900 nm, that it is safe to assume that light is completely absorbed by the water. Therefore, all our studies are conducted using a 1mm quartz cuvette.

4.5 System Design

Figure 4.10 gives the block diagram of the system. Jasco V-770 UV-VIS-NIR spectrophotometer forms the front end of our system.

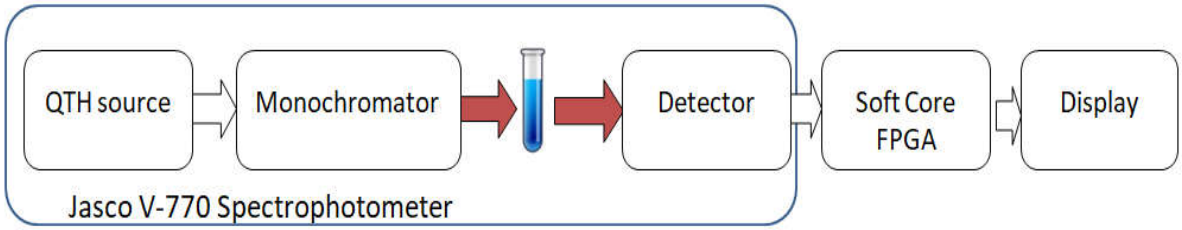

Figure 4.10: Block Diagram

The light source used is deuterium (D_2) lamp (187 to 350nm) for use in the UV region and a QTH (Halogen) lamp (330 to 3200nm) for use in the Visible and NIR region. The spectrophotometer houses a dual beam configuration and uses a single monochoramator. The light exiting the monochromator is split into two beams by a select mirror, one going to the target sample to be measured and the other to the reference sample. The beams are alternately incident on the detector i.e. photomultiplier or Peltier cooled PbS photoconductive detector.

The target sample and the reference are placed in a 1 mm quartz cuvette. As outlined above the aqueous samples contain the 5 different blood constituents. The absorbance spectrum is recorded for each sample. These spectra are then transferred to the soft-core FPGA platform.

We use the DE-0 Nano board which houses a Cyclone – IV FPGA to port a NIOS-II soft core, a 32-bit embedded processor. The building of the soft-core is discussed in detailed chapter 5.The PLSR algorithm is used to build the calibration model on the NIOS-II and the same calibration model is used to predict the concentration of the unknown sample, which are sent to the display device.

References

[1] J. W. Robinson, E. S. Frame, G. M. Frame II, “Undergraduate Instrumental Analysis”, CRC Press, 2014.

[2] “Oriel Product Training”, Newport Corporation [Online] Available at: https://www.newport.com/medias/sys_master/images/images/hfb/hdf/8797196451870/Light-Sources.pdf.

[3] "Technical information SD-12 Characteristics and use of infrared detectors", Hamamatsu PhotonicsK.K., [Online] Available at: https://www.hamamatsu.com/resources/pdf/ssd/infrared_kird9001e.pdf

[4] "V-770 UV-Visible NIR Spectrophotometer Specifications", JASCO Inc., [Online] Available at: https://jascoinc.com/ products/spectroscopy/uv-visible-nir-spectrophotometers/specifications/

The Field Programmable Gate Array (FPGA) is highly configurable logic device. The logic density is much higher than those offered by its predecessor such as Complex Programmable Logic Device (CPLD). Due to the versatility offered by FPGA, many are adopting it in product design. This chapter outlines the different steps required to configure a soft-core processor on an FPGA for our application of glucose estimation.

5.1 FPGA for Estimation of Glucose

The name of FPGA originates from the fact that a user can deploy a gate array that is programmable on the field of any workplace [1]. Broadly an FPGA consists of Configurable Logic Blocks (CLBs) with user programmable interconnect which enables developers to customize them for their application. This customization can be reprogrammed, if need arises in the future to accommodate new features in the application. Currently FPGA solutions are offered by Altera (Intel), Xilinx, Lattice semiconductor, Cypress, Microchip technology and Microsemi.

In FPGA the digital function is not implemented using AND and OR planes, instead a logic block is used for implementation of relatively large complex logic circuit. An FPGA consists of a huge number of independent CLBs, configurable I/O blocks, and programmable interconnection path. Depending on the manufacturer, the CLB may also be referred to as Logic Block (LB), a Logic Element (LE) or a Logic Cell (LC). All the resources of the device are uncommitted and these must be selected, configured and interconnected by a user to form a logic circuit for their application.

The various families of FPGAs manufactured by different manufactures differ primarily in the number of logic modules (form few hundred to hundreds of thousand), supply voltage range, power consumption, speed, architecture, process technology, number of pins, and type of packages, etc. The basic architecture of FPGA consists of an array of CLBs [2]. The logic blocks are surrounded by configurable input/output blocks [2]. There are rows and columns of programmable interconnection paths. The I/O blocks can be individually configured as input, output, or bidirectional. The architecture of FPGA is shown in Figure 5.1.

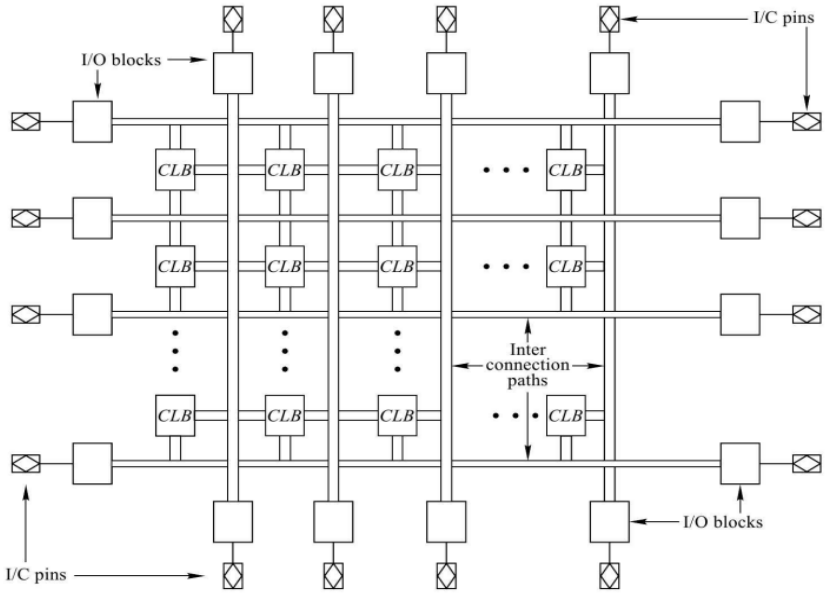

Figure5.1: The FPGA architecture [2]

5.1.1 Configurable Logic Blocks

The configurable logic blocks in FPGA are organized as an array of rows and columns. The logic blocks are connected to the I/O blocks through common row/column programmable interconnects. The common row/column interconnects are known as global interconnects. A logic block consists of a number of logic modules. The logic modules are the basic logic elements in an FPGA. The logic modules within a CLB are connected through local programmable interconnects. Figure 5.2 shows how a basic configurable logic block looks like.

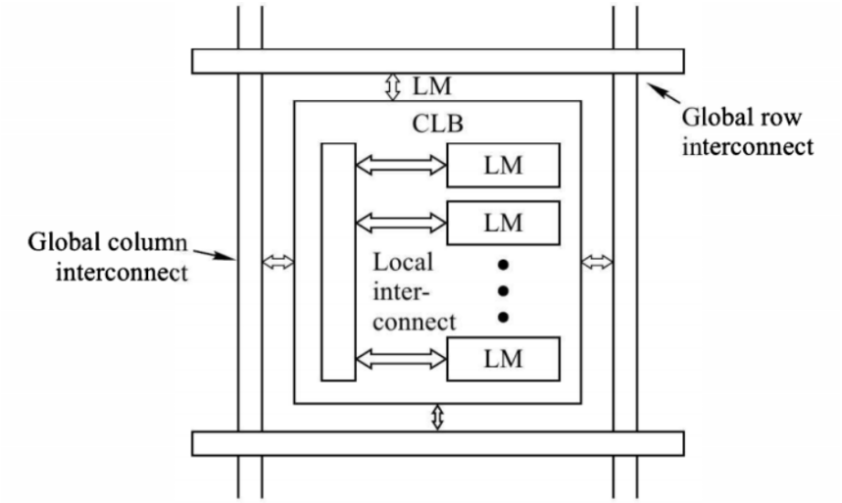

Figure5.2: Configurable logic block [2]

5.1.2 Logic Module

A logic module consists of a Look Up Table (LUT), a D-type flip-flop and a Multiplexer (MUX). Most of the FPGAs are based on 4 inputs LUT. Figure 5.3 gives the block diagram of a logic module with a 4 input LUT. Output of the LUT becomes the output of the logic module either directly or indirectly through a D-type flip-flop. Thus the output can be configured for combinational or registered.

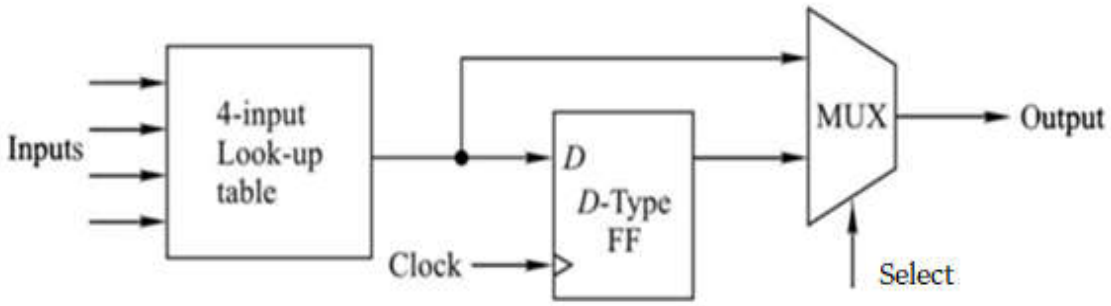

Figure5.3: A logic module [2]

5.1.3 Look Up Table

An LUT consists of a programmable memory and it can be used to generate logic function in SOP form. Figure 5.4 shows a LUT. It consists of a memory and a MUX. Since, it is an 8-bit memory, we require a 8:1 multiplexer. Larger LUTs would allow for more complex logic to be performed per logic block, thus reducing the wiring delay between blocks, as fewer blocks would be needed. This will require larger multiplexer and an increased chance of waste if all the functionality of larger LUTs were not to be used. On the other hand, smaller look up tables may require a design to consume a larger number of logic blocks, thus increasing wiring delay between blocks. Hence 4 input LUT structure makes the best tradeoff between area and delay for a wide range of applications. However, some FPGAs vendors have started offering 6 input LUT structure.

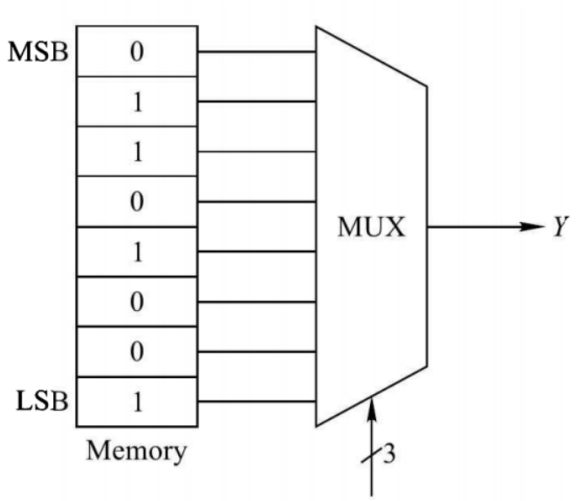

Figure5.4: A 3 input look up table [2]

5.2 Soft-core Processor for Embedded Systems

An Embedded system consists of software and hardware working to achieve a dedicated task. They have formed an integral part of our modern society and they play a vital role in our present gadget driven age. They find application in many places as entertainment electronics, automobiles, medical device, industrial control systems etc [3]. The core components of an embedded system are microprocessor/microcontroller, an on-board memory, an output device, an input device (for a user to enter data and control the device) and firmware (application software which runs on the above hardware). As manufactures are pushing for mobility and miniaturization, the embedded system designer has to adhere to tight constraints on area usage, size, power consumption and performance. The modern market requirements have also imposed tight time to market deadlines [4]. In order to reduce the time to market deployment, the designer need to reduce the time spent on development and debugging and this is done by using a hardware/software co-design methodology[5].

Designing each and every hardware component of the embedded system from scratch becomes time consuming, impractical and expensive for an embedded designer as the complexity of the embedded system increases. Hence, the prospect of using pre-designed and pre-tested Intellectual Property (IP) soft-cores in the application became more and more attractive. Soft-core processors are microprocessor with their architecture completely specified using Hardware Description Language (HDL). FPGA

are the most popular programmable hardware which are used to instantiate a soft-core processor.

The first stage in design flow of any design of soft-core processor is the description by a HDL. After this stage, synthesis and transformation of the design is carried out to form a configuration file for the FPGA. Once the configuration file is transferred to the FPGA it is transformed in to the required soft-core [7-13]. After the FPGA is configured as a soft-core processor, we use standard techniques to program a traditional discrete processor to harness its capabilities. Programming languages and Integrated Development Environments (IDE) are used for the above purpose. Many of the traditional peripherals such as memory, switches, buttons, LEDs, etc. which were interfaced with the discrete microprocessor, can also be interfaced with the soft-core processor. The interface logic required for the application can also be instantiated in the FPGA along with the soft-core processor as shown in the figure 5.5.

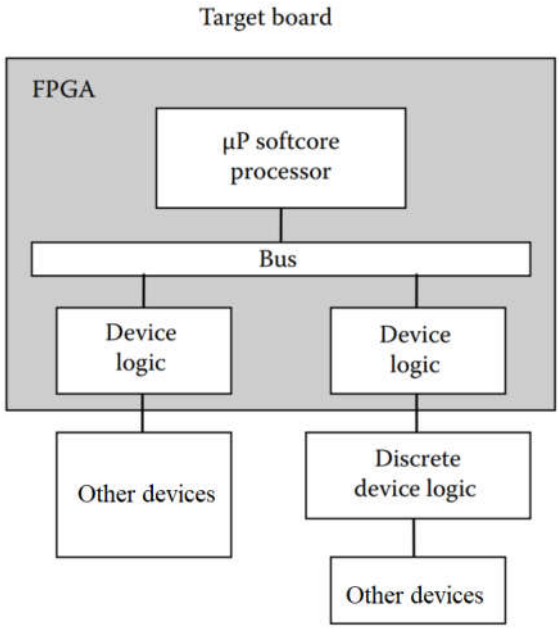

Figure 5.5: Interfacing of devices to a soft-core processor [7]

Many of the market players who offer FPGA solution, also supply these interface logic. The common interface logic used are General Purpose Input/Output(GPIO), Universal Asynchoronous Reciever/Transmitter(UART), Inter-Integrated Circuit(I^2C), Serial Peripheral Interface(SPI), etc. These logic interface packages offered by the different vendors are known as intellectual property or IP cores. These interface logic are also specified using a HDL. When a current day FPGA is configured as a soft-core

processor, it utilizes less than 1% of the resources present on it, which is contrary to the previous generation FPGAs. Many commercially available soft-core IP are available such as Nios II [14] by Altera [15], MicroBlaze [16] by Xilinx [17] and Mico32 [18] by Lattice [19].

Most of the vendors provide custom processor configuration tools, for example Altera has Quartus II software. This tool provides a graphical user interface for inclusion of different processor configuration and IPs for peripheral interfaces (PLLs, UART, etc.). For each component instanced, parameters can be specified. Other system features such as device memory address and IRQ numbering can also be specified. For Software development vendors also provide an IDE with assembler and C compilers necessary for the programming of these soft cores which are usually free to use.

5.2.1 ASIC v/s FPGA for soft-core

Different semiconductor devices can be utilized to realize a soft core. For instance an Application Specific Integrated Circuit (ASIC) or FPGA can be used to build a soft core. An FPGA affords flexibility and reusability, whereas ASICs are intended for specific applications such as a chip design for a digital voice recorder, DVD player and charge controller for lithium ion batteries.

To use an ASIC as a soft core, a gate level netlist is synthesized of the soft-core and any other desired logic. Logic gates are placed and routed as per the netlist, and from it photomasks are realized to fabricate the chip. To realize a soft-core on a FPGA, similar netlist is used to generate a configuration file, which is then used to configure the look up tables and configurable logic block present on a FPGA.

5.3 A survey of Soft-core processors

The various soft-core processors which are in the market today and various offering by the open source communities are described below.

5.3.1 Commercially Available Soft-cores

Altera and Xilinx are the major market players who offer FPGA solutions and NIOS-II, MicroBlaze and PicoBlaze are the soft-core solutions offered by them respectively.

NIOS-II soft core

NIOS-II is a 32-bit processor based on the popular Reduced Instruction Set Computer (RISC) architecture. There are thirty two 32-bit general purpose registers in NIOS-II soft-core [20, 21]. It employs load and store instructions to move data between memory and the large number of internal general purpose registers. The operation involving arithmetic and logic are performed in these general purpose registers. NIOS –II can also be used in the 16-bit instructions set mode, this improves the code density of the processor. Some 16 bit instruction can even be completed in 1 clock cycle. The performance of Altera FPGA is 30 to 80 MIPS. The NIOS-II is based on Harvard architecture as it has individual instruction and data buses [22].

The data path can be configured to either 16-bit having 1100 LEs or 32-bit having 1700 LEs. Byte addressing can be chosen to be either little endian or big endian. This must be selected at the configuration time. NIOS–II can function in three different modes. Any application runs in either user or supervisor mode. Figure 5.9 shows the NIOS-II soft core.

• Debug mode – allows features such as watch points and breakpoints used by software debugging tools.

• User mode – This mode prevents the execution of some instruction intended for system purpose only. Some of the features offered by the processor are also not accessible in this mode.

• Supervisor mode –On reset the processor enters the supervisor mode which allows it to execute perform all the possible functions and execute all the possible instructions

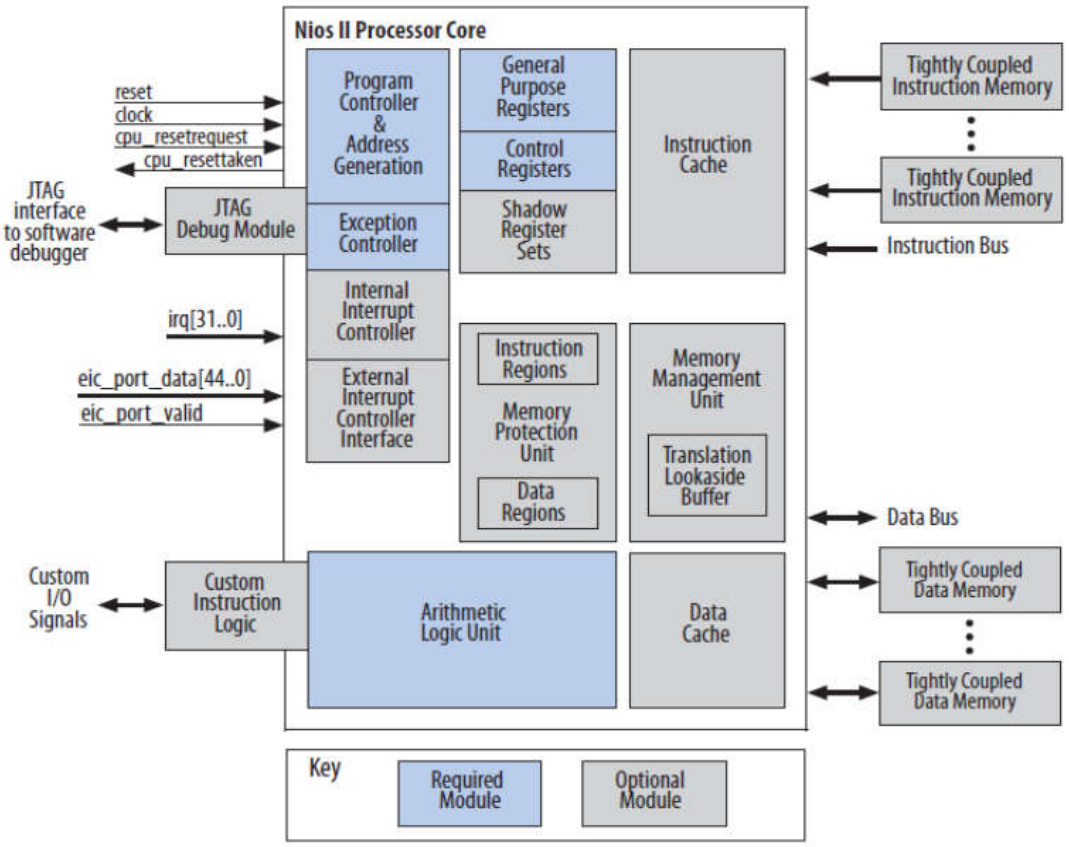

Figure 5.6: NIOS II soft-core Processor

It is feasible to build, debug & run software of a number of platforms utilizing the associated CAD tools such as Quartus II and Qsys system development tool. These tools help in rapid evaluation and development (validation / verification) of the embedded system. NIOS-II processor can be configured as per the requirements of the user, as such it offer three different configurations. The comparison between NIOS II Economy, Standard and Fast Processors is shown in table 5.1.

Table 5.1: NIOS-II versions

Features	**NIOS- II Fasts**	**NIOS- II Standard**	**NIOS- II Economy**
Objective	Optimized for high performance	Balanced for size and speed	Optimized for size
Logic Elements used	1400-1800	1200-1400	600-700
Caches(Instruction/ Data)	64 KB/64 KB	64 KB/None	None
Pipeline stages	6	5	1

Hardware Multiply	1 Cycle per MUL	3Cycles per MUL	Software Emulated
Custom Instruction	256 Custom instructions		

The number of Logic elements utilized are balanced in the standard configuration as compared to the others. The Hardware Multiply uses 3 Cycles/MUL unlike the fast variant having 1 Cycle/MUL. The NIOS II standard configuration provides real-time, high performance and deterministic results.

Micro Blaze and Pico Blaze

Xilinx offers the Spartan and Virtex families of FPGA solution. To go with these FPGA solutions, it also provides the soft IP cores needed for the optimal use of these FPGAs. MicroBlaze is a 32-bit soft-core optimized for embedded systems. It is based on Harvard architecture and can operate at up to 200MHz on a Vertex-4 FPGA chip. In addition, it features a three stage pipelining, 32-bit instructions, thirty two 32-bit general purpose registers, two levels of interrupts and a shift unit. On-chip Peripheral Bus (OPB) is used to interface on-chip and off-chip memories and other peripherals with the MicroBlaze soft-core[23].

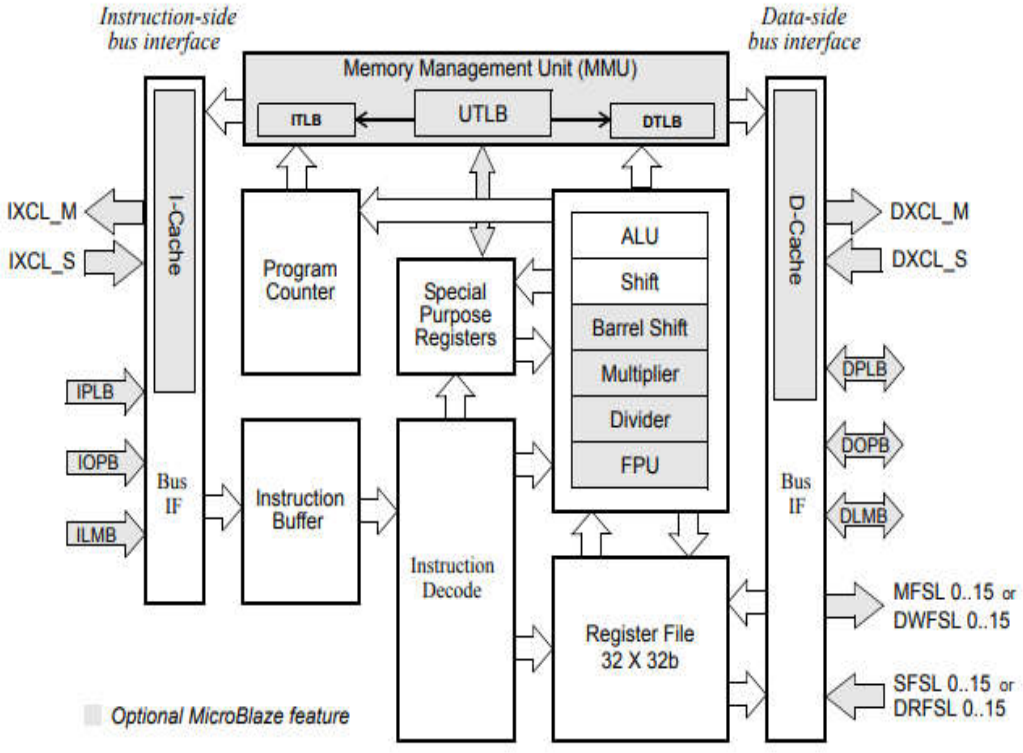

Figure 5.7: MicroBlaze soft-core block diagram [23]

Embedded Development Kit (EDK) by Xilinx is used to develop embedded application on MicroBlaze [23]. EDK bundle includes the Xilinx platform studio and a number of IP cores needed for MicroBlaze. PicoBlaze, an 8-bit offering of Xilinx which is intended for simple data processing applications. This processor is optimized for the Virtex-II, Virtex-II Pro and Spartan-3 series of FPGA [24].

5.3.2 Open-Source Cores

The open-source communities provide open-source cores which are free for use and do not require licensing [25]. The academia utilizes these cores heavily for research purposes and for development of embedded systems. An example of such an open-source core is the UT NIOS which is very popular in the academia [26]. Another core which is provided by Sun Microsystems is OpenSPARC processor which is heavily used in ASCI designs, but can also be used on an FPGA [27]. Below we discuss the LEON and OpenRISC 1200 cores which are readily available for the open-source community.

OpenRISC 1200

OpenRISC is one of the most popular open core, and features 32-bit and 64-bit RISC architecture which can finds its use in many automotive, consumer products, home entertainment and networking applications [25]. This processor is based on Harvard architecture with separate data and instruction caches of 8 KB each. It features a 32-bit instruction set architecture containing the OpenRISC basic instruction set, a five stage pipeline with most instruction requiring a single clock cycle. This processor can be utilized in wide range of applications and is optimized for high performance and low power consumption. Many real time operating systems are supported such as OAR RTEMS RTOS, µLinux and Linux. Many C/C++, Java and Fortran software development tools are available to develop embedded application on the OpenRISC.

LEON

LEON soft-core IP are provided by Gaisler Research along with the supporting development tools and is based on the SPARC V8 instruction set architecture [26]. Once synthesized on a target it requires the associated library called the GRLIB IP library [28]. Many successive version of this processor are developed by Gaisler Research such as the LEON2and theLEON3 processors.

5.3.3 Comparative Study of the Soft-cores

Companies such as Altera, Xilinx, Cypress, Lattice, and Microchip offer soft-cores customized to their FPGA solutions. NIOS-II, MicroBlaze, OpenRISC 1200, and LEON3 are few of the popular soft-cores. The NIOS-II features an expandable instruction set with up to 256 customizable instructions whereas MicroBlaze is not provided with this kind of ability. The highest operating frequency on an FPGA can be achieved with the NIOS-II and MicroBlaze. Both the NIOS-II and MicroBlaze are optimized for FPGA implementations, whereas the others are not optimized for a particular technology. Tabulated features and characteristics of different processor are given in table 5.2.

Table 5.2: Comparison of Soft-Core Processors

Category	NIOS II (Fast Core)	MicroBlaze	OpenRISC 1200	LEON3
Register File Size	32	32	32	2 to 32
Pipeline	6 Stages	3 Stages	5 Stages	7 Stages
Custom Instructions	Up to 256 Instructions	None	Unspecified limit	None
ISA	32-bit RISC	32-Bit RISC	32-bit RISC	32 or 64-bit RISC
Maximum frequency in MHz	200 (FPGA)	200 (FPGA)	300/185 (ASIC/FPGA)	400/125 (ASIC/FPGA)

5.4 DE-0 Nano Development Board

Figure 5.8: DE-0 Nano board

DE-Nano board is a FPGA platform featuring a powerful FPGA namely the Cyclone IV EP4CE22F17C6N [29]. It is apt for portable application due to its small compact size. This development board features a collection of interfaces such as general purpose input/output for extension of designs as well as on board SDRAM and EEPROM memory chips so that the application does not run out of data storage. In addition, push button and LEDs are included. If a design needs to have mobility, portable power is a necessity, therefore DE-0 Nano board offers 2 pin external power header for battery connection.

Table 5.3: Recourses of DE-Nano board [29]

Cyclone IV EP4CE22F17C6N FPGA	• 22,320 Logic elements (LEs) • 153 Maximum FPGA I/O pins • 594 Embedded memory (Kbits) • 4 General-purpose PLLs • 66 Embedded 18 x 18 multipliers
Configuration Status and Set-Up Elements	• FPGA Serial Configuration Device (EPCS) • On-board USB-Blaster circuit for programming
Expansion Header	• Two 40-pin Headers (GPIOs) provides 72 3.3V I/O pins • Two 5V power pins, two 3.3V power pins and four ground pins
Memory Devices	• 32MB SDRAM • 2Kb I2C EEPROM
General User Input/Output (GPIO)	• 8 green LEDs , 2 denounced push-buttons , 4 dip switches
G-Sensor	• ADI ADXL345, 3-axis accelerometer with high resolution (13-bit)
A/D Converter	• NS ADC128S022, 8-Channel, 12-bit A/D Converter
Clock System	• On-board 50MHz clock oscillator
Power Supply	• USB Type mini-AB port (5V) • Two DC 5V pins of the GPIO headers (5V) • 2-pin external power header (3.6-5.7V)

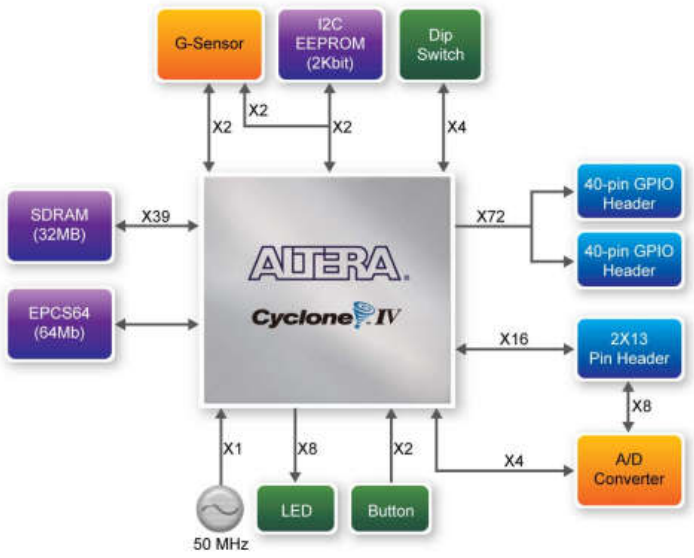

Figure 5.9: DE-0 Nano block diagram [29]

The table 5.3 gives the resources present on the board; all the features make this board most suitable for our application. Figure 5.9 gives the block diagram of DE-Nano board. In order to give the maximum flexibility, all the connections are accomplished through the cyclone IV FPGA. The Avalon switch fabric network provides the interconnection to all the components. Appropriate interfaces and IP cores are used to access various peripherals and memories such as SDRAM, I2C EEPROM, ADC, G-sensor, Dip switches, etc. present on the board.

5.5 Qsys System Integration Tool

Qsys system integration tool is supplied as a part of Quartus II CAD software. This tool is meant for the design of digital hardware systems which contain various components such as timers, input/output interfaces, memories and soft cores. Qsys automates the task of integrating various hardware components. Using traditional design methods one must put in a lot of man hours writing the HDL code for a desired design and its interconnections. Qsys Graphical User Interface (GUI) facilitates the process of adding the components by just a click-to-add the components and automatically generates the interconnect logic to connect these components together. Qsys generates HDL file that defines all the components of the system, as well as top-level HDL file that connects all the components together. User can choose either VHDL or Verilog as the choice of hardware description language [30].

5.5.1 SDRAM Interface to NIOS-II

For practical application such as ours we need to have large amount of memory. For this reason DE-Nano board features a SDRAM of 32 Mbytes or 256 Mbits of memory [29]. We need to interface this SDRAM chip with the NIOS-II soft core. The memory organization of this SDRAM is 4M x 16 bits x 4 banks. This SDRAM requires a careful timing control. In order to successfully access the SDRAM we need to include the SDRAM controller circuit IP through the Qsys system integration tool. This IP is located under memories and memory controller in the drop down menu on the left side of the user interface. All the necessary signals to successfully access the SDRAM chip are handled by it. The NIOS-II soft-core is connected to the memory and I/O interfaces through an interconnection network called as Avalon switch fabric. The figure 5.10 below shows a generic system which has instanced SDRAM controller along with few other peripherals.

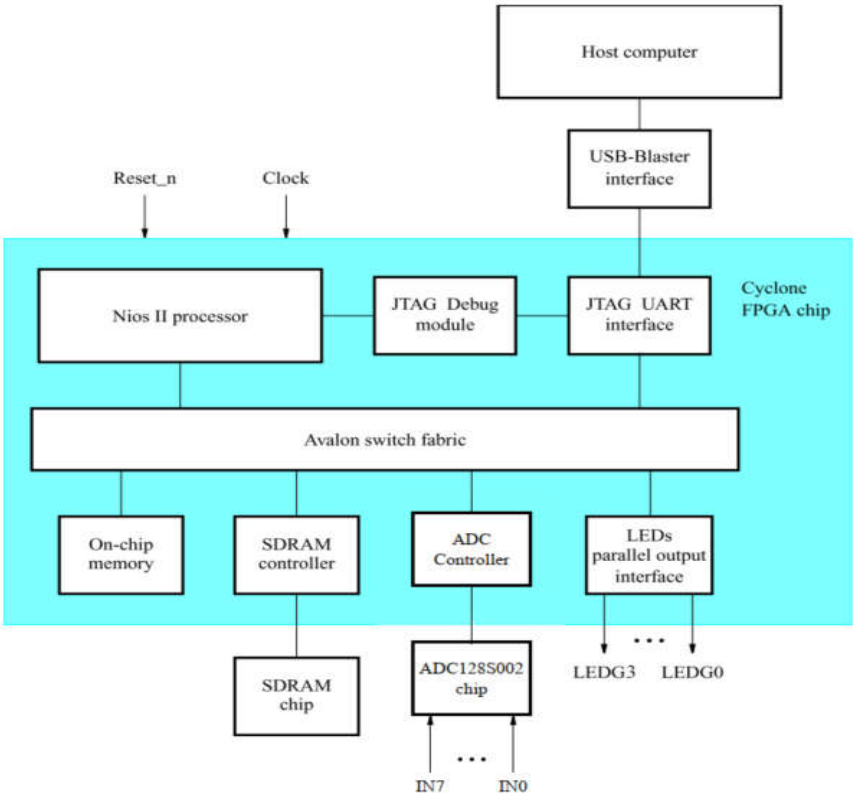

Figure 5.10: A generic NIOS-II system implemented on DE-Nano board

The necessary interface to access the SDRAM is shown in the figure 5.10. All necessary interface signals are generated by the SDRAM controller except the clock. The clock needs to be supplied separately and needs to meet the clock skew requirements. The

skew requirement need that the clock signal supplied to the NIOS-II processor lags the SDRAM clock by 3 nanoseconds [31,32]. This is accomplished by a phase locked loop circuit.

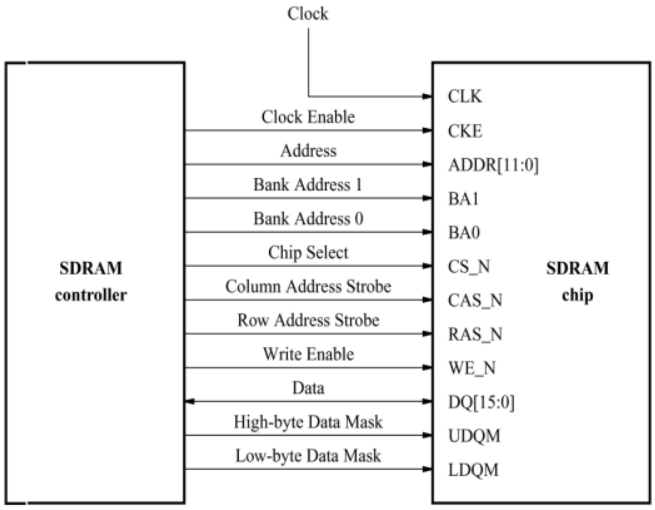

Figure 5.10: SDRAM controller interface [31]

5.5.2 ADC Controller Interface

The DE0-nano board is provided with an Analog to Digital Converter (ADC) onboard namely the ADC128S022 which provides eight channels with 12 bits of resolution. It is a successive approximation type and provides users with sampling rates of 50 to 200k samples per second. It comes with an internal track and hold circuit and an SPI interface. The 2x13 GPIO header which on the underside of the board is connected to the ADC.

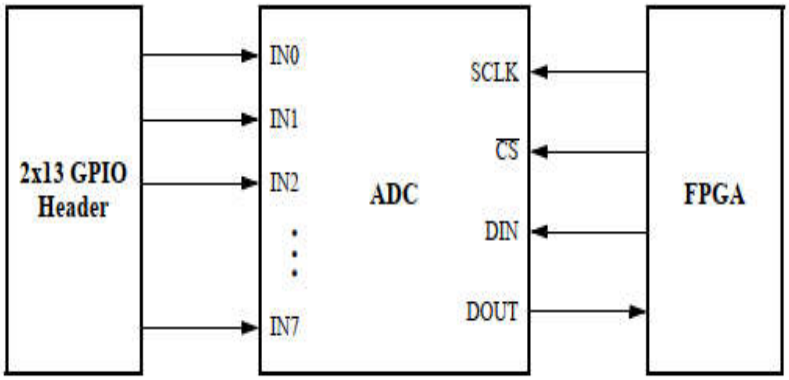

Figure 5.11: ADC128S022 interface to FPGA

Any analog signal (such as from temperature sensor) is fed to an ADC through one of the eight channels IN0 through IN7. The ADC connects to the FPGA through a four wire interface. The ADC is controlled by the SCLK and CS signals. The CS is used to select the chip and is an active low signal. SCLK is the clock signal required by the ADC. The DIN and DOUT pins are used to pass data and address between the chips. The SCLK frequency must be limited in the range of 0.8 to 3.2 MHz for proper functioning of the above ADC.

The DE0-Nano ADC Controller IP Core is used to interface with the above ADC and to provide the user with the digitized readings [33].The DE0-Nano ADC Controller IP core can be instantiated in a system using Qsys system development tool with its graphical user interface, and can be made part of the NIOS-II system. All the channels of the ADC are read in the ascending order once every cycle. The ADC controller core can define how many channels are active using a parameter called NUM_CH, which can be set by the user when the core is instantiated. Eight memory mapped registers, CH_0 to CH_7 are provided by the ADC controller for the reading and writing purpose. The controller must be operated by writing and reading from these registers. The core also allows users to specify the SCLK frequency and the desired range must be in the range of 0.8 to 3.2 MHz. For accessing the ADC reading each registers corresponds to each of the eight channels. If any channel is not in use, the respective register will have a zero constant. As soon as the conversion is complete the value is placed in the registers. This core is part of the university program IPs in the Qsys system integration tool. The ADC controller is also show in the generic NIOS-II system showed in figure 5.10 and interfaced through Avalon switch fabric network. The DE0-Nano ADC Controller core also comes with HAL C package to access the ADC. Figure 5.12 shows the NIOS-II instance generated in Quartus –II software along the ADC controller and SDRAM controller and figure 5.13 shows the hardware deployment of NIOS-II on DE-0 Nano board.

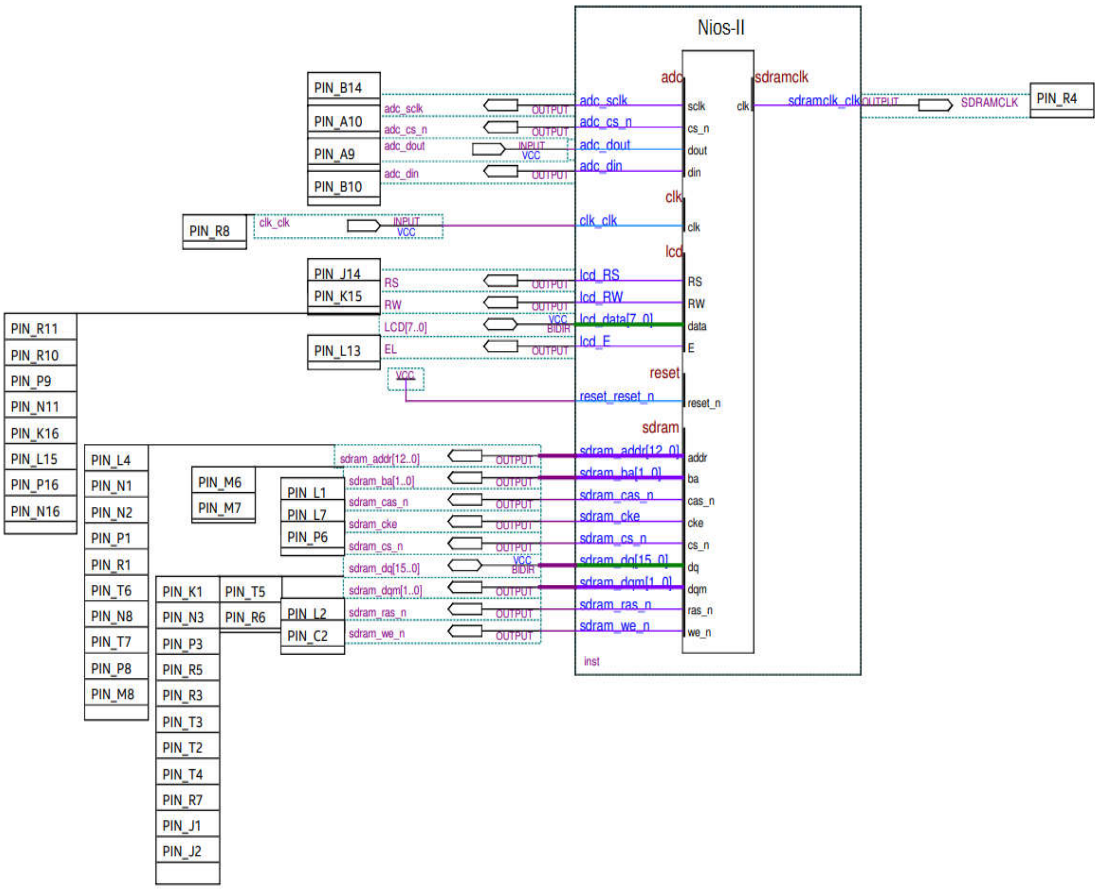

Figure 5.12: The NIOS-II instance generated in Quartus II software.

After compilation of the soft core, the programmer integrated in Quartus II software is used to program the user-specified SRAM object file (.sof) inside the FPGA. To estimate glucose we need to build calibration model which is done using PLS multivariate technique. **A 'C' program was ported to implement PLSR on the soft core. The same program is utilized to predict the unknown concentration of glucose for prediction samples.** To implement PLSR we have used the SIMPLS algorithm.

Figure 5.13: NIOS-II configured on DE-0 Nano board

5.5.3 Programming the NIOS-II Soft core

NIOS-II Software Build Tools (SBT) is used to program the NIOS-II soft-core which is built on the FPGA on DE-0 Nano board. It is collection of utilities targeted to build embedded C/C++applications for the soft-core. The C/C++ programming is accomplished using the Eclipse graphical user interface [34]. It provides identical support for both C and C++ development. It also provides editing, building and debugging for software development tasks. Nios II SBT provides Board Support Packages (BSP) which are specialized libraries containing system-specific support code. A BSP separates your application form details of systems such as memory map, processor configuration, available devices etc. The SBT also provides support for Altera Hardware Abstraction Layer (HAL). A UNIX like C/C++ runtime environment is provided by the HAL. The HAL also provides support for newlib C standard library routines, such as printf(). Figure 5.13 show the graphical user interface of NIOS-II SBT.

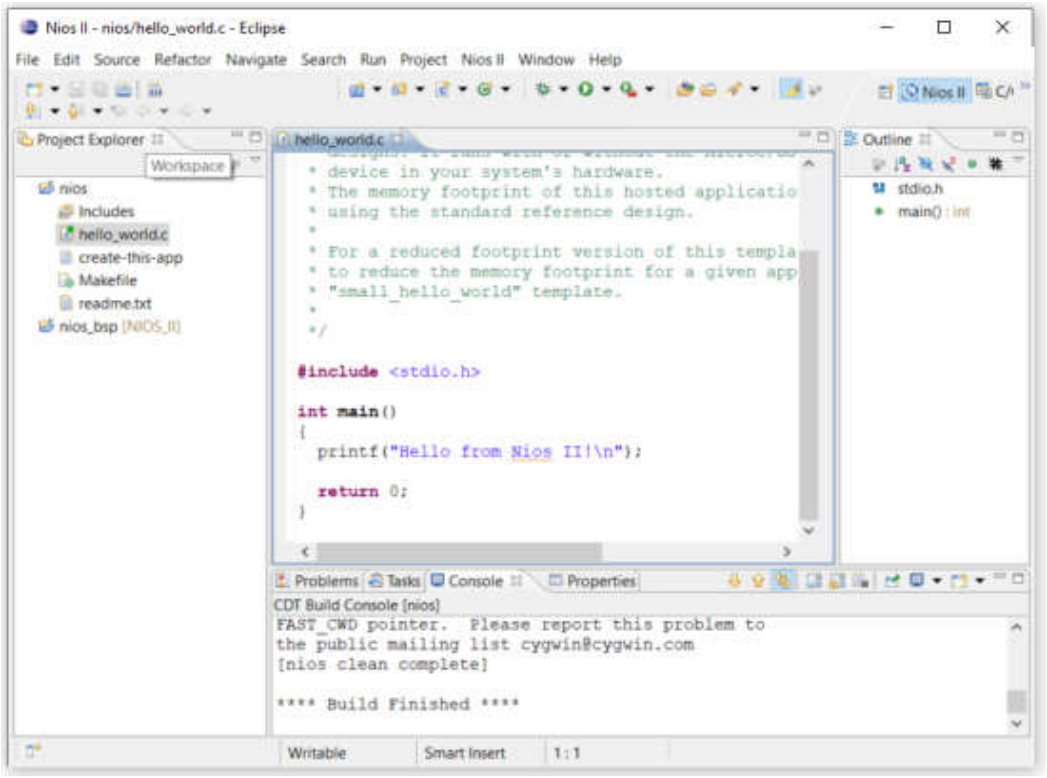

Figure 5.13: Graphical user interface of NIOS-II SBT

References

[1] H. Amano (Ed.), "Principles and Structures of FPGAs", Springer Singapore, 2018.

[2] R. P. Jain, "Modern Digital Electronics", Tata McGraw-Hill Education Pvt. Ltd., 2009

[3] P. Mishra, N. Dutt, "Architectural description languages for programmable embedded systems", IEE Proc. of Computers and Digital Techniques, Vol. 152, 2005, pp. 285–297.

[4] M. Chiodo, P. Giusto, A. Jurecska, H. C. Hsieh, et al. "Hardware-software codesign of embedded systems", IEEE Micro, Vol. 14, 1994, pp. 26-36.

[5] R. Ernst, "Codesign of Embedded Systems: status and trends", Proc. of IEEE Design and Test, 1998,pp. 45–54.

[7] B. M. Wilamowski (Ed.), J. D. Irwin (Ed.), "The Industrial Electronics Handbook", CRC Press, 2011.

[8] D. Arbinger, J. Erdmann, "Designing with an embedded soft-core processor", [Online] Available at: https://www.embedded.com/designing-with-an-embedded-soft-core-processor/

[9] "Soft Microprocessor", [Online] Available: http://en.wikipedia.org/wiki/Sof_processor

[10] "Listing of Soft Core Microprocessors", [Online] Available at: http://www.opencores.com/projects? cat=10&lang=0&stage=0&lic=0.

[11] "Field-Programmable Gate Array", [Online] Available at: http://en.wikipedia.org/wiki/Field-programmable_gate_array.

[12] "Soft Core Processor", [Online] Available: http://encyclopedia2.thefreedictionary.com/Sofcore.

[13] J.O. Hamblen, T.S. Hall, M.D. Furman, “Rapid Prototyping of Digital Systems, SOPC Edition”, Springer, 2008.

[14] “Altera Nios II Soft Core”, [Online] Available at: http://www.altera.com/nios2

[15] Altera company web page, [Online] Available at: http://www.altera.com

[16] “Xilinx MicroBlaze”, [Online] Available at: http://www.xilinx.com/microblaze

[17] Xilinx company web page, [Online] Available at: http://www.xilinx.com

[18] “Lattice Mico32”, [Online] Available at: http://www.latticesemi.com/en/Products/DesignSoftwareAndIP/IntellectualProperty/IPCore/IPCores02/LatticeMico32.aspx

[19] Lattice company web page, [Online] Available at: http://www.latticesemi.com

[20] “Nios II Processor Reference Guide”, [Online] Available at: https://www.intel.com/content/dam/www/programmable/us/en/pdfs/literature/hb/nios2/n2cpu-nii5v1gen2.pdf

[21] “Introduction to the Altera Nios II Soft Processor”, [Online] Available at: https://people.ece.cornell.edu/land/courses/ece5760/DE2/tut_nios2_introduction.pdf

[23] “MicroBlaze Processor Reference Guide”, [Online] Available at: https://www.xilinx.com/support/documentation/sw_manuals/xilinx11/mb_ref_guide.pdf

[24] “PicoBlaze 8-bit Embedded Microcontroller User Guide”,[Online] Availableat: https://www.xilinx.com/support/documentation/ip_documentation/ug129.pdf

[25] Website of Opencores.org, [Online] Avaialable at: www.opencores.org.

[26] UT NIOS Homepage, [Online] Available at: www.eecg.toronto.edu/˜plavec/utnios.html.

[27] “OpenSPARC T1 Microarchitecture Specification”, [Online] Available at: https://www.oracle.com/technetwork/systems/opensparc/t1-01-opensparct1-micro-arch-1538959.html

[28] “GRLIB IP Core User’s Manual”, [Online] Available at: https://www.gaisler.com/products/grlib/grip.pdf

[29] “DE-0 Nano User Manual”, [Online] Available at: https://www.ti.com/lit/ug/tidu737/tidu737.pdf

[30] “Introduction to the Altera Qsys System Integration Tool”, [Online] Available at: https://people.ece.cornell.edu/land/courses/ece5760/DE1_SOC/Introduction_to_the_Altera_Qsys_Tool.pdf

[31] “Using SDRAM on Altera’s DE0 Board with Verilog Designs”, [Online]Available at: ftp://ftp.intel.com/pub/fpgaup/pub/Intel_Material/12.0/Tutorials/Verilog/DE0/Using_the_SDRAM.pdf

[32] “Using SDRAM on Altera’s DE0 Board with VHDL Designs”,[Online] Available at: ftp://ftp.intel.com/Pub/fpgaup/pub/Intel_Material/11.1/Tutorials/VHDL/DE0-Nano/Using_the_SDRAM.pdf

[33] “Using the DE0-Nano ADC Controller”, [Online] Available at: ftp://ftp.intel.com/Pub/fpgaup/pub/ Intel_Material/16.1/Tutorials/Using_DE_Series_ADC.pdf

[34] “Nios II Software Build Tools”, [Online] Available at: https://www.intel.com/content/dam/www/programmable/us/en/pdfs/literature/hb/nios2/n2sw_nii52015.pdf

We are surrounded by complex phenomenon occurring around us, and in order to completely understand the underlying principle and to analyze them we need to employ multiple measurements. For instance, for successful prediction of the weather condition around us on a given day, myriad measurements needs to be carried out such as temperature, humidity in the atmosphere, wind conditions, pressure, etc. Using these measurements a model is built to predict the weather condition. The analysis of such a complex phenomenon necessitated the application of statistical methods called as multivariate techniques. When we consider only a single variable at a given instance of time we term it as univariate analysis. Many a times univariate analysis is not sufficient to understand a process or a system completely. A lot of information is lost when we employ univariate analysis. Hence we need to use multivariate analysis in order to bring out the hidden information lying latent in the available measurement data.

6.1 Multivariate Analysis

Multivariate techniques involve use of more than one variable at a given time in order to have a better understanding of a system. These techniques are efficient in identifying potential problems in a system and give an accurate insight of the behavior of data which is highly correlated. Multivariate techniques were an essential part of statistical analysis from the 1900s, but were not so popular. The advent of high speed computers and readily availability analytical software are responsible for the use of these techniques in different fields of research and industry.

The presence of overlapping spectral signatures in the NIR region as well as broad nature of these peaks rules out the use of univariate methods and calls for the use of multivariate calibration analysis to implement a successful prediction model. The process of multivariate calibration involves the relation of a chemical or physical property of interest to the spectral information by some mathematical model. Multivariate methods are found to be robust and enhance the selectivity of measurement. Sample containing multiple anlaytes are permitted for calibration in a multivariate analysis [1].

In our study spectroscopic measurements are done on a set of calibration samples; here calibration samples are those whose physical property of interest is determined using an independent reference method. These calibration samples and their reference readings

are together called as calibration data set. A mathematical model is formed using this calibration data set which relates the target property with the spectral data. This calibration model is then used for prediction of unknown values of the modeled property.

There are different multivariate calibration methods which can be employed for analysis in the near infrared region. The classical least-squares (CLS) and Inverse least-squares, multiple linear regression, Principal component analysis, Principal component Regression and Partial Least Squares Regression are few of the popular methods employed.

6.1.1 Classical Least-squares

Classical Least-Squares (CLS) is sometimes known as K-matrix calibration, as it originally involved the application of Multiple Linear Regression (MLR) to the expression of Beer-Lambert Law. This approach involves modeling the spectral data as a function of analyte concentration.

$$\mathbf{A = KC} \qquad \textbf{(6.1)}$$

We begin with calibration in classical least-squares, with concentration matrix **C** and the absorbance matrix **A**, for the known samples. We then solve for **K.** Each column in **K** contains the pure component spectra. Least-squares solution is found for the above equation i.e. we find the **K** such that it produces the least sum of squares of error. To handle the prediction of concentration of unknown samples, we use the calculated **K** matrix. It is found according to the following equation [2].

$$\mathbf{[K^T K]^{-1} K^T A_{unk} = C_{unk}} \qquad \textbf{(6.2)}$$

We use $\mathbf{[K^T K]^{-1}}$which is known as pseudo inverse of **K** and $\mathbf{K^T}$ which is the transpose of **K**. There are advantages and disadvantages associated with CLS. The main advantage of using CLS is that after calibration process, the estimates of true constituent spectra are determined. But it also requires the knowledge of the concentrations of all the constituents which are present in the sample which is many times impractical to know [1]. This can be circumvented by use of augmented CLS (ACLS) which relaxed the above criteria and gives a robust modeling with a complex matrix.

6.1.2 Inverse Least-squares (ILS)

This method so called because of the involvement of inverse expression of Beer-Lambert Law. This method is sometime called the P-matrix method. The ILS calibration model assumes that the concentration of sample could be predicted quantitatively from sample spectra [3].

$$\mathbf{C = PA} \qquad \textbf{(6.3)}$$

Where concentration matrix is denoted by **C** and absorbance matrix by **A.** In order to produce an inverse least square calibration we use calibration samples with known concentration, also known as training set. We then find the solution for **P** matrix in a least square manner. Each row will have a coefficient for each wavelength. This P matrix is used to predict the concentration of unknown samples according to the following equation [2].

$$\mathbf{C_{unk} = PA_{unk}} \qquad \textbf{(6.4)}$$

Employing an ILS model alleviates the need for complete knowledge of the calibration set constitution. With the ILS model, concentration (or any intrinsic property) is modeled as a function of instrument response.

6.1.3 Principal Component Analysis (PCA)

Principal Component Analysis (PCA) is a statistical method which characterized variance in spectral data [4,5]. PCA provides an interpretation and a better understanding of the sources of these variations. The original spectra contains group of correlated variable. PCA employs an orthogonal transformation to convert correlated variables into uncorrelated variables. Spectral variances are characterized as a set of orthogonal vectors typically referred to as principal components, eigenvectors, spectral loadings or loading vectors. The first principal components explain the maximum variance possible in the spectral data. The second principal component is chosen such that it is orthogonal to first principal components, and explains the maximum possible remainder of variation in the data. This process is continued as long as the desired amount of variation is explained by the principal components obtained.PCA is a powerful method for reducing the dimensionality of the spectral data matrix and eliminating noise.

$$\mathbf{X} = \mathbf{TP} + \mathbf{E} \qquad (6.5)$$

The orthogonal transformation decomposes the spectral data matrix **X** as shown in equation 6.5.**T** is termed as the scores matrix, **P** is the principal components matrix and **E** is the noise matrix and contains the noise which cannot be explained. The Singular Value Decomposition (SVD) algorithm is utilized to extract the principal components for the **X** matrix.

In building the PCA calibration model, usually the first k principal components are selected as the number of latent variables or factors. With a properly chosen of number of factors, the necessary information for concentration modeling can be included while principal components of interferences and noise can be excluded.

6.2 Partial Least Squares Regression for Glucose estimation

Partial Least Squares Regression (PLSR) was introduced by the Swedish statistician Herman Wold in the 1960s. PLSR finds its application in anthropology, chemometrics, biofinformatics, econometrics, marketing etc. PLSR has become the most widely used technique for quantitative analysis of NIR spectra as it overcomes most of the serious drawbacks of other multivariate techniques.

PCA is very efficient in finding latent variables which models the variation in the **X** block (spectral data). This highlights the noise removal capability of PCA from the spectral data. Problem arises if there is lot of variation in **X** that is not due to the analyte as such. Sometimes the analyte itself gives rise to only small variation in **X**, in this scenario the useful variation is hidden in the directions which PCA interpreted as noise. PLSR is able to cope with this situation by selecting the latent variable which is most relevant to the estimation of **Y**. In PLSR method, both **X** and **Y** are decomposed simultaneously to obtain a set of latent variables that describe maximum covariance between **X** and **Y**. Hence, the principal components obtained using PLSR method, could be relevant to a set of dependent variables that lead to better prediction accuracy.

PLSR finds its use in situation where the number of predictor variables in the spectral data are more as compared to the number of observations. PLSR also aids in the dimensionality reduction like PCA and is used to select a few predictor latent variables. PLSR can be used in any one of these condition namely, where the responses are

correlated or where number of predictor variable exceeds the number of observations or where the predictor variables are correlated. Compared to PCR, PLSR is more robust, faster, and requires a lower number of factors to establish the calibration model [1,6].

In PLSR, objective is to find linear components to model **X** and **Y** as given in equation 6.6.

$$\mathbf{X} = \mathbf{TP^T} + \mathbf{E} \quad \& \quad \mathbf{Y} = \mathbf{UQ^T} + \mathbf{F} \qquad \textbf{(6.6)}$$

Y is the response matrix with dimensions m/n, where m is the number of response variables and where n is the number of observations (number of spectra). Here, **X** is the spectral data matrix with dimensions n/k, and k is the number of wavelengths/data points in each spectrum (number of predictor/explanatory variables). $\mathbf{U} = \mathbf{YC} = (\mathbf{u_1},\ldots, \mathbf{u_Z})$ and $\mathbf{T} = \mathbf{XW} = (\mathbf{t_1},\ldots, \mathbf{t_Z})$ are the n/Z component score matrices for **X** and **Y** and respectively with Z representing the number of components which is less than or equal to k. $\mathbf{P} = (\mathbf{p_1}, \ldots, \mathbf{p_Z})$ and $\mathbf{Q} = (\mathbf{q_1}, \ldots, \mathbf{q_Z})$ are the m/Z and k/Z loading matrices for **X** and **Y** respectively. The m/Z matrix **C** and the k/Z matrix, **W** are the weight matrices [7].Mostly the contents of **X** and **Y** are centered by subtracting their means and normalized to by dividing with their standard deviations.

We have employed a calibration model using the PLSR methodology to estimate the glucose concentration on spectroscopic data. This process involves the development of a calibration model using a calibration data set having samples with known glucose concentration along with other analytes. Then this calibration model is used to predict the unknown glucose concentrations. In the next section we discuss the various algorithms for PLSR.

6.2.1 Algorithm to Implement PLSR

There are many algorithm proposed to implement PLSR, of which popular one are Non-linear Iterative Partial Least Squares (NIPALS) and Statistical Inspired Modification of PLS (SIMPLS) introduced by Wold et.al.[8] and DeJong et.al.[9] respectively. The SIMPLS algorithm is fast as compared to NIPLAS algorithm [10]. SIMPLS does not employ a breakdown of the data sets and as such is found to be fast and easy to interpret. We have used SIMPLS in our research work due to the advantages offered by it as outlined above.

6.2.2 NIPALS Algorithm

The simple NIPALS algorithm was introduced by Herman Wold [11]. It begins with centering and scaling matrix **X** and **Y**, and proceeds as follows. It must be noted that if a only one y-variable is present, the algorithm will be non-iterative This algorithm has found its application in chemometric and below are steps involved to implement as given in S. Wold et al. [12].

Step 1: A starting vector **u** is chosen **u** which is usually a column of **Y**. if **Y** has a single column then, **u** = **y**.

Step 2: The weights **w** of **X** are calculated as **w** = **X'u**/**u'u** (here **w** can be modified as $\|\boldsymbol{w}\| = 1.0$)

Step 3: The scores **t**, of **X** are calculated as **t** = **Xw**

Step 4: The weights **c**, of Y are calculated as **c = Y't/ t't**

Step 5:Get the updated set of scores of **Y as u** = **Yc**/ **c'c**.

Step 6: Convergence test is carried to check the change in **t**by $\| t_{old} - t_{new} \| / \| t_{new} \| < \varepsilon$, here the value of ε is "small" for example 10^{-6} or 10^{-8}. If not converged, go back to step 2, otherwise continue to to step 7. The process converges with one iteration if **Y** is a single variable matrix and goes on to step 7.

Step 7: The component calculated is removed from **X** and **Y** and these deflated matrices will be used to generate the next component.

p = X't/ t't

X = X - tp'

Y = Y - tc'

Step 8: If the number of desired components are not found go back to step 1 to find the next components

6.2.3 SIMPLS Algorithm

Statistical Inspired Modification of PLS **(**SIMPLS) algorithm models **X** and **Y** by decomposing as shown in equation 6.6. Let us assume the matrices **X** and **Y** are mean centered. The scores of the **X** and **Y** matrix must have maximum covariance; hence, a

constraint is added on the score vector to have a length of 1. The solution to the following maximization problem are the first score vectors $\mathbf{t_1}$and $\mathbf{u_1}$ and the statement for maximization problem is

$$\mathrm{cov}(\mathbf{t},\mathbf{u}) = \mathrm{cov}(\mathbf{Xw},\mathbf{Yc}) = \mathbf{t^T u} = (\mathbf{Xw})^{\mathrm{T}}\mathbf{Yc} = \mathbf{w^T X^T Y c} \Rightarrow \max \qquad \mathbf{(6.7)}$$

The equation 6.7 is under the constraints of $\|\mathbf{t}\| = \|\mathbf{u}\| = 1$. Singular value decomposition is used to find the weight vectors **w** and **c**. The largest singular value of covariance matrix $\mathbf{X^T Y}$ corresponds to the direction of **w** and **c** which gives the maximum of equation 6.7, and these vectors are names as $\mathbf{w_1}$ and $\mathbf{c_1}$ respectively. For the subsequent score vectors an additional constraint is required to ensure the orthogonality of the previous score vector and is specified by $\mathbf{u_a u_j} = 0$ and $\mathbf{t_a t_j} = 0$ for $1 \leqslant a < j \leqslant A$. Orthogonality is ensured by using the residual matrices to find the subsequent score vectors instead of **X** and **Y.**SIMPLS involves deflation of the $\mathbf{X^T Y}$ covariance matrix to calculate the residual matrices. Below are the steps followed to implement the SIMPLS algorithm [7].

For each h =1,…, Z, where Z is the number of components to be found.

Step 1: Mean center the explanatory and response variable matrices, and represents them as **X** and **Y** after mean centering. Calculate the covariance matrix $\mathbf{S_h} = \mathbf{X^T Y}$.

Step 2: The left singular vector of the matrix $\mathbf{S_h}$is taken as $\mathbf{w_h}$.

Step 3: Normalize $\mathbf{w_h}$using the expression $w_h = \mathbf{w_h} / \|\mathbf{w_h}\|$.

Step 4: $\mathbf{t_h}$the h^{th} component vector is calculated as$\mathbf{t_h} = \mathbf{X w_h}$ (when h=1, $\mathbf{t_1}$ is the first component vector)

Step 5: Normalize $\mathbf{t_h}$ as $t_h = \mathbf{t_h} / \|\mathbf{t_h}\|$.

Step 6: $\mathbf{p_h}$ the h^{th} loading vector of X is calculated as $\mathbf{p_h} = \mathbf{X^T t_h}$(when h=1, $\mathbf{p_1}$ is the first loading vector of **X)**.

Step 7: $\mathbf{q_h}$the h^{th} loading vector of **Y** is calculated as $\mathbf{q_h} = \mathbf{Y^T t_h}$. (when h=1, $\mathbf{q_1}$ is the first loading vector of **Y)**.

Step 8: Deflated covariance matrix $\mathbf{S}_{h+1}$ is calculated $\mathbf{S}_{h+1} = \mathbf{S}_h - \mathbf{v}_h(\mathbf{v}_h^T \mathbf{S}_h)$, where $\mathbf{v}_h = \mathbf{p}_h$(for h = 1)and $\mathbf{v}_h = \mathbf{p}_h - \mathbf{V}_{h-1}(\mathbf{V}_{h-1}^T \mathbf{p}_h)$ for a > 1 with $\mathbf{V}_{h-1} = (\mathbf{v}_1, \mathbf{v}_2, \dots, \mathbf{v}_{h-1})$.

Steps 2 to 8 are repeated till Z components are extracted.

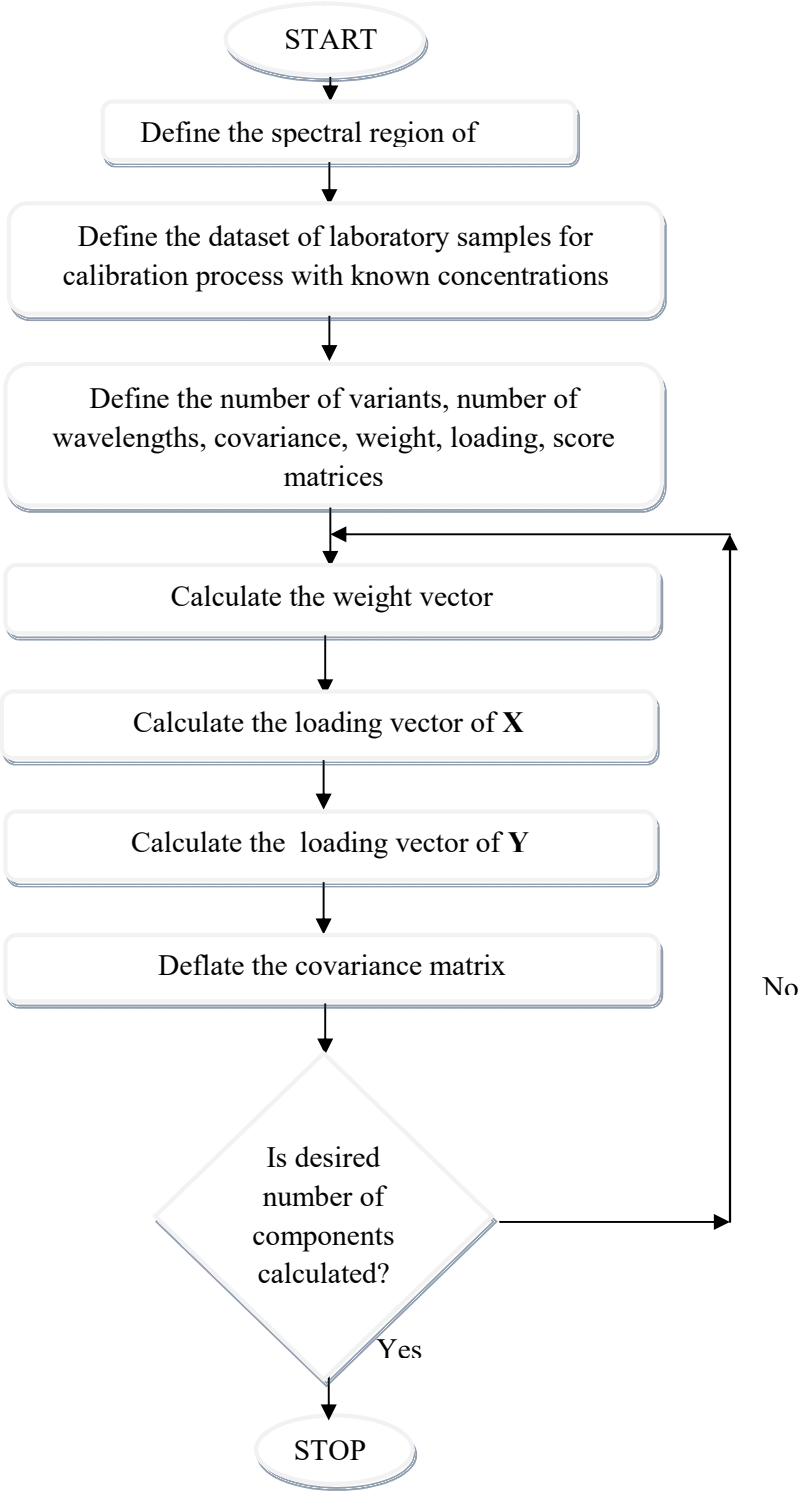

Figure 6.1: Flowchart for SIMPLS algorithm

As SIMPLS is very popular technique, and we have based our research on it. A C code is ported to the NIOS-II platform to implement the SIMPLS. Figure 6.1 gives the flowchart to implement SIMPLS

6.3 ParLes Software for Preliminary Analysis

ParLes is a shareware intends to be used for research and teaching purpose in spectroscopy and chemometric[13]. ParLes provides a lucid graphical user interface to implement various multivariate modeling techniques as well as various assessment statistics. ParLes is also intended for use in modeling in real time in field and laboratory setup.

The software structure is given by figure 6.2, here data import operation are shown by double lines, whereas rectangles with rounded edges represent assessment statistic offered by the software, circles represent the chemometric capabilities of the software, and trapeziums represent the saving option of the output of the analysis

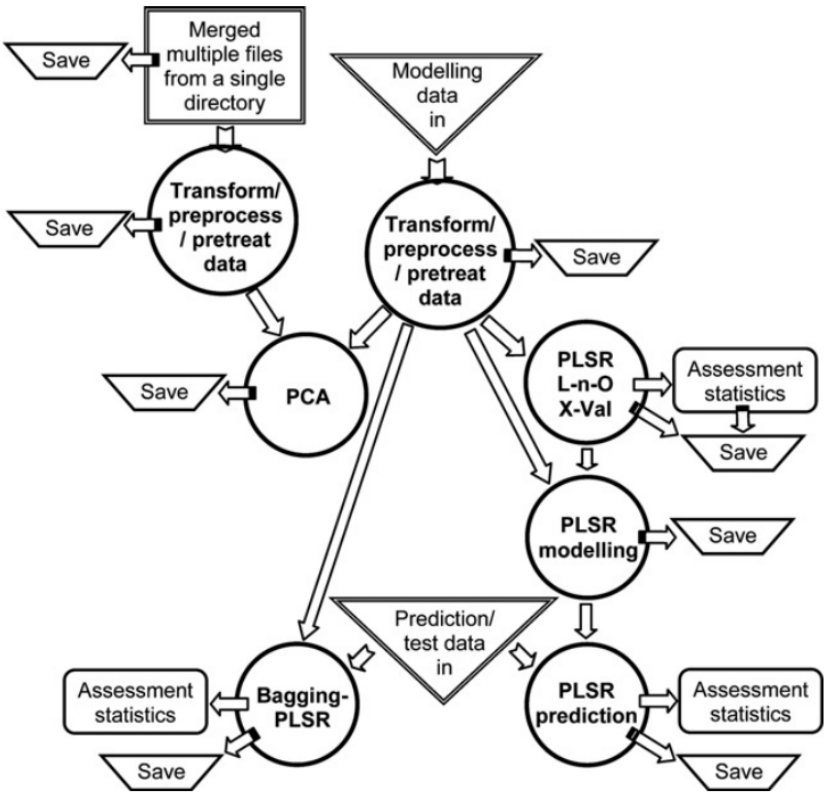

Figure 6.2: ParLes software structure

ParLes software was developed by Raphael A. Viscarra Rossel in LabVIEW, and provides a simple Graphical User Interface (GUI) to perform many multivariate algorithms. Figure 6.3 shows the opening screen of the GUI. Subsequently we need to choose the "Import data modeling" tab to import the data into the software as shown in figure 6.4. The spectroscopic data needs to be in the tab delimited ASCII format. The path of the file must be specified in the space provided under "Get file for modeling". Once that is done we need to specify the number of y variables present in the tab delimited ASCII file and to be considered for modeling. Once that is done the data is imported in the software by hitting the "import data for modeling button".

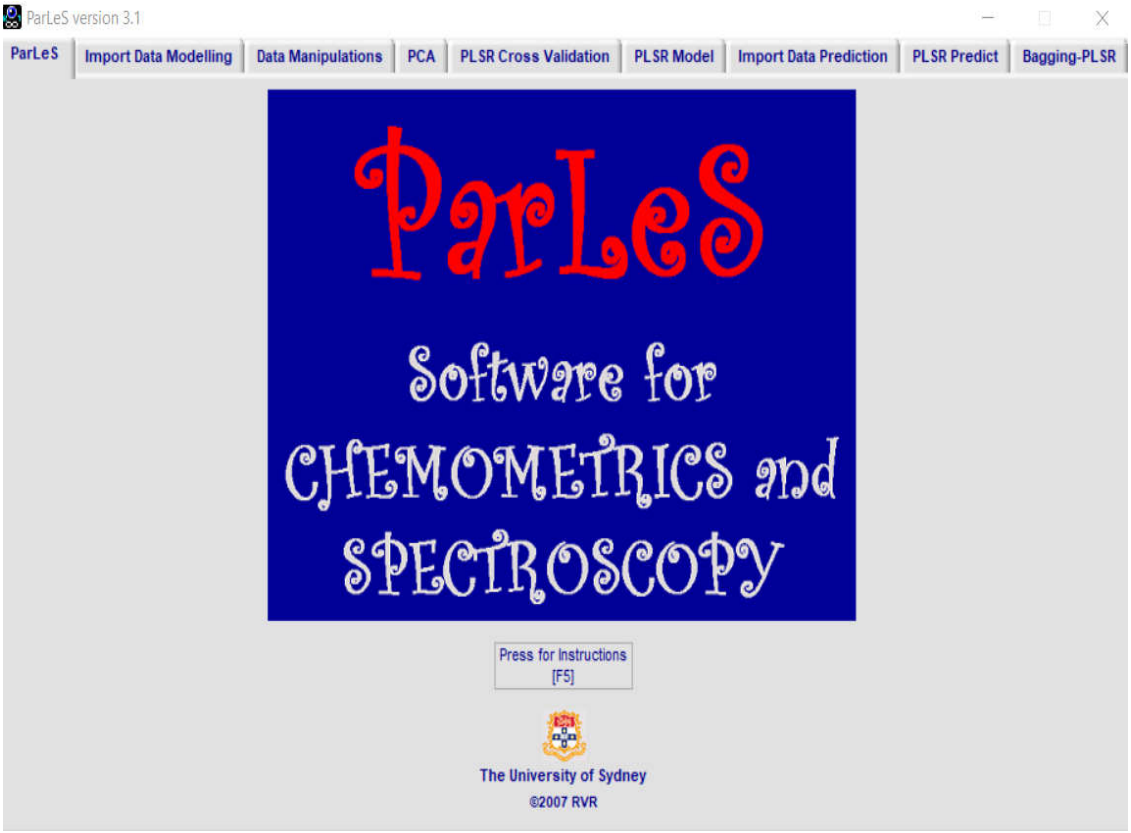

Figure 6.3: Opening screen of the ParLes software

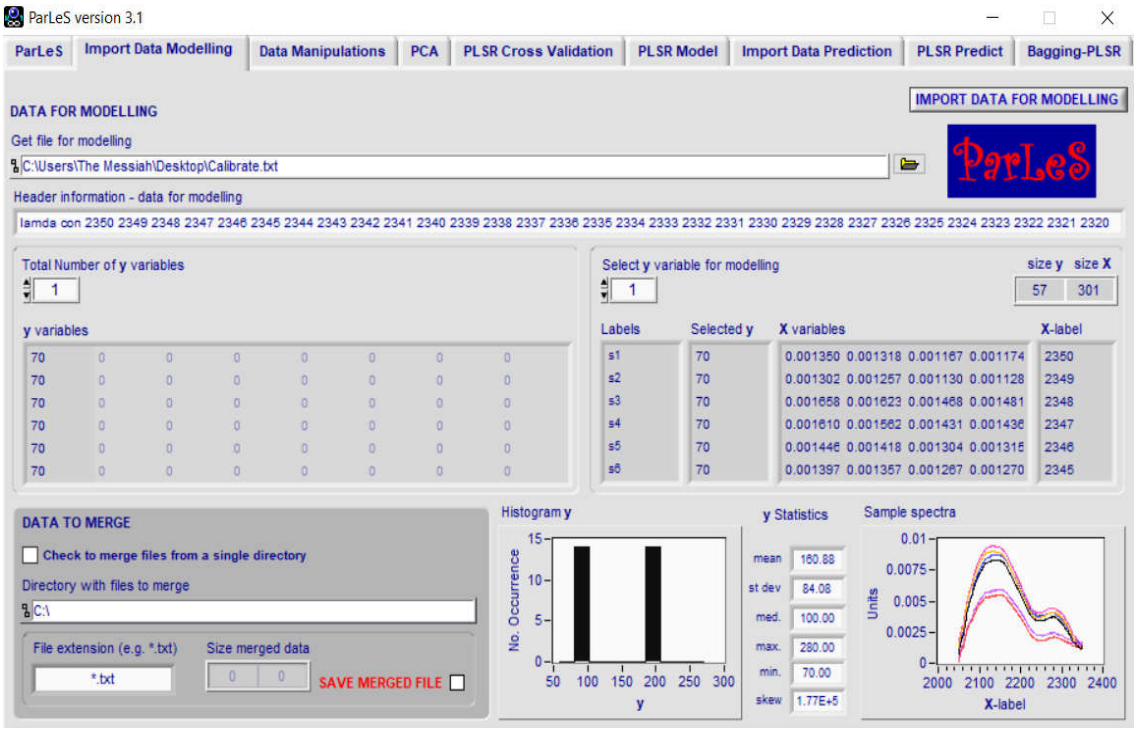

Figure 6.4: Import data for modeling in ParLes

Various preprocessing and transformation techniques are offered by the ParLes software (version 3.1), these can be accessed under the data manipulation tab in ParLes. Various transformations of reflectance spectra can be affected such as reflectance spectra (R) to log (1/R) or Kubelka Munk units. Also reverses also can be affected that is, log (1/R) to R units.

Various implement preprocessing such as multiplicative scatter correction (MSC), standard normal variate (SNV) transform and wavelet detrending can be performed. Different filtering methods such as median, Savitzky-Golay filtering are provided along with differentiation of spectra. Pretreatment of data is supported such as mean centering, variance scaling as can be seen in figure 6.5. Of the above options offered we have only mean centered out data.

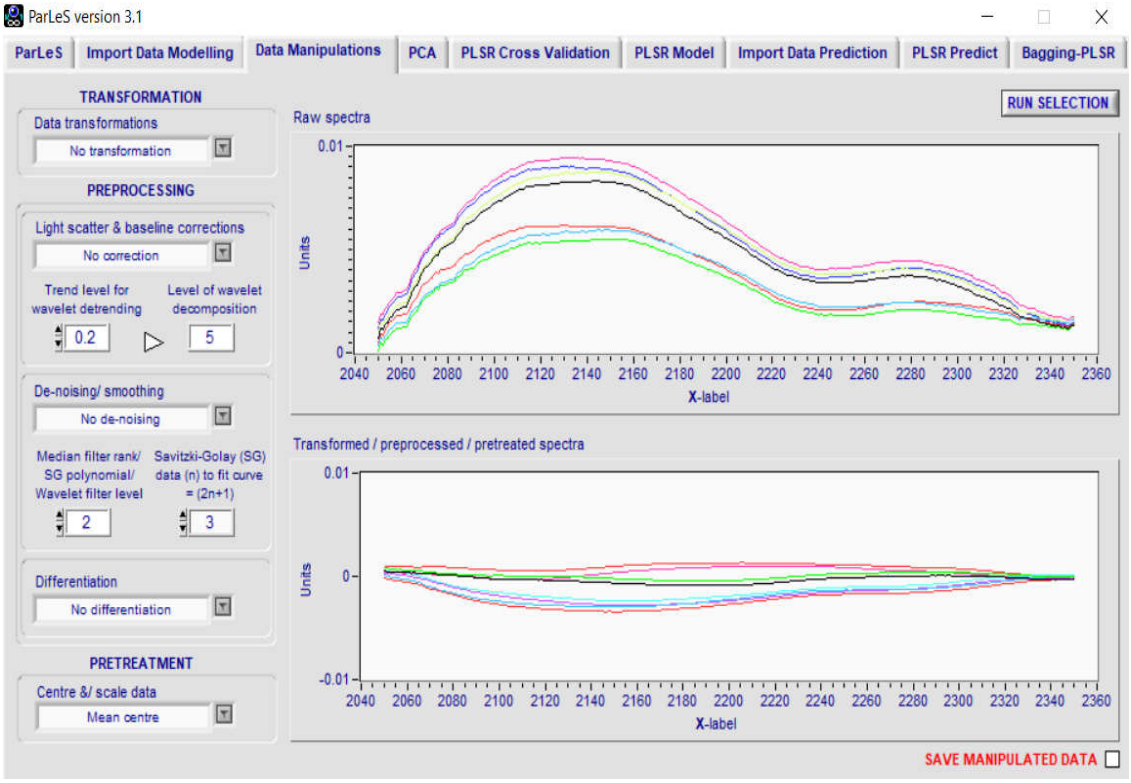

Figure 6.5: Data Manipulation in ParLes

Different modeling techniques are supported by the software such as PCA, PLSR, PLSR cross validation, Bagging-PLSR and separate tabs are provided for each of the modeling technique. Under the "PLSR Model" tab the parameters needed to build a PLSR model are specified as shown in figure 6.6. The number of factors required can be selected using the slide bar below "Select No. of factors for PLSR. The button "Run PLSR modeling" is used to build the model. Once the model is built we can use the various visualizations offered by the software various such as factors scores plot, plot of **t** versus **y**, B coefficients, and explained variance to better understand the model. The Explained variance visualization displays the percentage of variance explained by each of the factors generated.

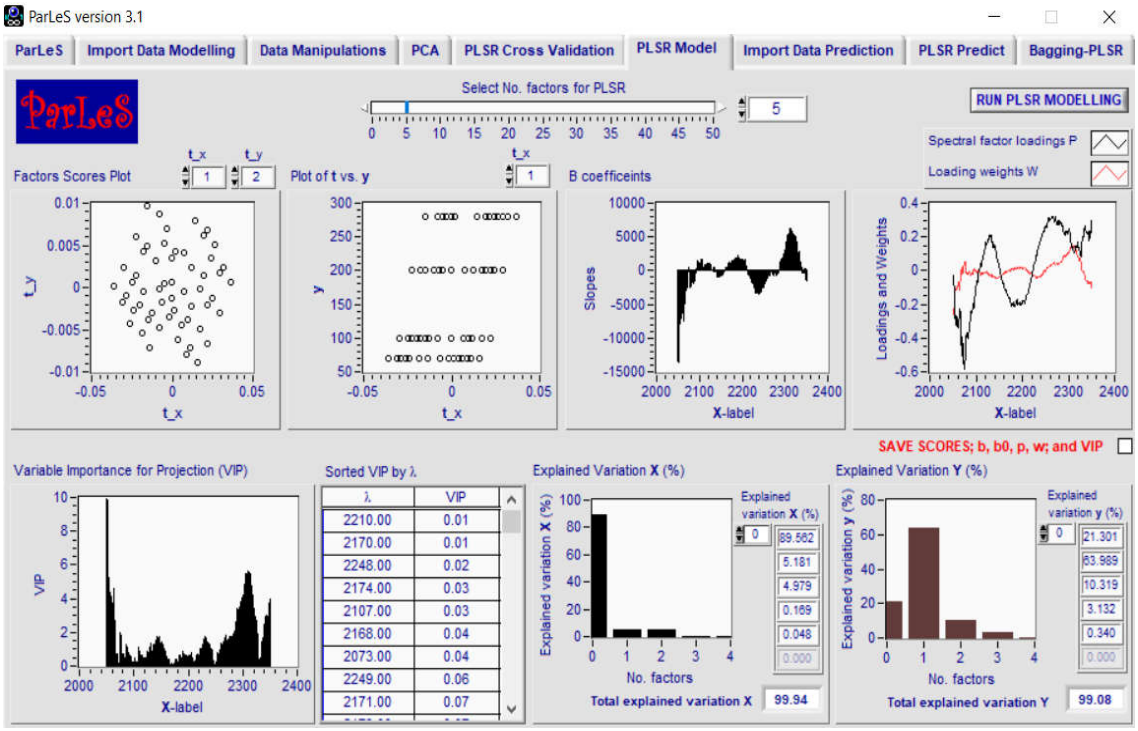

Figure 6.6: PLSR in ParLes

The “Import data prediction” tab is utilized to import the spectroscopic data of unknown samples for prediction using the built PLSR calibration model. Again, the prediction of spectroscopic data needs to be in the tab delimited ASCII format. The path of the file must be specified in the space provided under “Get file for prediction”. We need to specify the number of y variables present in the data to be imported and then hit the “Import data for prediction” button. Once the data is imported for prediction we must use the “PLSR predict” tab for prediction as shown in figure 6.7. The prediction is done by hitting the button” Run prediction”. The RMSE for prediction is displayed on the right hand side under Assessment statistics.

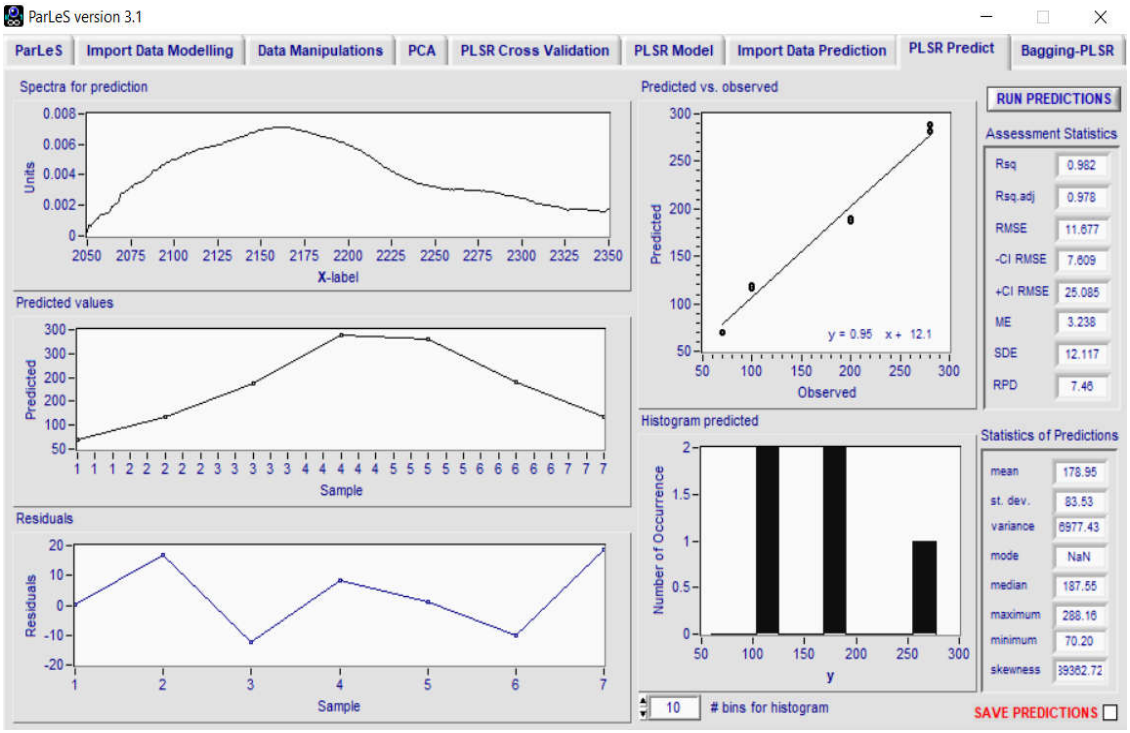

Figure 6.7: PLSR Prediction in ParLes

References

[1] J. Qian, "Glucose Monitoring in Various Matrices with Near-Infrared Spectrometry and Chemometrics", Doctoral Thesis, University of Iowa, 2013.

[2] R. Kramer, "Chemometric Techniques for Quantitative Analysis", CRC Press,1998.

[3] R.G. Krutchkoff, "Classical and Inverse Regression Methods of Calibration", Technometrics, Vol. 9, 1967, pp. 425-439.

[4] S. Wold, K. Esbensen, P. Geladi, "Principal Component Analysis", Chemometrics and Intelligent Laboratory Systems, Vol. 2, 1987, pp. 37-52.

[5] P. Nomikos, J.F. MacGregor, "Monitoring Batch Processes Using Multiway Principal Component Analysis", AlChE Journal, Vol. 40, 1994, pp. 1361-1375.

[6] M. J. Adams, "Chemometrics in Analytical Spectroscopy", Royal Society ofChemistry, 2004.

[7] A. Alin, C. Agostinelli, "Robust iteratively reweighted SIMPLS", J. of Chemometrics, Vol. 31(3), 2017, p. e2281.

[8] H. Wold, "Estimation of principal components and related models by iterative least squares" in Multivariate Analysis, P. R. Krishnajah (Ed.), Academic Press, 1966, pp. 391–420.

[9] S. DeJong, "SIMPLS, an alternative approach tp partial least squares regression", Chemometrics and Intelligent Laboratory Systems, Vol. 18, 1993, pp. 251–263.

[10] M. Andersson, "A comparison of nine PLS1 algorithms," J. Chemometrics, Vol. **23**(10), 2009, pp. 518-529.

[11] S. Wold, A. Ruhe, H. Wold, W.J. Dunn III, “The collinearity problem in linear regression, The partial least squares approach to generalized inverses”, SIAM J. Sci. Stat. Comput., Vol. 5 (3), 1984, pp. 735–743.

[12] S. Wold , M. Sjostrom, L. Eriksson, “PLS-regression: a basic tool of chemometrics”, Chemometrics and Intelligent Laboratory Systems, Vol. 58 (2), 2001, pp.109-130.

[13] R. A. V. Rossel, “ParLeS: Software for chemometric analysis of spectroscopic data”, Chemometrics and Intelligent Laboratory Systems, Vol. 90 (1), 2008, pp. 72-83.

In order to implement a successful non-invasive glucose sensing we need to detect transmitted near infrared radiation through the human tissue and the glucose absorption signatures. As we are implementing the sensing in the combination band, the overlapping signatures of the other human tissue constituents and the random fluctuation due to noise must be isolated. PLSR is a versatile technique which aids in the above process.

In this research work a system has been developed to estimate the glucose concentration non-invasively on an Altera NIOS-II soft-core platform using a DE-0 Nano board having a Cyclone-IV FPGA (EP4CE22F17C6N). We have used fixed wavelengths to probe the sample. We have focused out research in the combination band region which spans 2000 to 2500nm. A detailed study was carried out to test the robustness and performance of PLSR algorithm to estimate glucose concentration of unknown samples when subjected to input with absorbance at varying number of wavelengths points, First with the full absorbance spectrum, then with 10 fixed wavelengths and then with 5 fixed wavelengths. C code to implement PLSR using SIMPLS algorithm was ported to the NIOS-II platform in this research work. The C code is given at Annexure I.

7.1 Building of Multivariate Calibration Model

PLSR is a popular method used to analyze multivariate spectroscopic data and is discussed earlier in the chapter 6. PLSR is an extension of multiple linear regressions and widely used as exploratory analysis of the predictor variables and to identify outliers in the data. Laboratory samples having 5 major blood constituents namely glucose, urea, lactate, ascorbate and analine were prepared to simulate the blood matrix. Absorbance spectra of these 64 laboratory samples were recorded on a Jasco V-770 spectrophotometer. This spectrophotometer is equipped with a halogen lamp and a PbS detector for NIR range. The spectra were recorded in the range of 2050-2350nm having a total of 301 number of wavelength points. These constituents of the samples were made to have physiological relevant concentrations. Spectra of typical 15 of the above 64 samples are shown in the figure 7.1 and the corresponding concentration are tabulated below in table 7.1.

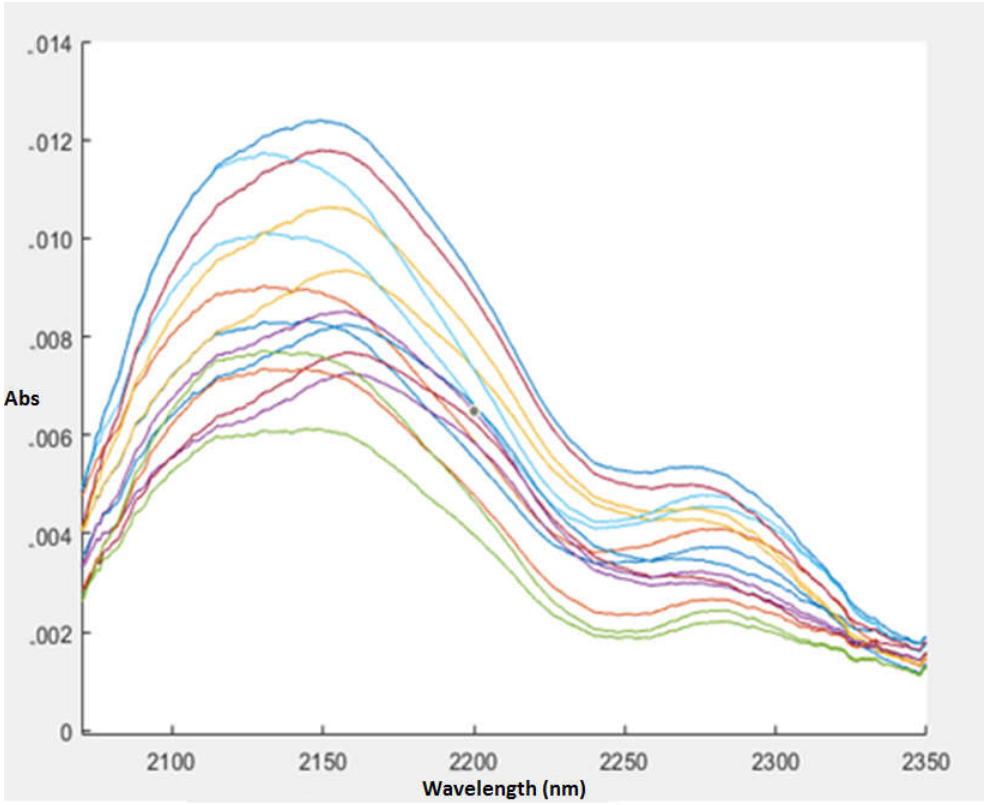

Figure 7.1: Spectra of typical 15 samples

Table 7.1: Concentration of typical 15 samples

Sample No	All above reading are in mg/dL				
	Urea	Lactate	Ascorbate	Analine	Glucose
1	11	12	2	10	70
2	11	22	2	10	70
3	20	12	2	10	70
4	20	22	5	28	70
5	11	12	5	10	100
6	11	22	5	10	100
7	20	22	2	28	100
8	11	12	2	28	200
9	11	22	2	10	200
10	20	12	5	28	200
11	20	22	5	28	200
12	11	12	5	28	280

13	11	22	5	10	280
14	20	12	5	10	280
15	20	22	5	28	280

The physiological relevant concentration ranges which were used in our research are given adjacent to the constituent.

- Alanine (10–28 mg/dL)
- Urea (11 –20 mg/dL)
- Lactate (12–22 mg/dL)
- Glucose (70–280 mg/dL)
- Ascorbate (2–5 mg/dL)

Three different cases were investigated using the same 64 absorbance recorded spectra. The different cases which were investigated are,

Case 1: Building multivariate PLSR model for glucose estimation using entire absorbance spectra in the range of 2050 – 2350nm.

Case2: Building multivariate PLSR model for glucose estimation using absorbance at 10 fixed wavelengths corresponding to glucose absorbance peaks, valleys, and slopes.

Case3: Building multivariate PLSR model for glucose estimation using absorbance at 5 fixed wavelengths corresponding to glucose absorbance peaks and valleys only.

Of the above 64 samples, 57 were used for the calibration of PLSR model and 7 samples were used as prediction set. For all the above cases a five component PLSR model was built. For each of the cases we have calculated the error and the percent error.

7.1.1 PLSR model using Full Spectra (Case 1): Glucose estimation using entire absorbance spectra in the range of 2050 – 2350nm.

In this case, we have investigated the performance of the multivariate PLSR algorithm for estimating the glucose concentration when we use the entire spectrum. Here we consider the first dataset to have the entire absorbance spectra of the above samples. It

must be noted that we used the entire range of points from 2050-2350nm a total of 301 sample points in each spectrum. 57 of the samples spectra were used to build the PLSR calibration model. The calibration model was built using 5 factors. The remaining 7 samples spectra were used to test the prediction of the calibrated model, as such these 7 samples were presented to the model as samples with unknown concentration and the predicted concentration were noted and compared with the concentration determined using the reference method. The PLSR model extracts five factors form a huge number of correlated variables, which models the covariance between the independent variables (spectral data)and the response variables (concentration data). The predicted values of these unknown samples are tabulated in the table 7.2

Table 7.2: Prediction results for case 1

Sr. no.	Actual Concentration in mg/dL					Predicted Glucose in mg/dL	Error	Percent Error
	Urea	Lactate	Ascorbate	Analine	Glucose			
1	20	12	5	28	70	70.20	0.20	0.29
2	20	12	5	10	100	117.04	17.04	17.04
3	11	22	2	10	200	187.55	12.45	6.22
4	11	12	5	28	280	288.16	8.16	2.91
5	20	22	5	28	280	281.08	1.08	0.39
6	20	12	2	28	200	190.10	9.90	4.95
7	11	12	5	10	100	118.53	18.53	18.53

7.1.2 PLSR model using fixed wavelengths (Case 2): Glucose estimation using absorbance at 10 fixed wavelengths corresponding to glucose absorption peaks, valleys, and slopes.

In this case, the investigation was done for the performance and robustness of PLSR model for the estimation of glucose when we use 10 fixed wavelengths. These 10 fixed wavelengths correspond to the peaks, valleys and slopes of the glucose absorbance spectrum as shown in figure 7.2. It can be seen that, as the glucose concentration

changes, the slopes before and after the peaks change. Hence it can be assumed that the slopes of the peaks and valleys correlate with the glucose concentration. Also, it can be seen from figure 7.2 that as the concentration of glucose increases, the height of the peaks increases. Instead of using the entire spectrum with a huge number of points we have attempted to build a calibration model using these fixed wavelengths. The precise values of wavelength chosen are 2085, 2127, 2180, 2246, 2264, 2278, 2290, 2312, 2324 and 2332nm and are represented by bars on the glucose absorbance spectra depicted in figure 7.2.

A separate second dataset is built using the same above absorbance spectra of the 64 laboratory samples. Each sample in the dataset contains absorbance at only 10 fixed wavelengths instead of the entire spectrum. From this new dataset 57 samples are used for building the calibration model and 7 samples are used to testing the prediction capability of the model. We have built the calibration model to have five factors. The 7 test samples were given to the model as unknowns and the predicted glucose concentration were recorded and tabulated in table 7.3.

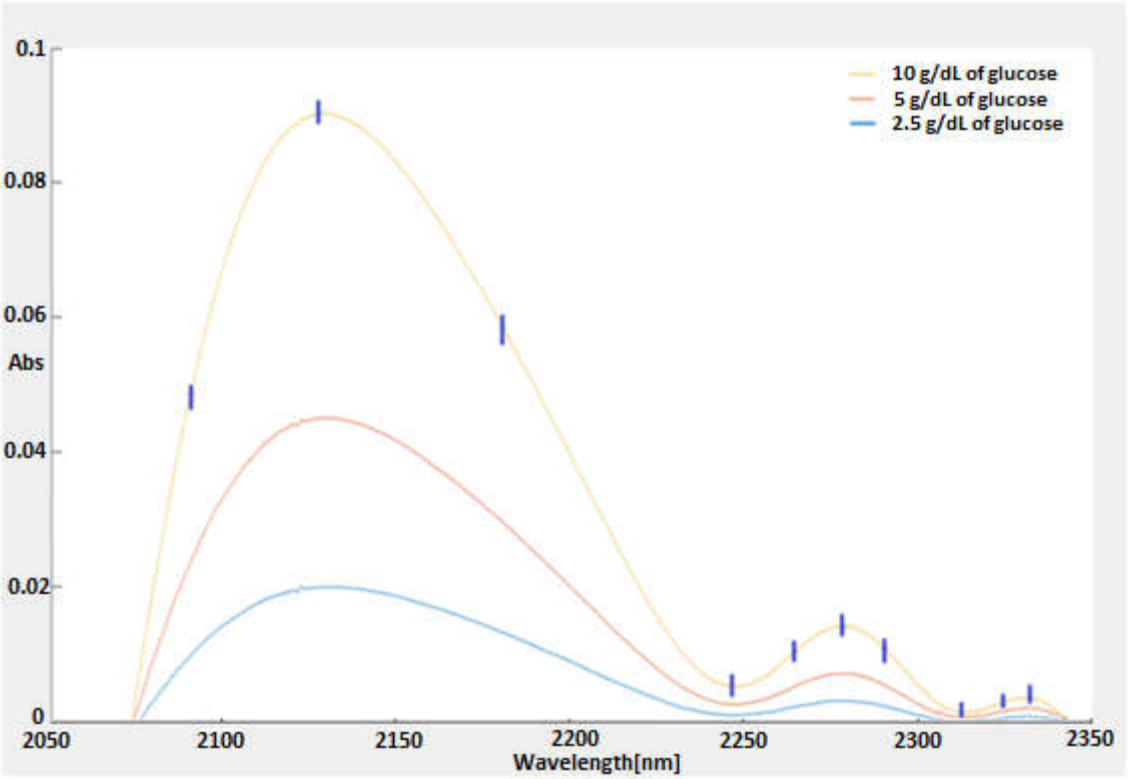

Figure 7.2: Pure glucose spectra at different concentrations

Table 7.3: Prediction results for case 2

Sr. no.	Actual Concentration in mg/dL					Predicted Glucose in mg/dL	Error	Percent Error
	Urea	Lactate	Ascorbate	Analine	Glucose			
1	20	12	5	28	70	60.96	9.04	12.91
2	20	12	5	10	100	119.99	19.99	19.99
3	11	22	2	10	200	195.33	4.67	2.34
4	11	12	5	28	280	279.49	0.51	0.18
5	20	22	5	28	280	275.99	4.01	1.43
6	20	12	2	28	200	195.70	4.30	2.15
7	11	12	5	10	100	120.63	20.63	20.63

7.1.3 PLSR model using reduced wavelengths (Case 3): Glucose estimation using absorbance at 5 fixed wavelengths corresponding to glucose absorption peaks and valleys only.

Here, we have investigated the robustness and perfomance of the PLSR model when subjected to a input dataset with absorbance at only 5 wevelengths corresponding to the glucose peaks and valleys in the combination band region. As explained earler the height of the glucose peaks change as the concentration changes, as such the peaks and valleys wavelengths of glucose contain information specific to its concentration. Hence, we have chosen these five wavelenghts to futher test the feasiblity and robustness of the method. The precise values of wavelengths which were chosen are 2127, 2246, 2278, 2312 and 2332nm.

Again a separate third dataset is built using the same above absorbance spectra of the 64 laboratory aqueous samples. From this new dataset 57 samples are used for building the calibration model and 7 samples were kept behind to test the prediction capability of the model. The calibration model was built by extracting five factors. The 7 test samples were given to the model as unknowns and the predicted glucose concentration were recorded and tabulated in table 7.4.

Table 7.4: Prediction results for case 3

Sr. no.	Actual Concentration in mg/dL					Predicted Glucose in mg/dL	Error	Percent Error
	Urea	Lactate	Ascorbate	Analine	Glucose			
1	20	12	5	28	70	56.74	13.26	18.95
2	20	12	5	10	100	120.63	20.63	20.63
3	11	22	2	10	200	199.33	0.67	0.33
4	11	12	5	28	280	275.18	4.82	1.72
5	20	22	5	28	280	273.12	6.88	2.46
6	20	12	2	28	200	197.89	2.11	1.05
7	11	12	5	10	100	121.18	21.18	21.18

7.2 Evaluation Criteria

The PLSR model for glucose estimation is assessed using Root Mean Square Error (RMSE) of the prediction. RMSE is calculated for each of the three cases. RMSE can be calculated using equation 7.1

$$\textbf{Root Mean Squred Error} = \sqrt{\frac{1}{N}\sum_{i=1}^{N}(\hat{y}_i - y_i)^2} \qquad (7.1)$$

Where $\hat{y}_i$ is the i^{th} predicted value and y_i is the actual observed value and N is the sample size. Table 7.5 gives the calculated values of RMSE for each of the three cases which were investigated.

Table 7.5: Results for the three cases investigated

Investigated Cases	RMSE
Case 1: Multivariate PLSR model for glucose estimation using entire absorbance spectra (2050 – 2350nm)	**11.67**
Case 2: Multivariate PLSR model for glucose estimation using absorbance at	**11.73**

10 fixed wavelengths corresponding to glucose absorption peaks, valleys, and slopes	
Case 3: Multivariate PLSR model for glucose estimation using absorbance at 5 fixed wavelengths corresponding to glucose absorption peaks and valleys only	**12.68**

In each of the three cases there were 7 samples in the prediction data set. The observed value and the predicted values were used to calculate the RMSE. In **case 1**, where a multivariate PLSR model for glucose estimation was built using the entire absorbance spectra in the range of 2050 – 2350nm produced an RMSE of prediction of 11.67. Next in **case 2**, where a multivariate PLSR model for glucose estimation was built using absorbance at 10 fixed wavelengths corresponding to glucose absorbance peaks, valleys, and slopes produced and RMSE of prediction of 11.73. In **case 3**, where a multivariate PLSR model for glucose estimation was built using absorbance at 5 fixed wavelengths corresponding to glucose absorbance peaks and valleys only, gave an RMSE of prediction of 12.68. The RMSE has increased form 11.67 to 12.68 when we went form case 1 to case 3, however the increase in RMSE is not found to be drastic and can be improved by using high intensity sources such as high intensity LEDs which offer high SNR as compard to the sources on the spectrophotometer.

7.3 Accuracy Testing of the Models

A thorough analysis of model accuracy on the basis of clinically relevant criteria needs to be carried out. To determine the clinical accuracy afforded by a glucose measuring technique we use error grids. The Primary method to measure the clinical accuracy of the glucose measuring device is Clarke Error Grid Analysis (EGA) which has become a gold standard. It was introduced by a team of five experts of university of Virginia in the year 1987 [1]. This method of representation uses a two-dimensional plot, where the X-axis represents the glucose values determined by a reference method and the Y-axis represents the values which are predicted by the technique under test. The grid is

divided into zones which indicate the amount of error from the reference reading. It is possible to analyze the distribution of points in the different zones of the grid and then quantify the degree of accuracy offered by the particular glucose measuring device or method. The diagonal of the EGA represent a perfect agreement between the predicted and reference values whereas the values above and below the diagonal represent overestimation and underestimation. The different zones represent different degree of accuracy and inaccuracy of glucose estimation. This method aims at maintaining the blood glucose levels between 70mg/dL - 180mg/dL and based on this assumption, the user will have to correct the values which are outside the range.

Zone A contain those values which are within 20% of the reference and also when the values lie in the hypoglycemic range when the reference is found to be less than 70mg/dL. The values are considered as clinically accurate as such these reading would result in a correct diagnosis.

Zone B contains those values which differ by greater than 20% from the reference value but result into only benign or no treatment.

Zone C contains those values which would lead to overcorrection, if the method was used for clinical practice. This overcorrection would result into glucose value falling below 70mg/dL or rise above 180mg/Dl.

Zone D represents contains those values which would lead to dangerous failure to detect glucose values outside the range of interest.

Zone E contains the values which would give erroneous treatment and would confuse treatment of hypoglycemia for hyperglycemia and vice-versa.

The values which lie in the zones A and B are clinically acceptable, but the values which lie in zones C, D, E can be regarded as potentially dangerous and there is a likelihood of making clinically significant mistakes [2][3]. For instance, if the patient's blood glucose is low, and the device being used to test says that it is high, the patient might take more insulin, lose consciousness and place his life in danger. On the other hand, if the true glucose value is high, and the device reads low, the patient might eat some food or drink fruit juice. The model accuracy testing is done using Clarke EGA for the three cases.

7.4.1 Accuracy of Model built using full Spectra in the range of 2050 – 2350nm

As discussed in section 7.1.1, the entire absorbance spectra of the samples were used for generation of the PLSR model. The prediction results are plotted on a Clarke EGA in figure 7.3

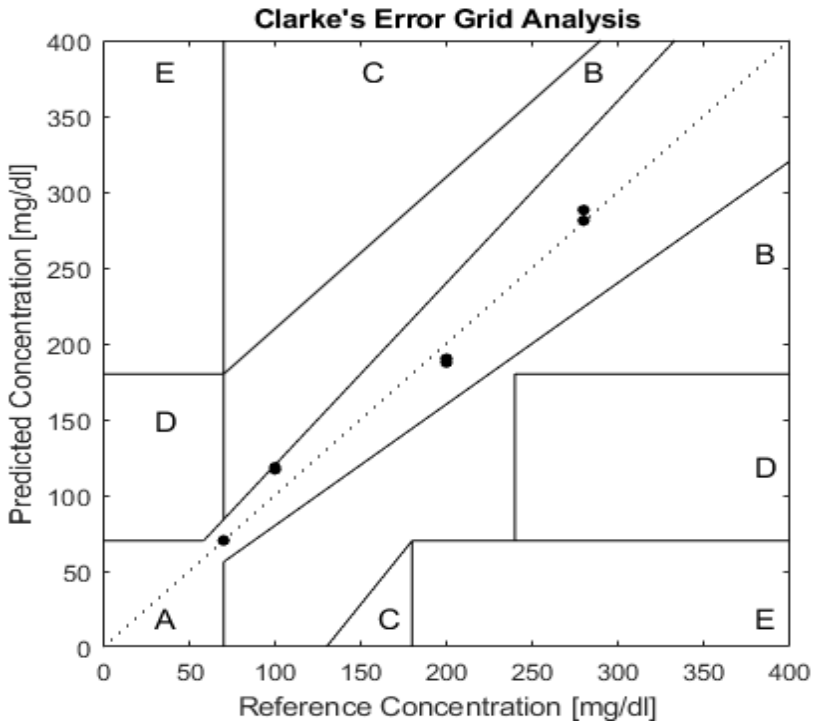

Figure 7.3: Clarke Error Grid Analysis for case 1

As can be seen in the Clarke EGA all the 7 samples used to test the robustness for prediction of the PLSR model lie in the A region.

7.4.2 Accuracy of Model built using fixed wavelengths corresponding to glucose absorption peaks, valleys, and slopes.

Here we have used the 10 fixed wavelengths corresponding to absorption peaks, valleys and slopes of glucose to build the PLSR model. The prediction result of 7 prediction samples is plotted on the Clarke EGA in figure 7.4.

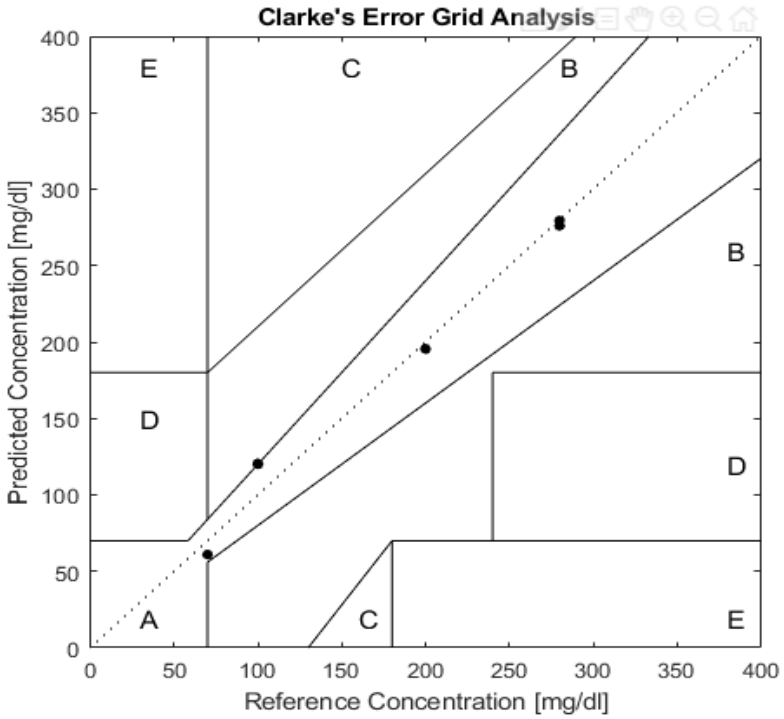

Figure 7.4: Clarke Error Grid Analysis for case 2

Here the EGA analysis shows that all the points lie inside the zone A except for one which lies on the boarder of zone A.

7.4.3 Accuracy of Model built using reduced wavelengths corresponding to glucose absorption peaks and valleys.

Here we have used the only the 5 fixed wavelengths corresponding to absorption peaks and valleys as discussed in the section 7.1.3 to build the PLSR model. The prediction result of 7 prediction samples is plotted on the Clarke EGA in figure 7.5.

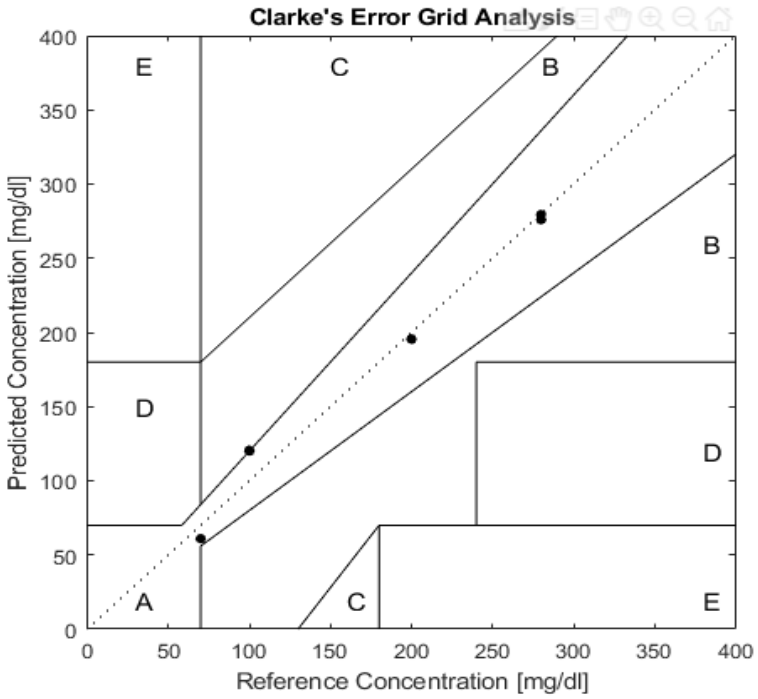

Figure 7.5: Clarke Error Grid Analysis for case 3

Here we found that out of the 7 samples, 5 lie in the zone A and 2 lie on the border of zone A.

7.5 Conclusion

In this research work I have extended the previous work done by our research group. A portable embedded solution was developed featuring a NIOS-II soft-core. It was built on a DE-0 Nano board having a Cyclone-IV FPGA. The focus of our attention was the combination band due to the relative transparency afforded by water in the human tissue. I have ported a C code to implement PLSR using SIMPLS algorithm on the NIOS-II platform. A rigorous study was performed to test the robustness and performance of PLSR algorithm for estimation of glucose concentration of unknown samples when subjected to input with absorbance at varying number of wavelengths points, First with the full absorbance spectrum, then with 10 fixed wavelengths and then

with 5 fixed wavelengths. The RMSE was found to be 11.67, 11.73 and 12.68 respectively for the three cases. The RMSE and the Clarke error grid analysis show that it is possible to estimate glucose using five fixed wavelengths corresponding to the absorbance peaks and valleys.

The aim here was to make a portable low power affordable device for glucose estimation. From the above results we have shown that we can reduce the number of wavelengths form a full spectrum (2050-2350nm) to 5 wavelengths without significantly affecting the accuracy. But by doing so we have significantly reduced the hardware requirements such as use of a white light source which is more power consuming, secondly, we have decreased the computation time and also the hardware resources by manifold. It is also now possible to replace these five fixed points by high intensity LEDs which can further improve the SNR thereby reducing the noise and thereby reducing the RMSE.

7.6 Future scope

As discussed, the SNR of the design can be imporved by using high intensity sources, the white light source can be replaced with high intensity LEDs to probe the sample. These sources are now available in the market at reasonable cost. Once this LED system is succesfully designed, PLSR algorithm can be implemented to validate its performance for glucose estimation. Investigation must be carried out on the front of finding out the influene of other blood constiuesnts using the LED system. One can intend to increase the sample complexity used in the present approach by using blood samples and then to use actual human tissue in a phased manner.

References

[1] W.L. Clarke, D. Cox, L.A. Gonder-Frederick, W. Carter, et al., "Evaluating Clinical Accuracy of Systems for Self-Monitoring of Blood Glucose", Diabetes Care, Vol. 10,1987, pp. 622–628.

[2] A. Maran, C. Crepaldi, A. Tiengo, G. Grassi, et al. "Continuous Subcutaneous Glucose Monitoring in Diabetic Patients", Diabetes Care, Vol. 25, 2002, pp. 347-352.

[3] B.P. Kovatchev, L.A. Gonder-Frederick, D.J. Cox, W.L. Clarke "Evaluating the Accuracy of Continuous Glucose-Monitoring Sensors", Diabetes Journal, Vol. 27, 2004, pp. 1922-1928.

ANNEXUREI

C code for SIMPLS Algorithm

```
#include <stdio.h>
#include <math.h>
#include <float.h>
#define ROW1 4
#define COL1 4
#define ROW2 4
#define COL2 4
#define N 4
double** minus(double** ,double**,int );
double addition(double** ,int ,int);
double** wpq(double** ,int ,int);
double**divide(double**, int,int,double);
double** column(double**,int,int);
void Jacobi_Cyclic_Method(double eigenvalues[COL1], double
*eigenvectors[COL1][COL1],double *A, int n);
double** identity(int);
double** transpose(double**,int,int);
double** init(double**,int,int);
double** set(double**,int,int);
void get(double**,int,int);
double** mul(double**,double**,int,int,int);

void main()
{
int i,j
double**matrix1,**matrix2,**AO,**MO,**trans,**CO,**AO_trans,**g,M[COL1][COL1];
double eigenvalues[COL1],**qh,**Wh,**Wh_mat,**Ch,**W,**ph,**p,**q,**vh;
double eigenvectors[COL1][COL1],Ch_sq,m=2.0,**X_pre;
double **v_trans,**C1,**p_trans,**M1,**A1,**q_trans,**B,**T,av_vh;
clrscr();
matrix1=init(matrix1,ROW1,COL1);
matrix2=init(matrix2,COL2,COL2);
set(matrix1,ROW1,COL1);
set(matrix2,ROW2,COL2);
clrscr();
trans=transpose(matrix1,COL1,ROW1);
AO=mul(trans,matrix2,COL1,COL2,ROW1);
```

```
MO=mul(trans,matrix1,COL1,COL1,ROW1);
CO=identity(COL1);
AO_trans=transpose(AO,COL2,COL1);
g=mul(AO_trans,AO,COL2,COL2,COL1);


        for(i=0;i<COL1;i++)
        {
             for(j=0;j<COL1;j++)
             {
                M[i][j]=*(*(g+i)+j);
             }
        }
        Jacobi_Cyclic_Method(eigenvalues,*eigenvectors,*M,COL1);
        qh=init(qh,COL1,COL1);
        for(i=0;i<COL1;i++)
        {
            for(j=0;j<COL1;j++)
            {
            if(i==j)
              qh[i][j]=eigenvalues[i];
            else
              qh[i][j]=0.0;
            }

        }

Wh=mul(AO,qh,COL1,COL1,COL2);
Wh_mat=column(Wh,COL1,COL1);
Ch=transpose(Wh_mat,1,COL1);
Ch=mul(Ch,MO,1,COL1,COL1);
Ch=mul(Ch,Wh_mat,1,1,COL1);

Ch_sq=sqrt(**Ch);
Wh_mat=divide(Wh_mat,COL1,1,Ch_sq);
W=wpq(Wh_mat,COL1,1);
Wh_mat=column(W,COL1,1);
ph=mul(MO,Wh_mat,COL1,1,COL1);
p=wpq(ph,COL1,1);
```

```
Wh_mat=column(W,COL1,1);
qh=mul(AO_trans,Wh_mat,COL2,1,COL1);
q=wpq(qh,COL2,1);
ph=column(p,COL1,1);
vh=mul(CO,ph,COL1,1,COL1);
av_vh=addition(vh,COL1,1);
av_vh=av_vh/m;
vh=divide(vh,COL1,1,av_vh);
v_trans=transpose(vh,1,COL1);
C1=mul(vh,v_trans,COL1,COL1,1);
C1=minus(CO,C1,COL1);
p_trans=transpose(ph,1,COL1);
M1=mul(ph,p_trans,COL1,COL1,1);
M1=minus(MO,M1,COL1);
A1=mul(CO,AO,COL1,COL2,COL1);
q_trans=transpose(q,1,COL1);
B=mul(W,q_trans,COL1,COL1,1);
T=mul(matrix1,W,ROW1,1,COL1);
get(T,ROW1,1);
ph=transpose(p,1,COL1);
X_pre=mul(T,ph,ROW1,COL1,1);
matrix1=transpose(matrix1,COL1,ROW1);
X_pre=transpose(X_pre,COL1,ROW1);
get(X_pre,COL1,ROW1);
printf("\n\t\t Thanks ");
getch();
free(matrix1);
free(matrix2);

} /* end main */

double** init(double** arr,int row,int col)
{
        int i=0,j=0;
        arr=(double**)malloc(sizeof(double)*row*col);
        for(i=0;i<row;i++)
        {
        for(j=0;j<col;j++)
```

```
            {
              *((arr+i)+j)=(double*)malloc(sizeof(double));
              *(*(arr+i)+j)=0.0;
            }
        }
return arr;
}
double** set(double** arr,int row,int col)
{
     int i=0,j=0;
    double val=0.0;
     for(i=0;i<row;i++)
    {
     for(j=0;j<col;j++)
      {
          printf("Enter value for row %d col %d :",(i+1),(j+1));
          scanf("%lf",&val);
         *(*(arr+i)+j)=val;
      }
    }

return arr;
}

void get(double** arr,int row,int col)
{
 int i=0,j=0;
for(i=0;i<row;i++)
{
      for(j=0;j<col;j++)
      {
         printf("%lf\t",*(*(arr+i)+j));
      }
      printf("\n");
}
}
```

```
double** mul(double** arr1,double** arr2,int row,int col,int col1)
{
double **result;
int i=0,j=0,k=0;
result=init(result,row,col);
 for(i=0;i<row;i++)
 {
        for(j=0;j<col;j++)
        {
            for(k=0;k<col1;k++)
            {
               *(*(result+i)+j)+=(*(*(arr1+i)+k))*(*(*(arr2+k)+j));
              if (k!=(col1-1))
              printf("+");
            }
            printf("\t");
        }
printf("\n");
}
return (result);
}
double** transpose(double** arr,int row1,int col1)
{
double **trans;
int i,j;
trans=init(trans,row1,col1);
   for(i=0;i<col1;i++)
  {
       for(j=0;j<row1;j++)
      *(*(trans+j)+i)=*(*(arr+i)+j);
   }
return trans;
}
```

```
double** identity(int dim)
{
double **CO;
int i,j;
CO=init(CO,dim,dim);
    for(i=0;i<dim;i++)
    {
        for(j=0;j<dim;j++)
        {
            if(i==j)
            {
               CO[i][j]=1.0;
            }
             else
            {
              CO[i][j]=0.0;
            }
        }
   }
return CO;
}
Void Jacobi_Cyclic_Method (double eigenvalues[N], double*eigenvectors[N][N],double
*A, int n)
{
int row, i, j, k, m;
double *pAk, *pAm, *p_r, *p_e;
double threshold_norm;
double threshold;
double tan_phi, sin_phi, cos_phi, tan2_phi, sin2_phi, cos2_phi;
double sin_2phi, cos_2phi, cot_2phi;
double dum1;
double dum2;
double dum3;
double r;
double max;
if ( n < 1) return;
if ( n == 1) {
```

```
eigenvalues[0] = *A;
*eigenvectors[0][0] = 1.0;
return;
}
for (p_e = eigenvectors, i = 0; i < n; i++)
for (j = 0; j < n; p_e++, j++)
if (i == j)
*p_e = 1.0; else *p_e = 0.0;
for (threshold = 0.0, pAk = A, i = 0; i < ( n - 1 ); pAk += n, i++)
for (j = i + 1; j < n; j++) threshold += *(pAk + j) * *(pAk + j);
threshold = sqrt(threshold + threshold);
threshold_norm = threshold * DBL_EPSILON;
max = threshold + 1.0;
while (threshold > threshold_norm) {
threshold /= 10.0;
if (max < threshold) continue;
max = 0.0;
for (pAk = A, k = 0; k < (n-1); pAk += n, k++) {
for (pAm = pAk + n, m = k + 1; m < n; pAm += n, m++) {

if ( fabs(*(pAk + m)) < threshold ) continue;
cot_2phi = 0.5 * ( *(pAk + k) - *(pAm + m) ) / *(pAk + m);
dum1 = sqrt( cot_2phi * cot_2phi + 1.0);
if (cot_2phi < 0.0) dum1 = -dum1;
tan_phi = -cot_2phi + dum1;
tan2_phi = tan_phi * tan_phi;
sin2_phi = tan2_phi / (1.0 + tan2_phi);
cos2_phi = 1.0 - sin2_phi;
sin_phi = sqrt(sin2_phi);
if (tan_phi < 0.0) sin_phi = - sin_phi;
cos_phi = sqrt(cos2_phi);
sin_2phi = 2.0 * sin_phi * cos_phi;
cos_2phi = cos2_phi - sin2_phi;
p_r = A;
dum1 = *(pAk + k);
dum2 = *(pAm + m);
dum3 = *(pAk + m);
*(pAk + k) = dum1 * cos2_phi + dum2 * sin2_phi + dum3 * sin_2phi;
```

```
*(pAm + m) = dum1 * sin2_phi + dum2 * cos2_phi - dum3 * sin_2phi;
*(pAk + m) = 0.0;
*(pAm + k) = 0.0;
for (i = 0; i < n; p_r += n, i++) {
if ( (i == k) || (i == m) ) continue;
if ( i < k ) dum1 = *(p_r + k);
else
dum1 = *(pAk + i);
if ( i < m ) dum2 = *(p_r + m); else dum2 = *(pAm + i);
dum3 = dum1 * cos_phi + dum2 * sin_phi;
if ( i < k ) *(p_r + k) = dum3; else *(pAk + i) = dum3;
dum3 = - dum1 * sin_phi + dum2 * cos_phi;
if ( i < m ) *(p_r + m) = dum3; else *(pAm + i) = dum3;
}
for (p_e = eigenvectors, i = 0; i < n; p_e += n, i++) {
dum1 = *(p_e + k);
dum2 = *(p_e + m);
*(p_e + k) = dum1 * cos_phi + dum2 * sin_phi;

*(p_e + m) = - dum1 * sin_phi + dum2 * cos_phi;
}
}
for (i = 0; i < n; i++)
if ( i == k ) continue;
else if ( max < fabs(*(pAk + i))) max = fabs(*(pAk + i));
}
}
for (pAk = A, k = 0; k < n; pAk += n, k++) eigenvalues[k] = *(pAk + k);
}


double** column(double** matrix,int row,int col)
{
int i,j,k=0;
double **column;
column=init(column,row,col);
for(i=0,j=(col-1);i<row;i++)
   {
```

```
        *(*(column+i)+k)=*(*(matrix+i)+j);
    }
return column;
}


double** divide(double** matrix,int row,int col,double Ch_sq)
{
int i,j,k=0;
double **divide;
divide=init(column,row,col);
for(i=0,j=(col-1);i<row;i++)
        {
          *(*(divide+i)+k)=*(*(matrix+i)+j) / Ch_sq;
        }
return divide;
}


double** wpq(double** matrix,int row,int col)
{
int i,j,k=0;
double **wpq;

wpq=init(wpq,row,col);
for(i=0;i<row;i++)
  {
     *(*(wpq+i)+k)= *(*(matrix+i)+k);
  }
return wpq;
}


double addition(double** matrix,int row,int col)
{
int i,j=col-1;
double add=0.0;
for(i=0;i<row;i++)
add+= *(*(matrix+i)+j);
```

```
return add;
}


double** minus(double** matrix1,double** matrix2,int col)
{
int i,j;
double **minus;
minus=init(minus,col,col);
for(i=0;i<col;i++)
{
        for(j=0;j<col;j++)
        *(*(minus+i)+j)=( *(*(matrix1+i)+j) - *(*(matrix2+i)+j) );
}
return minus;
}
```

ANNEXURE II

Program for LCD

```
#include"altera_avalon_lcd_16207_regs.h"
void lcd_int()
{
usleep(15000);
IOWR_ALTERA_AVALON_LCD_16207_COMMAND(LCD_BASE,0X38);
usleep(4100);
IOWR_ALTERA_AVALON_LCD_16207_COMMAND(LCD_BASE,0X06);
usleep(4100);
IOWR_ALTERA_AVALON_LCD_16207_COMMAND(LCD_BASE,0X0E);
usleep(4100);
IOWR_ALTERA_AVALON_LCD_16207_COMMAND(LCD_BASE,0X01);
usleep(2000);
}
int main()
{
int i;
char j[16]=" TEST ";
lcd_int();
        while(1)
        {
                IOWR_ALTERA_AVALON_LCD_16207_COMMAND(LCD_BASE,0X80);
                usleep(2000);
                for(i=0;i<16;i++)
                {
                        IOWR_ALTERA_AVALON_LCD_16207_DATA(LCD_BASE,j[i]);
                        usleep (30000);
                }

        }
return 0;
}
```

ANNEXURE III

Program for ADC interface

```
#include "altera_up_avalon_adc.h"
#include"altera_avalon_lcd_16207_regs.h"

void lcd_int()
{
        usleep(15000);
        IOWR_ALTERA_AVALON_LCD_16207_COMMAND(LCD_BASE,0X38);
        usleep(4100);
        IOWR_ALTERA_AVALON_LCD_16207_COMMAND(LCD_BASE,0X06);
        usleep(4100);
        IOWR_ALTERA_AVALON_LCD_16207_COMMAND(LCD_BASE,0X0E);
        usleep(4100);
        IOWR_ALTERA_AVALON_LCD_16207_COMMAND(LCD_BASE,0X01);
        usleep(2000);
}

int main()
{
        int i;
        alt_up_adc_dev *adc;
        unsigned int thousand, hundred, ten, unit;
        int count;
        int data;
        int channel;
        lcd_int();

        while(1)
        {
                data = 0;
                channel = 0;
                adc = alt_up_adc_open_dev ("/dev/ADC");
                while (adc!=NULL)
                {
                        alt_up_adc_update (adc);
                        count += 1;
                        data = alt_up_adc_read (adc, channel);
                        data=((data*3300)/4095);
                        thousand=(data/1000)+48;
```

```
                    hundred=((data/100)%10)+48;
                    ten=((data/10)%10)+48;
                    unit=(data%10)+48;

                IOWR_ALTERA_AVALON_LCD_16207_COMMAND(LCD_BASE,0XC0);
                    usleep(2000);
                    IOWR_ALTERA_AVALON_LCD_16207_DATA(LCD_BASE,thousand);
                    usleep (30000);
                    IOWR_ALTERA_AVALON_LCD_16207_DATA(LCD_BASE,hundred);
                    usleep (30000);
                    IOWR_ALTERA_AVALON_LCD_16207_DATA(LCD_BASE,ten);
                    usleep (30000);
                    IOWR_ALTERA_AVALON_LCD_16207_DATA(LCD_BASE,unit);
                    usleep (30000);
                    IOWR_ALTERA_AVALON_LCD_16207_DATA(LCD_BASE,'m');
                    usleep (30000);
                    IOWR_ALTERA_AVALON_LCD_16207_DATA(LCD_BASE,'g');
                    usleep (30000);
                    IOWR_ALTERA_AVALON_LCD_16207_DATA(LCD_BASE,'/');
                    usleep (30000);
                    IOWR_ALTERA_AVALON_LCD_16207_DATA(LCD_BASE,'d');
                    usleep (30000);
                    IOWR_ALTERA_AVALON_LCD_16207_DATA(LCD_BASE,'L');
                    usleep (30000);
            }
}
return 0;
}
```